Attitude Dynamics and Control of Satellites with Fluid Ring Actuators

Nona Abolfathi Nobari

Department of Mechanical Engineering
McGill University, Montreal
April, 2013

A thesis submitted to the Faculty of Graduate Studies and Research in partial fulfillment of the requirements of the degree of Doctor of Philosophy

Dedicated

to my parents, Shahla and Abbas, for their never-ending incredible support and sacrifice.

ABSTRACT

Successful mission of a satellite depends on maintaining a fixed orientation with respect to the Earth. However, the attitude angles of a satellite can be perturbed because of various natural disturbance sources, such as the Earth's gravity gradient, solar radiation pressure, and the Earth's magnetic field. Modeling the attitude dynamics and developing a controller to stabilize the attitude motion are quite important steps in the design of satellites. Although several actuators exist to control the attitude motion, a novel type considered in the thesis, shows promise of producing a high torque to mass ratio. This potential justifies the in-depth study reported. The novel actuator in question consists of a ring containing fluid, whose flow is regulated by a pump. The control torque is produced due to the variation of the angular velocity of the fluid.

In this thesis, first, a redundant actuator system composed of four fluid rings in a pyramidal configuration is studied. The dynamical model of the system is developed for a satellite travelling either in a circular or an elliptical orbit. The dynamical analysis of this system leads to an underdetermined system of nonlinear differential equations, whose solution without considering the control input (the torque produced by the pump pressure) shows that the fluid rings can damp out the attitude disturbances of a satellite in a circular orbit and the roll-yaw disturbances in an elliptical orbit. However, this passive damping effect is fairly slow; an active controller is hence designed in the next step. The effect of the failure of one fluid ring on the performance of the *attitude control subsystem* (ACS) of a satellite is also studied. It is observed that even in the case of failure of one fluid ring, the satellite can be stabilized by slight modification of the active controller. Later, a sliding mode controller is designed to cope with the uncertainties existing in the fluid model and in other parameters of the system. Although the results achieved are quite satisfactory, the chattering that exists in the steady response of the system is not

desirable; hence a switching controller consisting of a sliding mode and a PID control law is designed to eliminate this chattering effect.

Next, the theoretical results obtained are validated by conducting several experiments. To this end, first, a setup with one fluid ring is designed and built. Here, a single fluid ring is attached to a disk so as to verify the controllability of the system with a fluid ring and also the validity of the theoretical model. Although the experimental results confirm the theory developed in this thesis, the large torque-to-mass ratio expected is revealed to be only possible at the cost of a quite high input voltage to the pumps regulating the flow. Therefore, two novel applications of fluid rings are proposed: as an actuator for spin stabilized satellites, or as an auxiliary actuator in satellites with magnetic torquers.

Using fluid rings in spin stabilized satellites is proposed in the thesis, as an alternative to the commonly used micro-thrusters. Here, two fluid rings are mounted on the satellite while their axes of symmetry are aligned with the roll and yaw axes. To examine the feasibility and performance, a dynamical model of this spinning satellite with two fluid rings is developed. A controller is then designed to stabilize the attitude motion of this satellite.

The second novel actuator system developed here consists in using fluid rings as complementary actuators in satellites with two magnetic torquers. The dynamical model is formulated, and a controller is designed to investigate the performance of this system. The simulation of the system without the fluid ring shows that the satellite attitude can be stabilized by using only two magnetic torquers, however, slowly. Upon adding the active fluid ring actuator to the system, the stabilization time is reduced by a factor of 10. The failure of the fluid ring and each magnetic torquer is also studied.

RÉSUMÉ

La réussite d'une mission d'un satellite dépend du maintien d'une orientation fixe par rapport à la Terre. Toutefois, les angles d'attitude d'un satellite changent en raison d'excitations diverses. Un modèle dynamique est utile pour prédire l'attitude du satellite le développement un contrôleur pour stabiliser l'attitude est également importantes. Un nouvel actionneur pour le contrôle de l'attitude est proposé dans cette thèse. L'actionneur fluidique produit un couple élevé par rapport à la masse. L'actionneur en question se compose d'un anneau rempli par un fluide. L'écoulement de ce fluide est régulé par une pompe. Le couple de commande est produit par la variation du moment cinétique du fluide.

Un système d'actionnement redondant composé de quatre anneaux de fluide dans une configuration pyramidale est d'abord étudié. Le modèle dynamique du système est développé pour un satellite voyageant dans une orbite circulaire ou elliptique. L'analyse dynamique de ce système mène à un système sous-déterminé d'équations différentielles non-linéaires. La solution, sans tenir compte du couple produit par le contrôleur, montre que les anneaux de fluide peuvent agir comme régulateurs passifs, ce qui amortit les perturbations d'attitude d'un satellite sur une orbite circulaire et les perturbations en roulis-lacet selon une orbite elliptique. Cependant, cet effet d'amortissement passif est assez lent. Par conséquent, le contrôleur actif fut conçu. Les résultats obtenus montrent que les angles d'attitude du satellite sont stabilisés rapidement. De plus, l'effet de la défaillance d'un anneau liquide sur la performance du sous-système de contrôle d'attitude (SCA) du satellite est étudié. On constate que, même dans le cas de défaillance d'un anneau de fluide, le satellite peut être stabilisé par la modification du contrôleur actif. En raison des limites de ressources de calcul dans les applications spatiales, un modèle simple de l'écoulement du fluide est adopté ici. Un contrôleur au mode glissant est donc conçu pour être robuste aux incertitudes dans le modèle hydraulique et dans les

paramètres du système. Bien que les résultats obtenus soient assez satisfaisants, l'effet importun du 'chattering' existe dans l'état stationnaire du système. Un contrôleur hybride composé d'un contrôleur au mode glissant avec une loi de commande PID est conçu pour éliminer cet effet.

Les résultats théoriques sont validés expérimentalement. À cette fin, une première configuration consistant en un anneau de fluide est conçue et construite. Puis un test sur un anneau de fluide unique attaché à un disque est effectué pour vérifier si le système peut être contrôlé, et si le modèle théorique représente le comportement réel. Bien que les résultats expérimentaux confirment la théorie développée dans cette thèse, le grand couple à rapport de masse nécessite un coût de tension d'entrée très élevé pour les pompes de régulation du débit. Par conséquent, deux nouvelles applications d'anneaux de fluide sont proposées dans cette thèse: comme actionneur pour les satellites stabilisés de spin, ou comme actionneur auxiliaire avec magnéto-coupleurs.

L'utilisation des anneaux de liquide dans les satellites stabilisés par rotation est le premier champ d'application proposé comme une alternative aux courants micro-propulseurs. Dans ce système, deux anneaux de fluide sont montés sur le satellite alors que leurs axes de symétrie sont alignés avec les directions de roulis et de lacet. Pour vérifier la faisabilité et la performance, un modèle dynamique de ce satellite en rotation avec deux anneaux de fluide est développé. Ensuite un contrôleur modifié est conçu pour stabiliser l'attitude du satellite.

Le deuxième système d'actionneur est développé en utilisant les anneaux de fluide comme actionneurs complémentaires dans les satellites avec magnéto-coupleurs. Un modèle dynamique est développé, et un contrôleur est également conçu pour étudier la performance de ce système. Le système est d'abord examiné sans l'utilisation de l'anneau de fluide. Les résultats montrent que le satellite est stabilisé par seulement deux magnéto-coupleurs, mais lentement. Après l'ajout de l'actionneur actif de l'anneau de fluide dans le système, le temps de stabilisation est réduit par un facteur de dix. L'échec de l'anneau de fluide et de chaque couple magnétique sont testés.

ACKNOWLEDGEMENTS

First and foremost, I wish to thank my supervisor Professor Arun K. Misra, whose great knowledge helped me a lot to walk in this path. In fact, this thesis became possible because of his guidance and support. By now, not only he is my professional role-model for his knowledge, but also for his kind treatment. Indeed, his patience and kindness softened the difficult days of PhD studies. With his fatherly behaviour, he taught me how to enter and remain in the research world.

I could never imagine that someone can make me feel like I have a brother, until I met Dr. Bijan Deris. His encouragement and support made the life in Montreal much more pleasant. The fact that, at every moment of a day or a night, he has always been open to receive me and my husband is very sweet. I also wish to thank his wife, Shiva Varshovi, for her peaceful personality that calmed me down and sweetened the unpleasant taste of the difficult moments of my graduate student life.

I wish to thank Sara Shayan Amin, who has always been there for me when I needed her the most. She, with her high energy, was a boost for me to walk in this path more and more strongly. For the first time in Montreal, she gave me the sweet taste of having a close friend. She is one of the reasons that living in Montreal became more pleasant for me. I would also like to thank Dr. Hamid Dalir, whose optimism always motivated me toward my goals.

I thank Dr. Afshin Taghvaiepour: as a very good friend, he helped me to be much more aware of different aspects of human personality, and thus, to try to improve mine. In the first days in Montreal, I and my husband were received by a close friend, Tara Khani,

and his husband, Majid Fekri. Their kindness cannot be forgotten as they helped me to start my PhD without worrying about a shelter in the very first days.

I want to thank Tara Mirmohammadi, Pamela Woo, and Mohammad Jalali Mashayekhi because of their helps and also the friendly environment they made at the office. I also would like to thank Bahareh Ghotbi, Atefeh Nabavi, and Nazanin Aghaloo because of all pleasing moments that we had together all this time. I would also like to thank Mehdi Paak and Dr. Vahid Raeesi for our technical discussions on *fluid structure interactions* and *robust controller design*.

I wish to thank my father- and mother-in-law, Mr. Ebrahim Alizadeh and Taraneh Yarahmadi, for their everyday support. I am always aware of their kindness in treating me like a princess and wishing me all the best of the worlds. Not only because of that, but also I want to thank them mostly because of their son, Danial, whose unconditional support has always been there for me. During all this time, Danial got so tough on himself to soften the way ahead of me as much as he could. My sister, Nila, with her everyday phone calls and kind voice unbelievably reduced the sadness of being far apart. She always stayed beside me in my happiness, sadness and became a great support from thousands of miles away. Finally, I reached to my parents, Shahla and Abbas; I thank them at the end, because I believe in their patience. I owed my success to my parents because of their incredible support and sacrifice. One should be a parent to understand the meaning of the unconditional love that they always offered me. In fact, only hearing "*my daughter"* from them was more than enough to forget all the sorrow. Mom and dad: I love you because of everything you did, which I cannot describe; I dedicate this thesis to you.

CLAIM OF ORIGINALITY

The originality of the main ideas and research results presented in this thesis are claimed here. The most significant ones are listed below:

(i) The main claim of novelty of this thesis is that, for the first time, a thorough feasibility analysis of using fluid ring systems for attitude control is reported, which highlights the advantages of this system quantitatively.

(ii) A more accurate dynamical model compared to what exists in the literature is developed for a system consisting of a satellite and a set of fluid ring actuators.

(iii) Although a PID controller could stabilize the system understudy, another contribution of the thesis is to propose a switching application of a sliding mode controller and a PID so as to cope with the model uncertainties and avoid chattering in the system response.

(iv) The feasibility of using fluid ring actuators was demonstrated through the experiments.

(v) A novel application of fluid ring actuators is suggested that indicates using fluid rings for stabilizing the attitude angles of spinning satellites. Henceforth, a dynamical model is developed and a controller is designed for the system proposed.

(vi) A new hybrid actuator consisting of a fluid ring and two magnetic torquers is proposed. Moreover, the dynamical model of this system is developed; the effect of failure of an actuator of this new hybrid system was also evaluated.

NOMENCLATURE

Roman symbols

A	Fluid ring cross-sectional area
$\boldsymbol{b}$	Earth's geomagnetic field vector
c_1 , c_2	Non–dimensional physical parameters defined in Eqs. (2.24) and (5.35)
d	Cross-sectional diameter of fluid rings
$\hat{d}$	Non–dimensional geometric parameter of fluid rings defined in Eqs. (2.24) and (5.35)
e	Orbit eccentricity
f	Friction coefficient
I_a, I_t	Moments of inertia of a spinning satellite in axial and tangential directions
I_d	Moment of inertia of a disk
I_f	Fluid moment of inertia
$\boldsymbol{I_{fi}}$	Inertia matrix of the i th fluid ring about its axis of symmetry
$\hat{\boldsymbol{I}}_{\boldsymbol{fi}}$	Non-dimensional inertia matrix of the ith fluid ring

I_{ji}	Moment of inertia of the ith ring about the jth axis of the ith fluid ring body frame
$\boldsymbol{I_r}$	Inertia matrix of a rigid body about its centroidal principal axes
$\boldsymbol{I_s}$	Satellite inertia matrix about its principal axes at its center of mass
$\hat{\boldsymbol{I}}_{\boldsymbol{s}}$	Non-dimensional moment of inertia matrix of the satellite
I_{xx}, I_{yy}, I_{zz}	Diagonal terms of the inertia matrix of the satellite
$\boldsymbol{k}$	Sliding mode controller gain vector
$\boldsymbol{K}$	Feedback controller matrix obtained from the pole placement method
K_1, K_3	Non–dimensional inertia parameters in Eq. (2.23)
K_d, K_i, K_p	Non–dimensional gains of a PID controller
K_{ij}	Non–dimensional inertia of the fluid rings in Eq. (2.23)
K_R, K_t	Non–dimensional inertia of the fluid ring in a spinning satellite
K_v	Non–dimensional gain of the modified PID controller
m_{1i}, m_{2i}	Components of the reaction moment exerted on a satellite by the ith fluid ring in the X and Y directions
$\boldsymbol{m_{coil}}$	Magnetic dipole moment
n	Mean orbital rate

$\boldsymbol{P}$	Error covariance matrix
$\boldsymbol{q_1}$,$\boldsymbol{q_2}$	Vectors spanning a plane *P* whose normal is parallel to the Earth's magnetic vector
$\boldsymbol{Q}$	A matrix composed of $\boldsymbol{q_1}$,$\boldsymbol{q_2}$
$\boldsymbol{R_i}$	Rotation matrix transforming vectors from the satellite frame to the ith fluid ring frame
R_n	Reynolds number
r	Fluid ring radius
$\boldsymbol{r_c}$	beimg the position vector of the satellite with respect to the Earth
r_{imp}	Impeller radius
s	A sliding surface used in the sliding mode control law
T	Non–dimensional time parameter
u_ω^c	Control input for impeller speed in the experiments
v_1^c, v_3^c	Control inputs defined in Eqs. (5.36) and (5.37)
V_{app}	Applied voltage
V_e	Electromotive voltage
$\boldsymbol{w}(k)$	Kalman filter gain

Greek symbols

α_i, γ_i	Pyramidal configuration angles (Euler angles describing the orientation of the ith fluid ring)
$\dot{\beta}$	Fluid angular velocity
$\dot{\beta}_i$	Fluid angular velocity relative to the ith ring
β_i'	Non-dimensional fluid angular velocity
δ	Error signal
η_i	Sliding mode gain
θ	Disk angle
θ_i	Attitude angles of the satellite, $i = x, y, z$
$\boldsymbol{\theta}$	Array of attitude angles of the satellite
$\boldsymbol{\theta'}$	Non-dimensional rate of attitude angles array
$\boldsymbol{\theta_d}$	Array of desired attitude angles
$\Theta, \dot{\Theta}$	True anomaly and orbital rate
Θ'	Non-dimensional orbital rate
λ	Design parameter of the sliding mode controller
μ	Fluid viscosity
ν	$\Omega + n$
ξ	Damping factor

ρ	Fluid density
σ	Fluid shear stress acting on the wall of the ring
τ^c	Control torque
$\hat{\tau}^c$	Non-dimensional control torque
τ_a	Torque produced by a fluid ring
$\boldsymbol{\tau_{ext}}$	External torque exerted on a satellite
τ_f	Fluid friction torque
τ_{f_i}	Fluid friction torque in the ith ring
$\hat{\tau}_{f_i}$	Non-dimensional fluid friction torque in the ith ring
$\boldsymbol{\tau_{gt}}$	Gravity gradient torque exerted on the satellite
$\hat{\boldsymbol{\tau}}_{\boldsymbol{gt}}$	Non-dimensional gravity gradient torque exerted on the satellite
$\boldsymbol{\tau_{gt_{fi}}}$	Gravity gradient torque exerted on the fluid rings
$\hat{\boldsymbol{\tau}}_{\boldsymbol{gt_{fi}}}$	Non-dimensional gravity gradient torque exerted on the fluid rings
$\boldsymbol{\tau_m}$	Magnetic torque
τ_p	Pump pressure torque
$\boldsymbol{\tau_r}$	Reaction torque
$\boldsymbol{\omega}$	Satellite angular velocity defined in its own body frame

$\hat{\boldsymbol{\omega}}$	Non-dimensional angular velocity of the satellite
$\boldsymbol{\omega_f}$	The absolute angular velocity of the fluid defined in the body frame of the fluid ring
ω_{imp}	Impeller angular velocity
Ω	Spin rate of a spinning satellite

TABLE OF CONTENTS

ABSTRACT i

RÉSUMÉ iii

ACKNOWLEDGEMENTS v

CLAIM OF ORIGINALITY vii

NOMENCLATURE ix

TABLE OF CONTENTS xv

TABLE OF FIGURES xix

TABLE OF TABLES xxvii

INTRODUCTION 1

1.1 Background 1

1.1.1. Reaction/Momentum Wheels 2

1.1.2. Control Moment Gyros 4

1.1.3. Micro-thrusters 5

1.1.4. Magnetic Torque Rod Actuators 6

1.2. Motivation 7

1.3. Review of the Literature on Fluidic Actuators 8

1.4. Objectives of the Thesis 11

1.5. Thesis Organization 11

ATTITUDE DYNAMICS OF A RIGID SATELLITE WITH FLUID RINGS 13

2.2 Dynamical Model of a Rigid Satellite with Fluid Rings 13

2.1.1. Non-dimensionalization of the equations of motion 19
2.3 Numerical Results with Passive Fluid Rings 21
2.4 Summary 29
DESIGNING OF CONTROLLERS FOR SATELLITES WITH FLUID RINGS 31
3.1 PID Controller 32
3.2. Failure Analysis 38
3.3. Designing a Sliding Mode Controller 41
3.3.1. Dynamical behaviour of the system with the sliding mode controller 44
3.4. Switching Control Law 46
3.5. Summary 48
EXPERIMENTAL RESULTS 49
4.1. Design of the Experimental Setup 49
4.1.1. Material selection 50
4.1.2. Fluid selection 50
4.1.3. Pump selection 51
4.2. Preliminary Analysis 52
4.3. Experiment with a Single Fluid Ring System 55
4.3.1. Designing a Kalman filter 56
4.3.2. Single fluid ring system experiment 59
4.4. Three Dimensional (3D) Control Experiment 63
4.5. Summary 68
SPINNING SATELLITES WITH FLUID RING ACTUATORS 69
5.1. Development of the Dynamical Model 70
5.2. Small Angle Approximation 73

5.2.1. Non-dimensionalization 76
5.3. Design of a Controller for the Linear Model 77
5.3.1. Numerical results for the linear model 79
5.4. Design of the Controller for the Nonlinear Model 81
5.4.1. Numerical results for the nonlinear system 82
5.5. Summary 85
A HYBRID ATTITUDE CONTROLLER CONSISTING OF ECTROMAGNETIC TORQUE RODS AND A FLUID RING 87
6.1. Dynamics Modeling 88
6.2. Simulation and Results 93
6.3. Failure Study 97
6.3.1. Failure of the fluid ring 98
6.3.2. Failure of one magnetic coil 101
6.4. Summary 105
CONCLUDING REMARKS AND RECOMMENDATIONS FOR FUTURE WORK 107
7.1. Summary and Findings 108
7.2. Recommendations for Future Work 110
REFERENCES 111

TABLE OF FIGURES

Figure 1.1: A reaction/momentum wheel (Wertz, 1999) 3

Figure 1.2: Singular configuration of CMGs (Leeghim et al. 2009)..... 5

Figure 1.3: Magnetic torquer designed by Vectronic Aerospace..... 6

Figure 1.4: A fluid ring actuator (Patel and Kumar, 2009)..... 8

Figure 1.5: Fluidic actuator proposed by Maynard (1988) 9

Figure 1.6: Fluid loop configurations proposed by Lurie et al. (1991)..... 9

Figure 1.7: A dual-function actuator consisting of a fluid loop and a permanent magnet 10

Figure 1.8: Fluid loop prototype used by Kelly et al. (2004)..... 10

Figure 2.1: A satellite with three orthogonal fluid rings..... 14

Figure 2.2: Pyramidal configuration of the fluid rings in a satellite 15

Figure 2.3: (a) LVLH reference frame of a satellite; (b) Free body diagram of a fluid ring 15

Figure 2.4: Attitude motion of the satellite in a circular orbit in the absence of damping torques: (a) Roll angle; (b) Pitch angle; (c) Yaw angle 22

Figure 2.5: Attitude motion of a satellite in an elliptical orbit with the eccentricity of 0.05 in the absence of damping torques: (a) Roll angle; (b) Pitch angle; (c) Yaw angle . 23

Figure 2.6: Attitude motion of the satellite in a circular orbit in the presence of damping torques of four fluid rings: (a) Roll angle; (b) Pitch angle; (c) Yaw angle..... 24

Figure 2.7: Attitude motion of a satellite in an elliptical orbit with the eccentricity of 0.05 in the presence of damping torques of four fluid rings: (a) Roll angle; (b) Pitch angle; (c) Yaw angle..... 25

Figure 2.8: Attitude angles for the pyramidal angle $\gamma = 5°$: (a) Roll angle; (b) Pitch angle; (c) Yaw angle..... 26

Figure 2.9: Attitude angles for the pyramidal angle $\gamma = 45°$: (a) Roll angle; (b) Pitch angle; (c) Yaw angle 27

Figure 2.10: Attitude angles for the pyramidal angleγ=**85°:** (a) Roll angle; (b) Pitch angle; (c) Yaw angle 27

Figure 3.1: Attitude angles of the controlled system with PID gains $K_p = 5000$, $K_d = 10$, and $K_i = 0.5$ (circular orbit): (a) Roll angle; (b) Pitch angle; (c) Yaw angle..... 33

Figure 3.2: Control torque components with PID gains $K_p = 5000$, $K_d = 10$, and $K_i = 0.5$ (circular orbit case); (a) Roll angle; (b) Pitch angle; (c) Yaw angle..... 34

Figure 3.3: Fluid angular velocity with PID gains $K_p = 5000$, $K_d = 10$, and $K_i = 0.5$ (circular orbit case) 35

Figure 3.4: Attitude angles of the controlled system with various pyramidal angles using 36

Figure 3.5: Attitude angle differences upon varying the pyramidal angle γ with PID gains $\mathrm{K_p} = 5000$, $\mathrm{K_d} = 10$, and $K_i = 0.5$: (a) Difference of attitude angles between $\gamma = 5°$ and 45°; (b) Difference of attitude angles between $\gamma = 45°$ and 85° (circular orbit case) 37

Figure 3.6: Response of the system subject to the failure of one fluid ring with using PID gains $K_p = 5000$, $K_d = 10$, and $K_i = 0.5$ (circular orbit case): (a) Satellite attitude angles; (b) Fluid angular velocity in the rings; (c) Resultant control torque 39

Figure 3.7: Response of the system associated with the failure of one fluid ring using the gains $K_p = 5000$, $K_d = 10$, $K_i = 0.5$, and $K_v = -0.5$ (circular orbit case): (a) Satellite attitude angles; (b) Fluid angular velocity in the rings; (c) Control **torque** 40

Figure 3.8: Sliding hypersurface for the roll direction..... 42

Figure 3.9: Attitude angles after applying the sliding mode controller (circular orbit case) 44

Figure 3.10: Components of the control torque resulting from the sliding mode controller: (a) Roll direction; (b) Pitch direction; (c) Yaw direction (circular orbit case) 45

Figure 3.11: Attitude angles after applying the switching controller (circular orbit case) 46

Figure 3.12: Control torque resulting from the switching controller; (a) Roll direction; (b) Pitch direction; (c) Yaw direction (circular orbit case) 47

Figure 3.13: Satellite attitude angles using a PID controller with the nominal parameter values 48

Figure 3.14: Satellite attitude angles using a PID controller subject to the $\pm 15\%$ uncertainty in the nominal parameter values 48

Figure 4.1: The fluid ring used in the experimental validation phase 52

Figure 4.2: Angular velocity of the impeller versus the applied voltage 53

Figure 4.3: Fluid ring with its base mounted on the simulator 54

Figure 4.4: Fluid angular velocity $\dot{\beta}$ versus the impeller angular velocity ω_{imp} using a sinusoidal input voltage 54

Figure 4.5: The block diagram of the controllers used between the model and the plant. 56

Figure 4.6: The block diagram of a system with a Kalman filter 56

Figure 4.7: Theoretical and experimental plots of the impeller angular velocity versus time 61

Figure 4.8: Theoretical and experimental plots of the attitude angle of the disk versus time 61

Figure 4.9: The theoretical and experimental plots of the disk angular velocity versus time 62

Figure 4.10: The experimental control torque versus time 62

Figure 4.11: Input voltage which is applied to the fluid ring system 62

Figure 4.12: (a) Cubic satellite floating on the simulator; (b) Hardware-in-the-loop experimental setup 63

Figure 4.13: Attitude angles found from the theoretical model 64

Figure 4.14: Theoretical and Experimental angular velocities of the roll-axis impeller... 64

Figure 4.15: Theoretical and Experimental angular velocities of the pitch-axis impeller 64

Figure 4.16: Theoretical and Experimental angular velocities of the yaw-axis impeller.. 65

Figure 4.17: Desired fluid angular velocity in the: (a) Roll-axis ring; (b) Pitch-axis ring; (c) Yaw-axis ring 66

Figure 4.18: Applied voltage to the pumps on different rings versus time: (a) roll-axis; (b) pitch-axis; (c) yaw axis 67

Figure 5.1: A cylindrical satellite with two fluid rings 70

Figure 5.2: Three coordinates frames used in dynamical modeling 71

Figure 5.3: Free body diagrams of the satellite and two fluid rings (only moment vectors are shown) 71

Figure 5.4: Roll and yaw angles using the linear controller with $p_i = -10$ 80

Figure 5.5: Control torque in the roll and yaw directions using the linear controller with $p_i = -10$ 80

Figure 5.6: Fluid angular velocity using the linear controller with $p_i = -10$ 80

Figure 5.7: Pitch angle θ_2 while using the modified PD controller with the gains obtained from the linear controller: $K_{p1_i} = 364$; $K_{d1_i} = -25$; $K_{p2_i} = 140$; and $K_{d2_i} = -23$ 83

Figure 5.8: Roll and yaw angles (θ_1 and θ_3), while utilizing the modified PD controller with the gains obtained from the linear controller: $K_{p1_i} = 364$; $K_{d1_i} = -25$; $K_{p2_i} = 140$; and $K_{d2_i} = -23$ 83

Figure 5.9: Control torque produced by the modified PD controller with the gains obtained from the linear controller: $K_{p1_i} = 364$; $K_{d1_i} = -25$; $K_{p2_i} = 140$; and $K_{d2_i} = -23$ 83

Figure 5.10: Angular velocity of the fluid, while using the modified PD controller with the gains obtained in the linear controller: $K_{p1_i} = 364$; $K_{d1_i} = -25$; $K_{p2_i} = 140$; and $K_{d2_i} = -23$ 84

Figure 5.11: Roll and yaw angles (θ_1 and θ_3), while using the modified PD controller with the gains of $K_{p1_i} = 350$; $K_{p2_i} = 140$; $K_{d1_1} = -25$; $K_{d2_1} = -5$; $K_{d1_2} = -5$; and $K_{d2_2} = -25$ 84

Figure 5.12: Control torque produced by the modified PD controller with the gains of $K_{p1_i} = 350$; $K_{p2_i} = 140$; $K_{d1_1} = -25$; $K_{d2_1} = -5$; $K_{d1_2} = -5$; and $K_{d2_2} = -25$. 85

Figure 5.13: : Angular velocity of the fluid, while using the modified PD controller with the gains of $K_{p1_i} = 350$; $K_{p2_i} = 140$; $K_{d1_1} = -25$; K_{d2_1} =−5; K_{d1_2}=−5; and $K_{d2_2} = -25$ 85

Figure 6.1: A satellite with two magnetic coils and one fluid ring 88

Figure 6.2: The control torque vector decomposition 89

Figure 6.3: The attitude angles of a satellite using two magnetic coils with PID gains $K_p = 50$, $K_d = 60$, and $K_i = 1$ 93

Figure 6.4: Torques produced in the satellite using only two magnetic coils with PID gains $K_p = 50$, $K_d = 60$, and $K_i = 1$: (a) Control torque; (b) Torque produced by the magnetic coils in the roll direction; (c) Torque produced by the magnetic coils in the pitch direction; (d) Torque produced by the magnetic coils in the yaw direction; (e) Magnetic dipole moments 94

Figure 6.5: The attitude angles of a satellite using two magnetic coils and one active fluid ring with PID gains $K_p = 70$, $K_d = 100$, and $K_i = 0$ 95

Figure 6.6: Torques produced in the satellite using two magnetic coils and one fluid ring with PID gains $K_p = 70$, $K_d = 100$, and $K_i = 0$: (a) Control torque; (b) Torque produced by the pump; (c) Fluid friction torque; (d) Torque produced by the magnetic coils; (e) Magnetic dipole moments 97

Figure 6.7: Attitude angles of the satellite in the case of failure of the fluid ring with PID gains $K_p = 60$, $K_d = 30$, and $K_i = 1$ 98

Figure 6.8: Torque produced in the satellite with the fluid ring failure with PID gains $K_p = 60$, $K_d = 30$, and $K_i = 1$: (a) Control torque; (b) Fluid friction torque; (c) Torque produced by the magnetic coils;(d) Magnetic dipole moments 100

Figure 6.9: Stabilization of attitude angles in the case of failure of the roll-axis magnetic coil with PID gains $K_p = 12$, $K_d = 2$, and $K_i = 0.01$ 101

Figure 6.10: The torque produced in the case of failure of the roll-axis coil with PID gains $K_p = 12$, $K_d = 2$, and $K_i = 0.01$: (a) Control torque; (b) Torque produced by the fluid ring; (c) Torque produced by the magnetic coils; (d) Magnetic dipole moment in the pitch direction 102

Figure 6.11: Stabilization of attitude angles in the case of failure of the pitch-axis coil with PID gains $K_p = 450$, $K_d = 15$, and $K_i = 0.01$ 103

Figure 6.12: Torques produced in the case of failure of the pitch-axis coil with PID gains $K_p = 450$, $K_d = 15$, and $K_i = 0.01$: (a) Control torque; (b) Torque produced by the fluid ring; (c) Magnetic dipole moment in the roll direction; (d) Torque produced by the magnetic coils 104

TABLE OF TABLES

Table 2.1: Stability condition of a satellite in a circular orbit 28

Table 2.2: Stability condition of a satellite in an elliptical orbit with the eccentricity of 0.05 28

Table 4.1: Fluid properties 50

Chapter 1

INTRODUCTION

1.1 Background

A satellite is required to maintain a specific orientation in order to complete its mission objectives, such as communication and imaging. However, the satellite attitude can be disturbed due to different natural sources, such as the Earth's gravity gradient, solar radiation pressure, aerodynamic forces, and the Earth's magnetic field. These disturbances usually cause rotational oscillations of the satellite, but at times they can cause the satellite to tumble. To avoid this, the design of any satellite should include an attitude stabilization scheme, which normally involves an attitude control subsystem.

Several methods of attitude stabilization of satellites have been developed over the last five decades, which can be divided into two groups: passive and active. The most fundamental passive method is *gravity gradient stabilization* (Wie, 1998). In this method, the principal axes of the satellite are required to be aligned with the local vertical and local horizontal (LVLH) reference frame whose origin is located at the center of mass of the satellite. The axes of maximum and

minimum moment of inertia should be aligned with the axes which are perpendicular to the orbital plane and directed to the center of the Earth. If this condition holds, the satellite attitude angles remain stable even in the presence of small perturbations (Wie, 1998).

Another passive stabilization method is to spin up a satellite about one of its principal axes. In fact, spinning causes the satellite to resist changing its attitude (Hughes, 1986). The reason behind is that the disturbance torques are not large enough to significantly change the direction of the bias angular momentum produced in the spinning direction.

Other passive methods involve energy dissipation, such as using liquid, magnetic, or nutation dampers to reduce the attitude variations. However, it should be pointed out that energy dissipation can sometimes be destabilizing. For instance, a satellite spinning about its axis of minimum moment of inertia can become unstable, if energy dissipation occurs (Leimanis, 1965; Hughes, 1986; and Fortescue and Stark, 1995).

There are some drawbacks in relying on passive methods as the primary techniques of attitude stabilization, such as their slow action and their lack of ability for tracking desired attitude. Therefore, passive methods are often utilized only to improve the performance of active methods. In fact, the focus of research on satellite attitude dynamics and control is generally on the active alternatives; hence, a literature survey on these methods is in order.

1.1.1. Reaction/Momentum Wheels

Reaction wheels, momentum wheels, or control moment gyros are the most common attitude actuators utilized in satellites. A reaction wheel has zero initial angular velocity; a resistant torque can be produced by accelerating or decelerating the rotation of the wheel. Momentum wheels are the counterpart of reaction wheels; they have a non-zero initial angular velocity, by changing which the magnitude of the resistance torque can be controlled[1] (Schaub and Junkins, 2003). Figure 1.1 shows a reaction/momentum wheel.

There are some drawbacks associated with reaction and momentum wheels, such as their relatively small capacity to produce torque and also the saturation problem (Wie, 1998). The

[1] Although control moment gyros are modifications of simple momentum wheels, they are considered here as another type of attitude control actuators and will be discussed later.

latter implies that the wheel cannot speed up any further so as to produce larger torques; in fact, the saturation occurs because of various restrictions, such as motor maximum capability, bearing friction, and maximum voltage available. Despite the abovementioned disadvantages, due to their simple functionality and control, these actuators are commonly used in the space industry. Extensive research has been conducted on reaction/momentum wheels so as to minimize their energy consumption and improve their performance (Kaplan, 1976; Barba and Aurbrun, 1976; Hablani, 1994; Tsiotras et al. 2001; Richie and Lappas, 2007; Zhang et al. 2009; Navabi and Nasiri, 2010; Ye et al. 2011).

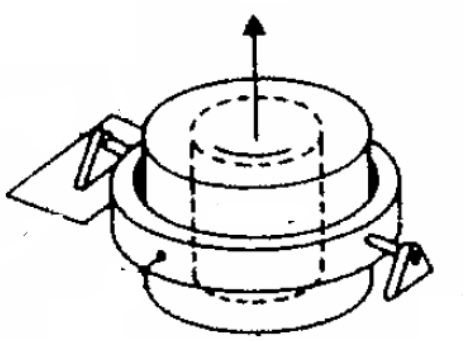

Figure 1.1: A reaction/momentum wheel (Wertz, 1999)

Optimization of the configuration of a set of reaction/momentum wheels used in a satellite is also a subject of interest. Recently, Ismail and Varatharajoo (2010) examined different configurations of reaction wheels in a satellite in order to find the optimum configuration based on the power consumption and the momentum produced. They proposed 11 different structures with three reaction wheels, for which the dynamical models were developed and PD controllers were designed. The same procedure was followed for four reaction wheels in eight different configurations. The results showed that there is no significant difference in the momentum produced in various cases, the minimum total torque level also varying only slightly. It was shown that the pyramidal configuration of four reaction wheels is neither an optimum nor the worst case. However, the pyramidal configuration is used in several research articles (Marshall et al. 1991; Hablani, 1994; Lee et al. 2009; Li and Kumar 2011), the reason for this selection being the symmetry of the system that proves helpful in the case of failure of a control actuator.

Due to its high importance, the failure analysis of control actuators is thoroughly discussed in the literature (Vadali and Junkins, 1984; Hablani, 1994; Battagliere et al. 2010; Haga and Saleh

2011; Horri and Palmer, 2012). For instance, Godard et al. (2010) studied this problem by considering a redundant set of four reaction wheels in a satellite. In their model, they also considered saturation of the reaction wheels, external disturbance torques, and model uncertainties. To control the satellite in the case of failure of one reaction wheel, they designed an adaptive controller. The results were validated with a hardware-in-the-loop simulation, which proved the robustness of the control algorithm proposed.

1.1.2. Control Moment Gyros

Control moment gyros (CMGs) are the momentum wheels with the capability of rotating about two axes: the axis of symmetry and an axis orthogonal to the former. In this type of actuators, the spinning rate of the wheel is fixed, the effective torque being produced via rotating the wheel about the second axis, called the gimbal axis (Schaub and Junkins, 2003). This operation allows producing quite large torques, which makes CMGs the most desirable choice in agile space systems. The most significant disadvantage of CMGs is that they have singularities at certain gimbal angles which are perpendicular to the plane of the allowable torques (Figure 1.2). At the singularities, CMGs cannot produce the torque required, despite consuming more energy. Different control strategies have been proposed to avoid these singularities or, at least, handle them efficiently (Kennel, 1970; Li and Bainum, 1990; Krishnan and Vadali, 1996; Kurokawa, 1997; McMahon and Schaub 2010; Leeghim and Park 2009; Lappas and Wie 2009; Akiyama 2010). For example, Sands et al. (2009) developed a decoupled control strategy to solve the singularity problem of CMGs. The theoretical results were verified by an experiment in which the simulator test bed allows for a free-floating satellite. As an alternative solution, Nanamori et al. (2008) suggested using a geometric method to solve the singularity problem. In this method, the initial gimbal angles were chosen by an optimization algorithm, so as to reduce the possibility of falling into singularities in the operation range of the CMGs.

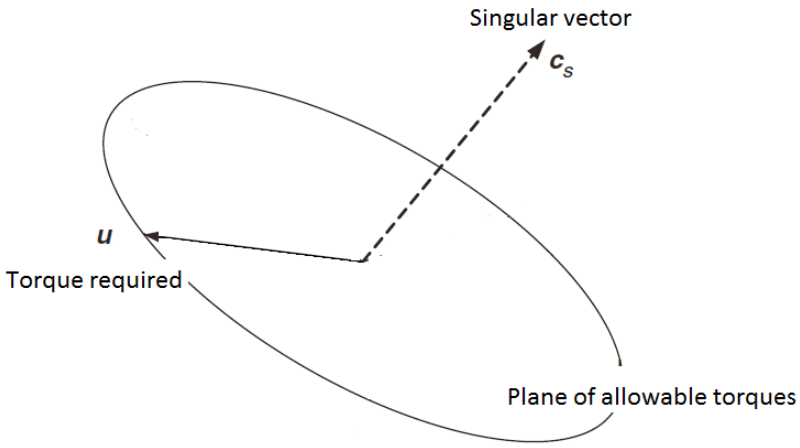

Figure 1.2: Singular configuration of CMGs (Leeghim et al. 2009)

A few researchers have suggested using double-gimbal CMGs to avoid singularities (Wie, 1998; Ahmed and Bernstein, 2002; Bolandi et al., 2006), a solution that is more costly and complex for the dynamical modeling view point(Wie, 1998). McMahon and Schaub (2010), Richie and Lappas (2007), and Jin and Hwang (2011) have designed variable-speed control moment gyroscopes to produce the exact effective torque required at the cost of increasing the difficulty of dynamical modelling and controller design.

1.1.3. Micro-thrusters

Micro-thrusters are another type of attitude actuators, which are of considerable importance for their low modeling complexity. For more than four decades, these actuators have been utilized in various types of satellites (Kazinczy and Leibing, 1975; Stenmark and Lang, 1997), such as spinning satellites (Jiang et al. 2008; Raus et al. 2010; Ayoubi and Longuski 2009). For instance, recently, Tang et al. (2011) used micro-thruster actuators in a small spinning satellite for the three-dimensional attitude control. The authors suggested a dual-phase fuel thruster, which is composed of compressed cold-gas and liquid nitrogen. Srikant and Akella (2010) used cold-gas proportional thrusters for the control of attitude motion of a satellite. Micro-thrusters can also be augmented by other types of attitude actuators; as an example, Liu et al. (2010) suggested a combination of thrusters and a single-pitch bias momentum wheel for attitude control.

1.1.4. Magnetic Torque Rod Actuators

The Earth's magnetic field was introduced earlier in this chapter as a source of environmental disturbance. On the other hand, this effect has been used for satellite attitude stabilization for more than four decades (Steyn, 1994; Maeda et al., 1997; Sun et al., 2003; Hur-Diaz et al. 2008; Forbes and Damaren 2010; Kataoka and Kawai 2010; Kim et al. 2011). A magnetic torque rod, also known as magnetic torquer, is an actuator (Figure 1.3), which produces torque by interacting with the Earth's magnetic field.

Figure 1.3: Magnetic torquer designed by Vectronic Aerospace

Indeed, a magnetic torquer is a rod core wrapped by an electric conductor. In the presence of a magnetic field and electric current in the wire, a torque is produced. The simple functionality, low mass, and low energy consumption have made magnetic torquers quite popular for applications in small satellites (Steyn, 1994; Maeda et al., 1997; Sun et al., 2003).

The drawback of magnetic torquers is that they cannot produce torque in the direction of the geomagnetic field vector. Moreover, the estimation of the magnitude of the geomagnetic field vector is not accurate, something which reduces the accuracy of attitude stabilization. In the literature, the means of increasing the accuracy of magnetic torque rods and also producing torque in all directions have been investigated (Hur-Diaz et al. 2008; Forbes and Damaren 2010; De Ruiter 2011). For instance, De Ruiter (2011) studied a spinning satellite equipped with three magnetic torque rods mounted on three directions of roll, pitch, and yaw. The failure of one or two magnetic torquers was then handled by modifying the control law developed for the complete system. Das et al. (2010) studied the performance of three magnetic torquers in a small satellite. They also considered the case of failure of one magnetic torquer, for which a modified control law was designed. Wang et al. (2010) combined a passive stabilizer method, based on aerodynamics drag, with magnetic torquers to control the satellite attitude angles. To exploit the

drag force in attitude stabilization, these researchers determined the appropriate position of the center of pressure and the centroid of a satellite. The results showed that this hybrid controller can asymptotically stabilize the attitude motion.

Chen et al. (2008), and Soyali and Jafarov (2011) compared the performance of two different actuator systems: a system including only magnetic torquers; another combining magnetic torquers with a bias momentum wheel. The results showed that the settling time and power consumption is lower, for the former case, while adding a bias momentum wheel can reduce the steady-state error. Further, Forbes and Damaren (2010) considered a combination of magnetic torquers and reaction wheels as control actuators for attitude stabilization. They calculated the torque to be produced by different components via decomposing the control torque: the component of the control torque parallel to the Earth's magnetic field vector is produced by reaction wheels, the rest by the magnetic torquers. They studied the cases of using one, two, and three reaction wheels. The results are significant, especially in the case of saturation of the reaction wheels.

1.2. Motivation

As mentioned in Section 1.1, several methods of attitude stabilization, passive or active, have been developed so far. Among various active methods, wheels, being currently the most popular type, are typically used either as reaction/momentum wheels or CMGs. The downside of reaction wheels is that they do not produce a large torque to mass ratio. The CMGs are much better in this regard, their main drawback being the existence of singularities at some gimbal angles. These shortcomings of the CMGs and reaction wheels motivated us to seek an alternative attitude control actuator. An ideal solution should compete with the CMGs in terms of the torque to mass ratio, without introducing any singularity.

Fluidic-based attitude actuators, originally utilized as passive controllers in spacecraft, have recently been proposed as promising attitude control actuator by Kumar (2009). In this type of actuator, fluid is circulated inside a ring, henceforth referred to as a *fluid ring*, as shown in Figure 1.4. The principle of operation to produce the torque is similar to that of a reaction wheel with the difference that, for the fluid ring actuator, the distribution of the fluid ring mass is concentrated around the ring periphery, contrary to a reaction wheel whose mass distribution is quite uniform. Therefore, the moment of inertia of a fluid ring is expected to be larger than a reaction wheel with

the same mass; hence, in principle, for a certain angular acceleration, a fluid ring is likely to produce a larger torque compared to a reaction wheel.

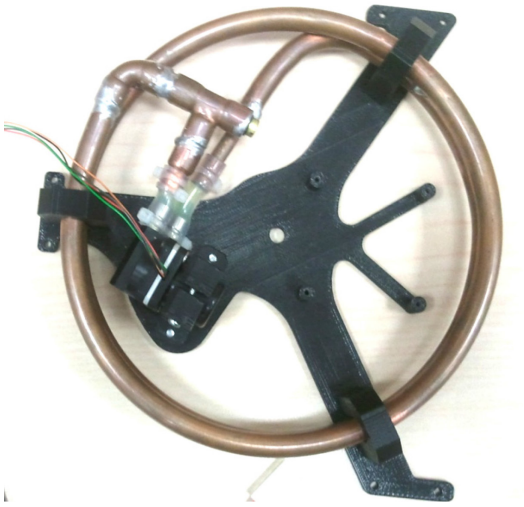

Figure 1.4: A fluid ring actuator (Patel and Kumar, 2009)

As nothing is perfect, fluid rings have their own drawbacks, namely, the complexity in modeling the fluid flow, fluid leakage, and several other challenges. Nevertheless, the promising potential of fluid rings to produce a quite large torque to mass ratio justifies an in-depth investigation of the feasibility analysis of utilizing this type of actuators.

1.3. Review of the Literature on Fluidic Actuators

The literature on fluidic actuation in attitude stabilization is not that extensive. The very early work on this concept was done by Maynard (1988). This author proposed a fluidic actuator to neutralize the disturbance torque exerted on spacecraft, ocean ships, and other suspended systems. In his invention, the author considered an actuation system consisting of two triangular and three rectangular loops, as shown in Figure 1.5. The loops can be equipped with reservoir(s) to control the flow of the fluid. Further, as an auxiliary advantage, the fluid inside the loops was expected to remove heat from spacecraft.

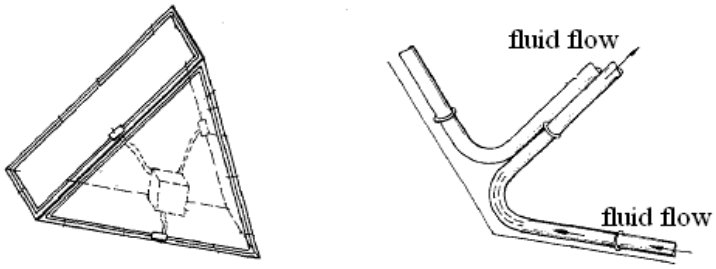

Figure 1.5: Fluidic actuator proposed by Maynard (1988)

The research on fluidic actuators was extended later by Iskenderian (1989), Lurie and Schier (1990), and Lurie et al. (1991). These researchers considered further detailes of the system, such as using pumps, and also hydraulic actuators and valves to control the fluid flow. Although the fluid loops can have any shape so as to fit into the available space in a satellite, to obtain the maximum torque possible, the fluid should flow at the largest feasible distance around the satellite. Accordingly, six different possible configurations of the fluid loops were proposed, three of which are illustrated in Figure 1.6. In Figure 1.6 (a), the fluid loops are attached to the satellite, like solar sails, on three orthogonal directions so as to be able to produce control torque in any arbitrary direction. Figure 1.6 (b) shows three orthogonal circular fluid loops with slightly different diameters around a satellite. A tetrahedral configuration of fluid loops is shown in Figure 1.6 (c).

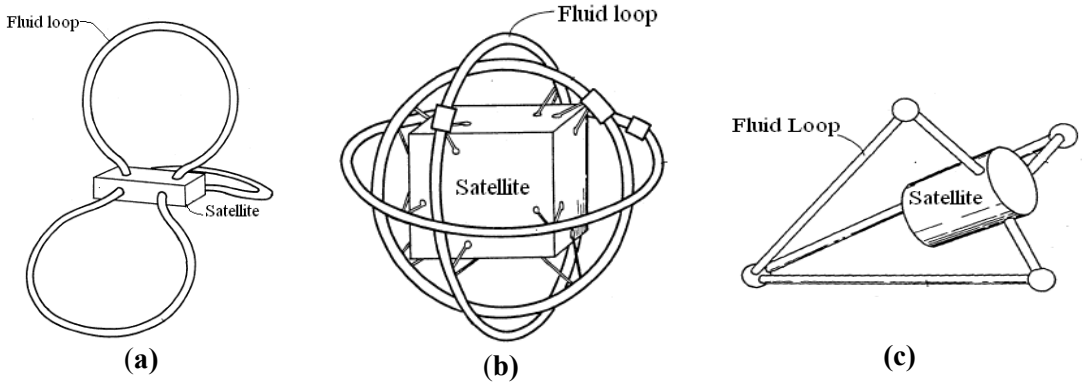

Figure 1.6: Fluid loop configurations proposed by Lurie et al. (1991)

In another study, Laughlin, et al. (2002) proposed a dual-function system to both measure the attitude angles of a satellite and generate a control torque. This system consists of a permanent magnet and a loop filled with a conductive fluid, as illustrated in Figure 1.7. The

satellite attitude motion causes the fluid to rotate in the loop. However, since the fluid is conductive and subject to a magnetic field, a voltage is produced that can be used to determine the satellite attitude angles. On the other hand, upon applying a voltage to the fluid, an electric field is produced, whose interaction with the permanent magnetic field produces the torque required, to stabilize the satellite attitude.

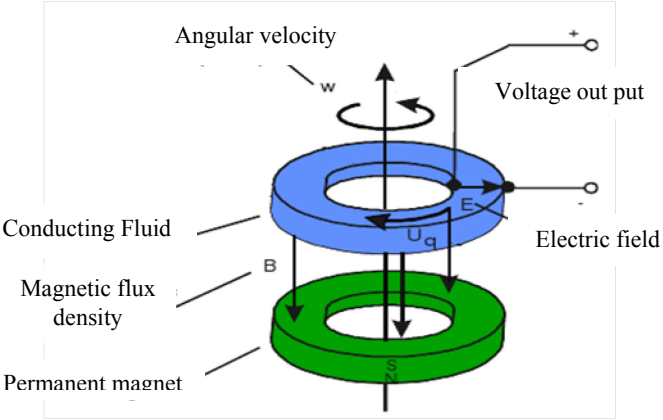

Figure 1.7: A dual-function actuator consisting of a fluid loop and a permanent magnet (Laughlin et al. 1991)

The aforementioned studies, although proposing fluidic actuators, deal only with the concepts and do not involve a rigorous feasibility analysis for real applications. In this regard, Kelly et al. (2004) tested the performance of a *fluidic momentum controller* (FMC) in an experimental setup with two fluid loops whose axes of symmetry are parallel. The experiment was conducted in *NASA's Reduced Gravity Student Flight Program*. A CAD model of the setup is shown in Figure 1.8.

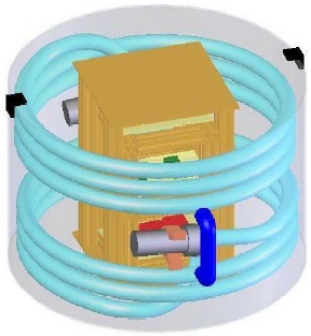

Figure 1.8: Fluid loop prototype used by Kelly et al. (2004)

Kumar (2009) also proposed a similar fluidic actuator. This actuator, called the *fluid ring*, is a circular loop filled with fluid. This author examined the three dimensional attitude control of a satellite with fluid rings mounted on three orthogonal axes. To study the attitude motion of this satellite, a dynamical model was developed; however this model does not include all reaction moments transferred between the satellite and the fluid rings. In fact, a complete dynamical analysis of a satellite with fluid rings has not been performed yet. The failure of a fluid ring leaves it as a damper in the system, which may cause instability due to energy dissipation. Despite its significance, to the best knowledge of the author, a detailed analysis of the feasibility of using fluid rings as attitude actuators as well as their failure analysis has not been reported in the literature.

1.4. Objectives of the Thesis

The main goal of the thesis is to report the results of a rigorous feasibility analysis of fluid ring actuators. In this regard, the objectives of this research can be listed as follows:

i. Dynamic analysis to investigate the feasibility of using fluid rings as attitude control actuators.
ii. Conducting experiments to verify the validity of the model developed.
iii. Exploring the feasibility of using fluid ring actuators in various scenarios, such as in a spinning satellite or in conjunction with magnetic torquers.

1.5. Thesis Organization

The overall goal of this research, as mentioned above, is first to investigate the feasibility of using fluid rings as attitude control actuators; second, to find possible solutions to their drawbacks. An additional goal is to conduct experiments to verify the theoretical results.

This thesis is organized into seven chapters:

In Chapter 1, the motivation behind this study was discussed; a review of the literature was also presented.

In Chapter 2, the dynamical models of a satellite with three orthogonal and four fluid rings in a pyramidal configuration are developed. The damping effect of the fluid rings on the satellite behaviour is also accounted for.

A PID controller is designed to stabilize the satellite attitude motion in Chapter 3. Here, the case of failure of a fluid ring is also examined. To cope with the uncertainties in the system model, the PID controller is then replaced by a sliding mode controller to add robustness to the system behavior.

Chapter 4 outlines the procedure followed to build an experimental setup. The results of the numerical simulations are then compared to those from experiments.

Experimental results obtained in Chapter 4 suggest the application of fluid rings where a relatively low control torque is required. Hence, in Chapter 5, a spinning satellite is considered to carry two fluid rings as auxiliary attitude actuators. The dynamical model of this system is obtained; a controller is then designed to stabilize the attitude angles.

In Chapter 6, the feasibility of using a fluid ring along with magnetic torque rod actuators is explored. Modeling the dynamics of the system, a controller is then designed and implemented to check the validity of the idea.

The thesis closes with the summary and concluding remarks in Chapter 7; directions for future research are also recommended.

Chapter 2

ATTITUDE DYNAMICS OF A RIGID SATELLITE WITH FLUID RINGS

In this chapter, the dynamical model of a satellite with a set of fluid rings is developed. Two different cases are examined: three orthogonal fluid rings; and four fluid rings in a pyramidal configuration. The dynamical model of a rigid satellite including three fluid rings is developed to analyze the feasibility of using fluid rings as attitude control actuators. The results obtained from this model will be used later in Chapter 4 in the three dimensional control experiments. Using four fluid rings in the pyramidal configuration in a satellite provides a redundant set of actuators for the system. The passive performance of this system as well as the effects of varying the pyramidal configuration angle are studied in this chapter.

2.2 Dynamical Model of a Rigid Satellite with Fluid Rings

The system considered consists of a satellite with three or four fluid rings, as depicted in Figures 2.1 and 2.2. In the model developed, it is assumed that the center of mass of each of the fluid rings coincides with that of the satellite. A local vertical and local horizontal (LVLH)

reference frame, with its origin located at the center of mass of the satellite, is defined such that (Wie, 1998): X_0 is along the local horizontal; Y_0 is perpendicular to the orbital plane in which the satellite travels; and Z_0 is directed towards the center of the Earth; this is illustrated in Figure 2.3(a). In the equilibrium configuration, the principal axes of the satellite, X, Y, and Z axes, are aligned with the LVLH reference frame. The instantaneous orientation of the satellite is described relative to the LVLH frame by three rotation angles θ_1, θ_2, and θ_3 about X, Y, and Z axes of the body frame[1], respectively.

Before proceeding, let us recall the notation convention that is used throughout the whole thesis: vectors are denoted by boldface lower case, matrices by boldface upper case letters.

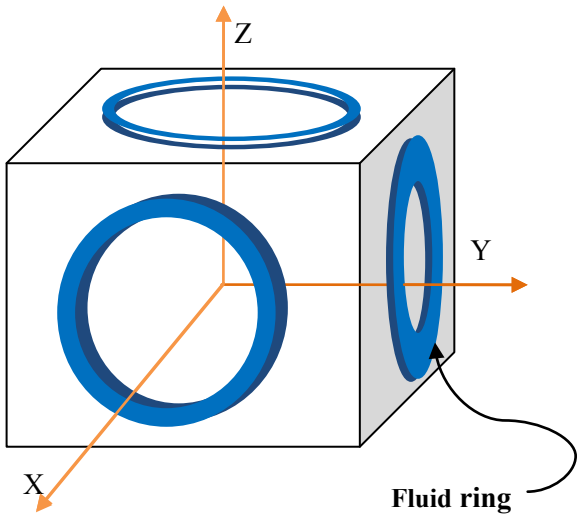

Figure 2.1: A satellite with three orthogonal fluid rings

To derive the equations governing the attitude motion of the satellite in question, the Euler equations are used. Generally speaking, the Euler equation governing the rotational motion of a rigid body is

$$\boldsymbol{I_r\dot{\omega} + \omega \times I_r\omega = \tau_{ext}} \tag{2.1}$$

For the sake of numerical calculation, in Eq. (2.1), the absolute angular velocity $\boldsymbol{\omega}$ and the absolute angular acceleration $\boldsymbol{\dot{\omega}}$ are expressed in the body fixed frame, with the origin located

[1] Body frame refers to a reference frame that is attached to the satellite.

either at the center of mass or at a point with zero velocity. For a satellite, since there is no point of zero velocity, Eq. (2.1) is written assuming that the origin of the body fixed frame is located at the center of mass of the satellite. Further, $\boldsymbol{I_r}$ denotes the inertia matrix of the rigid body with respect to the same body fixed reference frame. The term $\boldsymbol{\tau_{ext}}$ is, in turn, the summation of all external applied torques about the origin of the reference frame.

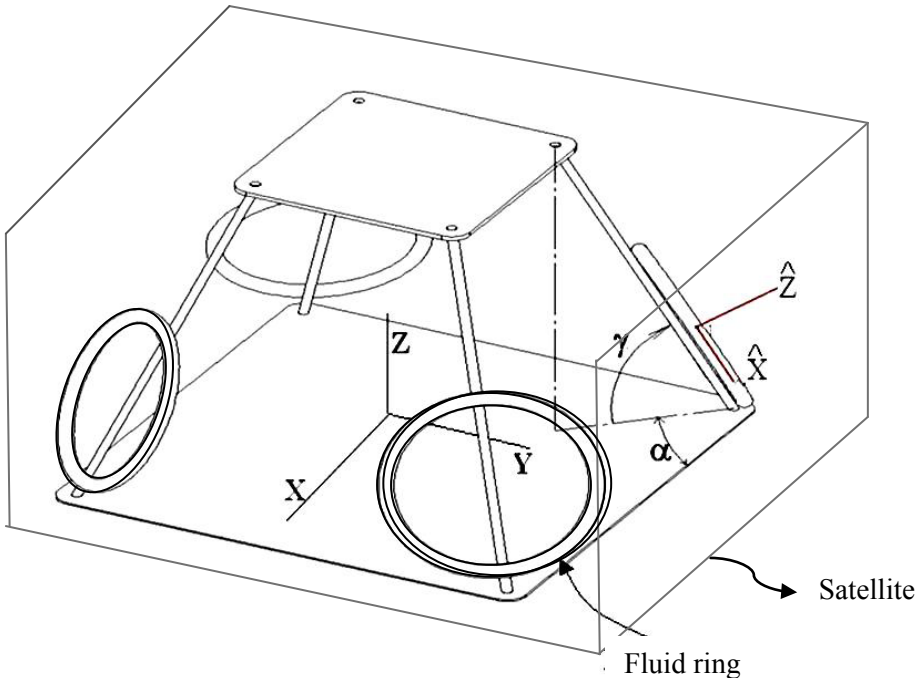

Figure 2.2: Pyramidal configuration of the fluid rings in a satellite

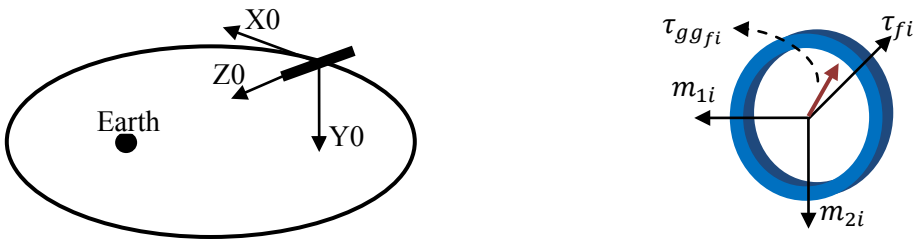

Figure 2.3: (a) LVLH reference frame of a satellite; (b) Free body diagram of a fluid ring

The models shown in Figures 2.1 and 2.2 consist of a rigid satellite and the fluid rings. Separating the satellite from the fluid rings, the equations of motion can be derived for each component; the free body diagram of a fluid ring is illustrated in Figure 2.3 (b). Further, the reaction moments transferred between the fluid rings and the satellite and the gravity gradient torque are external torque acting on both systems. Accordingly, the equations of attitude motion of the satellite, excluding the fluid rings, can be written as:

$$\boldsymbol{I_s\dot{\omega} + \omega \times I_s\omega = \tau_{gg} + \sum_{i=1}^{k} R_i\tau_{r_i}} \tag{2.2}$$

where k is either three or four depending on the number of the fluid rings. The term τ_{gg} is the gravity gradient torque given by $\tau_{gg} = (3n^2/\|r_c\|^2)r_c \times I_s.r_c$ (Wie, 1998), r_c beimg the position vector of the satellite with respect to the Earth; $\tau_{r_i} = [m_{1i} \quad m_{2i} \quad \tau_{fi}]^T$ is the moment vector exerted by the ith fluid ring on the satellite; m_{1i} and m_{2i}, shown in Figure 2.3 (b), are the reaction moments stemming from the detachment of the each fluid ring from the satellite in its free body diagram; τ_{fi} is the friction torque produced by the fluid viscosity, to be discussed later in this section. Further, $\boldsymbol{R_i}$ is the rotation matrix transforming the vectors from the body fixed frame of the ith fluid ring into that of the satellite. For a satellite with three orthogonal fluid rings, transformation matrices $\boldsymbol{R_i}$ for i=1,...,3 can be found as:

$$\boldsymbol{R_1 = C_z(0)C_{y'}(0), \qquad R_2 = C_z(\pi/2)C_{y'}(0), \qquad R_3 = C_z(0)C_{y'}(-\pi/2)} \tag{2.3}$$

where $\boldsymbol{C_j(\psi_i)}$ is a rotation matrix of the angle ψ_i about the j axis; for instance,

$$\boldsymbol{C}_z(\psi_1) = \begin{bmatrix} \cos(\psi_1) & \sin(\psi_1) & 0 \\ -\sin(\psi_1) & \cos(\psi_1) & 0 \\ 0 & 0 & 1 \end{bmatrix} \tag{2.4}$$

For a satellite with four fluid rings in a pyramidal configuration, $\boldsymbol{R_i}$ is

$$\boldsymbol{R_i = C_z(\alpha_i)C_{y'}(\gamma_i)} \tag{2.5}$$

where γ_i is the angle between the plane of the ith fluid ring and the base of the satellite, while α_i is the angle between the diagonal of the rectangular base and its edge; these angles are shown in Figure 2.2.

The equation of motion of the ith fluid ring in its body frame is found upon substituting appropriate values into Eq. (2.1) as:

$$\boldsymbol{I_{fi}\dot{\omega}_f + \omega_f \times I_{fi}\omega_f = \tau_{ext}} \tag{2.6}$$

where $\boldsymbol{I_{fi}}$ is the moment of inertia of the ith fluid ring with respect to its body fixed frame. For the sake of simplicity, it is assumed that the axes of the body fixed frames of the satellite and the fluid rings coincide with the principal inertia axes. Therefore, $\boldsymbol{I_{fi}}$ is a diagonal matrix whose diagonal entries are

$$\begin{aligned} I_{x_i} = I_{y_i} &= \pi\rho A r^3 \\ I_{z_i} &= 2\pi\rho A r^3 \end{aligned} \tag{2.7}$$

where ρ is the fluid density, A and r are the cross-sectional area and the radius of the fluid ring, respectively.

Furthermore, in Eq. (2.6), $\boldsymbol{\tau_{ext} = -\tau_{r_i} + R_i^T \tau_{gg_{fi}}}$, where $\boldsymbol{\tau_{gg_{fi}}}$ is the gravity gradient torque exerted on the ith fluid ring. Having $\boldsymbol{\tau_{gg_{fi}}}$ in the body fixed frame of the satellite, the rotation matrix $\boldsymbol{R_i^T}$ is used to find the coordinates of $\boldsymbol{\tau_{gg_{fi}}}$ in the body fixed frame of the fluid ring. In Eq. (2.6), the angular velocity of the fluid $\boldsymbol{\omega_f}$ is

$$\boldsymbol{\omega_f = R_i^T \omega + \dot{\beta}_i} \tag{2.8}$$

where $\boldsymbol{\dot{\beta}_i} = [0 \quad 0 \quad \dot{\beta}_i]^T$, with $\dot{\beta}_i$ denoting the relative angular velocity of the fluid inside the ith loop with respect to the satellite. Again, in Eq. (2.8), the rotation matrix $\boldsymbol{R_i^T}$ transforms the angular velocity of the satellite $\boldsymbol{\omega}$ from its body frame to that of the fluid ring. The angular acceleration of the fluid is found upon obtaining the derivative of the fluid angular velocity with respect to time:

$$\boldsymbol{\dot{\omega}_f = R_i^T \dot{\omega} + \ddot{\beta}_i + R_i^T \omega \times \dot{\beta}_i} \tag{2.9}$$

Substituting Eqs. (2.8) and (2.9) into Eq. (2.6), the equation of motion of the ith fluid ring is obtained as:

$$\boldsymbol{I_{fi}}\left(\boldsymbol{R_i^T}\dot{\boldsymbol{\omega}} + \ddot{\boldsymbol{\beta}}_{\boldsymbol{i}} + \boldsymbol{R_i^T}\boldsymbol{\omega} \times \dot{\boldsymbol{\beta}}_{\boldsymbol{i}}\right) + \boldsymbol{R_i^T}\boldsymbol{\omega} \times \boldsymbol{I_{fi}}\left(\boldsymbol{R_i^T}\boldsymbol{\omega} + \dot{\boldsymbol{\beta}}_{\boldsymbol{i}}\right) = -\boldsymbol{\tau_{r_i}} + \boldsymbol{R_i^T}\boldsymbol{\tau_{gg_{fi}}} \tag{2.10}$$

Let us recall that, in Eq. (2.2), $\boldsymbol{\tau_{r_i}} = [m_{1i} \quad m_{2i} \quad \tau_{fi}]^T$. The reaction moments m_{1i} and m_{2i} can be found from Eq. (2.10) as:

$$m_{1i} = -\boldsymbol{e_1^T}\{\boldsymbol{I_{fi}}\left(\boldsymbol{R_i^T}\dot{\boldsymbol{\omega}} + \ddot{\boldsymbol{\beta}}_{\boldsymbol{i}} + \boldsymbol{R_i^T}\boldsymbol{\omega} \times \dot{\boldsymbol{\beta}}_{\boldsymbol{i}}\right) + \boldsymbol{R_i^T}\boldsymbol{\omega} \times \boldsymbol{I_{fi}}\left(\boldsymbol{R_i^T}\boldsymbol{\omega} + \dot{\boldsymbol{\beta}}_{\boldsymbol{i}}\right) - \boldsymbol{R_i^T}\boldsymbol{\tau_{gg_{fi}}}\} \tag{2.11}$$

$$m_{2i} = -\boldsymbol{e_2^T}\{\boldsymbol{I_{fi}}\left(\boldsymbol{R_i^T}\dot{\boldsymbol{\omega}} + \ddot{\boldsymbol{\beta}}_{\boldsymbol{i}} + \boldsymbol{R_i^T}\boldsymbol{\omega} \times \dot{\boldsymbol{\beta}}_{\boldsymbol{i}}\right) + \boldsymbol{R_i^T}\boldsymbol{\omega} \times \boldsymbol{I_{fi}}\left(\boldsymbol{R_i^T}\boldsymbol{\omega} + \dot{\boldsymbol{\beta}}_{\boldsymbol{i}}\right) - \boldsymbol{R_i^T}\boldsymbol{\tau_{gg_{fi}}}\} \tag{2.12}$$

where $\boldsymbol{e_1} = [1 \quad 0 \quad 0]^T$, and $\boldsymbol{e_2} = [0 \quad 1 \quad 0]^T$. Since $\boldsymbol{e_j^T}\ddot{\boldsymbol{\beta}}_{\boldsymbol{i}}$ for $j = 1,2$ and $i = 1, \ldots, 4$ vanishes identically, upon replacing m_{1i} and m_{2i} in Eq. (2.2) from the relations (2.11) and (2.12), the equations of motion of the satellite can be obtained free of the fluid angular acceleration terms. The equations thus resulting can then be solved by a stable numerical integrator.

Prior to proceeding with the numerical solution of the equations obtained, it is necessary to obtain an expression for the fluid friction torque τ_f. This torque is produced by the shear stress resulting from the motion of the fluid relative to the ring. In fact, the shear stress σ can be calculated from the below equation (Kumar, 2009):

$$\sigma = \frac{1}{8} f \rho r^2 \dot{\beta}^2 \tag{2.13}$$

where f is the friction coefficient, to be introduced hereafter. The flow in the ring can be either laminar or turbulent. In the case of laminar flow (the Reynolds number R_n of less than 2300), the friction coefficient can be found as (Shames, 1992):

$$f = 64/R_n \tag{2.14}$$

On the other hand, for a turbulent flow, the friction coefficient can be obtained as:

$$f = 0.3164 R_n^{-1/4} \tag{2.15}$$

The friction torque τ_f is now calculated by integrating the shear stress over the wetted area of the loop multiplied by its moment arm:

$$\tau_f = sgn(\dot{\beta})2\pi^2\sigma r^2 d = 16\pi^2 r^3 \mu\dot{\beta} \tag{2.16}$$

where μ is the viscosity of the fluid. In obtaining Eq. (2.16), it is assumed that the cross-sectional diameter of the fluid ring d is much smaller than the radius r of the ring itself.

Before proceeding to numerically solve Eq. (2.2), a relation between the angular velocity $\boldsymbol{\omega}$ of the satellite and $\dot{\theta}_1$, $\dot{\theta}_2$, and $\dot{\theta}_3$ denoting the roll, pitch, and yaw angular rates is required. From the kinematics of the rotational motion of the satellite, the relation sought is obtained in vector form as (Schaub and Junkins, 2003):

$$\begin{bmatrix}\dot{\theta}_1\\ \dot{\theta}_2\\ \dot{\theta}_3\end{bmatrix} = \frac{1}{c\theta_2}\begin{bmatrix}c\theta_2 & s\theta_1 s\theta_2 & c\theta_1 s\theta_2\\ 0 & c\theta_1 c\theta_2 & -s\theta_1 c\theta_2\\ 0 & s\theta_1 & c\theta_1\end{bmatrix}\begin{bmatrix}\omega_1\\ \omega_2\\ \omega_3\end{bmatrix} + \frac{\dot{\Theta}}{c\theta_2}\begin{bmatrix}s\theta_3\\ c\theta_2 c\theta_3\\ s\theta_2 s\theta_3\end{bmatrix} \tag{2.17}$$

where $c\theta_i$ and $s\theta_i$ denote $\cos\theta_i$ and $\sin\theta_i$, respectively. Further, the orbital rate $\dot{\Theta}$ is given by (Wie, 1998):

$$\dot{\Theta} = \frac{n[1 + ecos(\Theta)]^2}{(1 - e^2)^{\frac{3}{2}}} \tag{2.18}$$

where n is the mean orbital rate and e is the eccentricity of an orbit.

2.1.1. Non-dimensionalization of the equations of motion

To enhance the applicability of the results and to reduce the numerical errors, the equations of motions obtained in the foregoing section are converted to non-dimensional form. To this end, a new time variable T is defined as:

$$T \equiv nt \tag{2.19}$$

The non-dimensional angular velocity terms are also defined as per the relations below:

$$\hat{\omega} \equiv \frac{\omega}{n}, \qquad \beta_i' \equiv \frac{\dot{\beta}_i}{n}, \qquad \theta' \equiv \frac{\dot{\theta}}{n}, \quad \Theta' \equiv \frac{[1 + ecos(\Theta)]^2}{(1 - e^2)^{\frac{3}{2}}} \tag{2.20}$$

The equations of motion of the satellite and the fluid rings can now be expressed in terms of the non-dimensional variables as:

$$\hat{\boldsymbol{I}}_s \hat{\boldsymbol{\omega}}' + \hat{\boldsymbol{\omega}} \times \hat{\boldsymbol{I}}_s \hat{\boldsymbol{\omega}} = \hat{\boldsymbol{\tau}}_{gg} + \sum_{i=1}^{k} \boldsymbol{R}_i \hat{\boldsymbol{\tau}}_{\boldsymbol{r}_i}, \quad \text{for } k = 3 \text{ and } 4 \tag{2.21}$$

$$\hat{\boldsymbol{I}}_{fi}\left(\boldsymbol{R}_i^T \hat{\boldsymbol{\omega}}' + \boldsymbol{\beta}_i'' + \boldsymbol{R}_i^T \hat{\boldsymbol{\omega}} \times \boldsymbol{\beta}_i'\right) + \boldsymbol{R}_i^T \hat{\boldsymbol{\omega}} \times \hat{\boldsymbol{I}}_{fi}\left(\boldsymbol{R}_i^T \hat{\boldsymbol{\omega}} + \boldsymbol{\beta}_i'\right) = \boldsymbol{R}_i^T \hat{\boldsymbol{\tau}}_{gg_{fi}} - \hat{\boldsymbol{\tau}}_{\boldsymbol{r}_i}, \quad \text{for } i = 1, \ldots, 4 \tag{2.22}$$

where $\hat{\boldsymbol{I}}_{\boldsymbol{s}}$ and $\hat{\boldsymbol{I}}_{fi}$ are the non-dimensional inertia matrices of the satellite and the fluid ring:

$$\hat{\boldsymbol{I}}_{\mathbf{s}} = \begin{bmatrix} k_1 & 0 & 0 \\ 0 & 1 & 0 \\ 0 & 0 & k_3 \end{bmatrix}, \qquad \hat{\boldsymbol{I}}_{\boldsymbol{fi}} = \begin{bmatrix} k_{xi} & 0 & 0 \\ 0 & k_{yi} & 0 \\ 0 & 0 & k_{zi} \end{bmatrix} \tag{2.23}$$

Here, k_1, k_3, and k_{ji} are non-dimensional inertia ratios, as defined below:

$$\begin{gathered} k_1 \equiv \frac{I_{xx}}{I_{yy}}, \qquad k_3 \equiv \frac{I_{zz}}{I_{yy}} \\ k_{zi} \equiv \frac{I_{zi}}{I_{yy}} = \frac{\pi}{2} a_1 \hat{d}^2, \qquad k_{xi} = k_{yi} \equiv \frac{\pi}{4} a_1 \hat{d}^2 \end{gathered} \tag{2.24}$$

where I_{xx}, I_{yy}, and I_{zz} are the diagonal entries of the satellite inertia matrix. Further, $\hat{d}$ and a_1 are the non-dimensional geometrical and physical parameters associated with the fluid rings:

$$\hat{d} \equiv d/r, \qquad a_1 \equiv (\rho \pi r^5)/I_{yy} \tag{2.25}$$

Also, $\hat{\tau}_{fi}$ is the non-dimensional fluid friction torque, which is given by:

$$\hat{\tau}_{fi} = -16\, \pi\, a_1 a_2 \hat{d} \beta_i' \tag{2.26}$$

where $a_2 = \mu/(\rho r n D)$.

2.3 Numerical Results with Passive Fluid Rings

In this section, a $100\,kg$ satellite with the shape of a rectangular prism is considered for numerical simulations. The length, width and height of the satellite are assumed to be $1\,m$, $1.5\,m$, and $0.8\,m$, respectively. Further, four identical fluid rings of radius $0.2\,m$ with the cross-sectional diameter of $0.02\,m$ are considered to be mounted on the satellite. The principal moments of inertia of this satellite about its center of mass are $I_{xx} = 24.08\,kgm^2$, $I_{yy} = 27.08\,kgm^2$, and $I_{zz} = 13.67\,kgm^2$; the dimensions of the satellite, and hence, the moments of inertia obtained lead to a gravity gradient stabilized satellite. The satellite is assumed to be located in an orbit with the semi-major axis of $7000\,km$ (altitude of $622\,km$). The initial attitude angles, attitude angular rates, and relative angular velocity of the fluid in the fluid rings are chosen as $\pi/36$ rad, 10^{-4} rad/s, and zero, respectively. To investigate the performance of the fluid rings as dampers, the equations of motion developed are solved using the Runge-Kutta method.

In order to highlight the damping effect of fluid rings on the attitude motion of satellites, first, the plots of the satellite attitude without fluid rings in the circular and elliptical orbit are demonstrated in Figures 2.4 and 2.5, respectively. As can be seen, the attitude motion of the satellite travelling in the circular orbit is stable, but not asymptotically. In an elliptical orbit, again, the pitch motion is stable, however not asymptotically, while the roll and yaw motions are not stable at all.

Figure 2.6 shows the dynamical behaviour of the satellite with four fluid rings in a pyramidal configuration with $\gamma = 60°$, and $\alpha = 45°$. It can be observed that the satellite attitude is asymptotically stabilized in the roll, pitch, and yaw directions while using fluid rings only passively. However, the satellite attitude angles are reduced by approximately 50% of the initial value in the roll direction and 70% in the pitch and the yaw directions after 50 orbits. Hence, the damping effect is not fast enough, as the fluid friction torque is not sufficiently large.

Figure 2.7 corresponds to the same satellite moving in an elliptical orbit with the same value of the semi-major axis ($7000\,km$), but with the eccentricity of 0.05. As can be seen, the roll and yaw angles become asymptotically stable, while in the pitch direction the satellite attitude angle θ_2, although remains bounded, undergoes steady state oscillations about its equilibrium state. The

reason for the oscillation is a force term in the equation of motion of the system due to the orbit eccentricity; this force is related to the rate of change of the true anomaly[1] of the satellite.

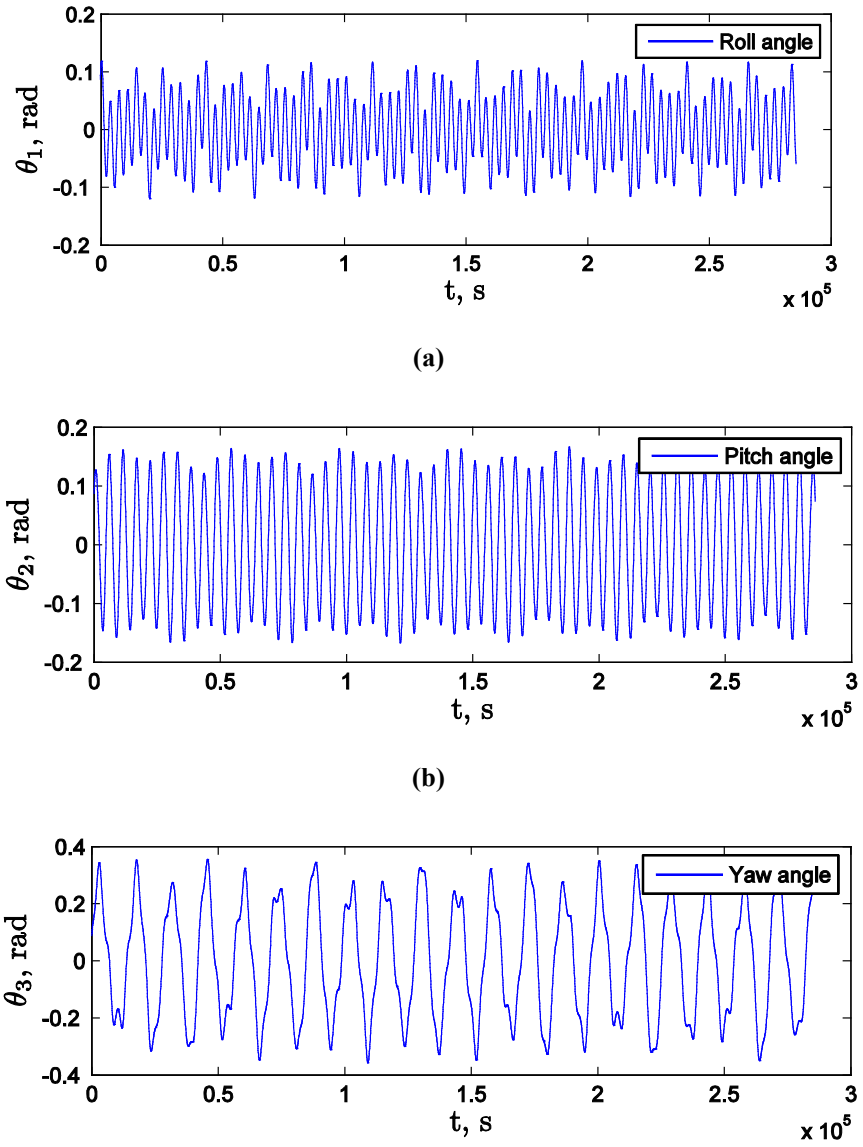

Figure 2.4: Attitude motion of the satellite in a circular orbit in the absence of damping torques: (a) Roll angle; (b) Pitch angle; (c) Yaw angle

[1] True anomaly is the angle between a satellite's radial vector and the perigee of the orbit (Schaub and Junkins, 2003).

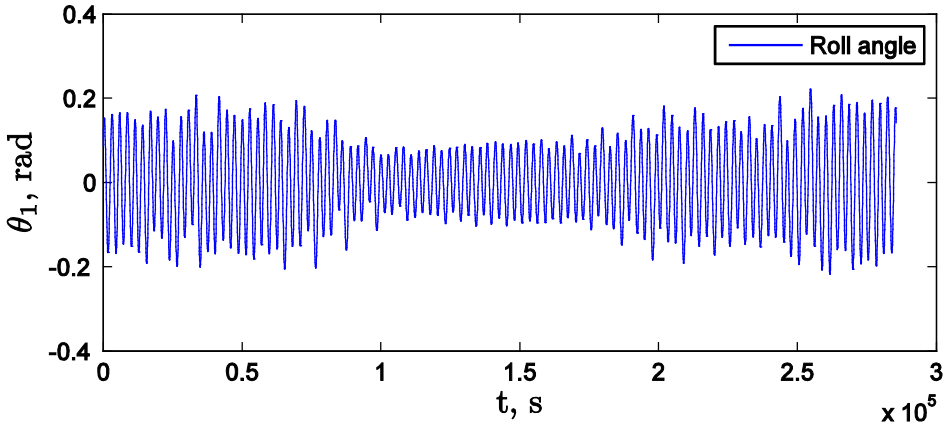

(a)

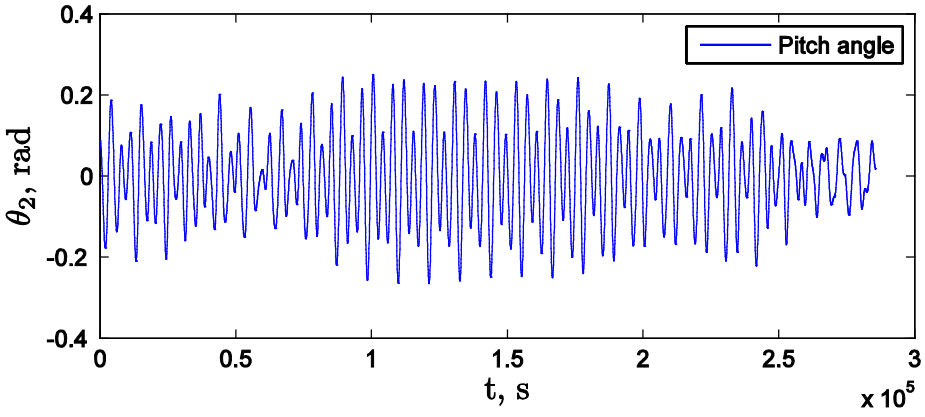

(b)

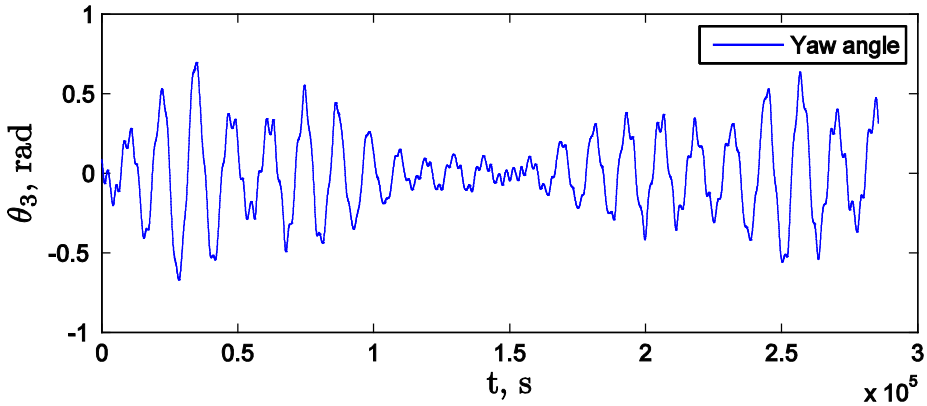

(c)

Figure 2.5: Attitude motion of a satellite in an elliptical orbit with the eccentricity of 0.05 **in the absence of damping torques: (a) Roll angle; (b) Pitch angle; (c) Yaw angle**

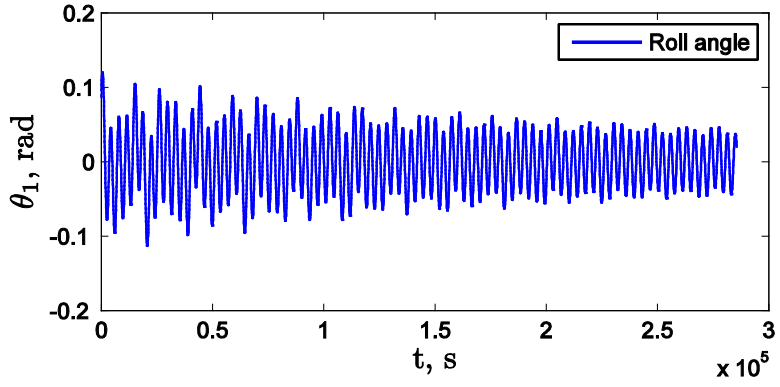

(a)

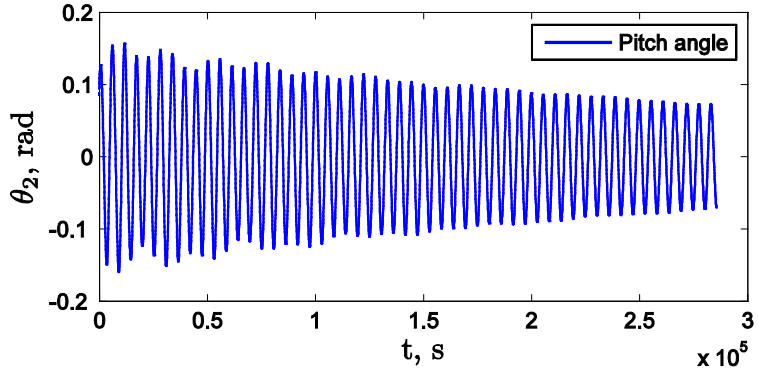

(b)

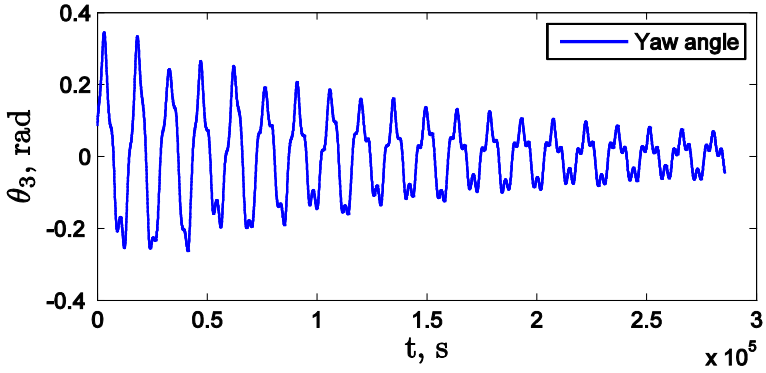

(c)

Figure 2.6: Attitude motion of the satellite in a circular orbit in the presence of damping torques of four fluid rings: (a) Roll angle; (b) Pitch angle; (c) Yaw angle

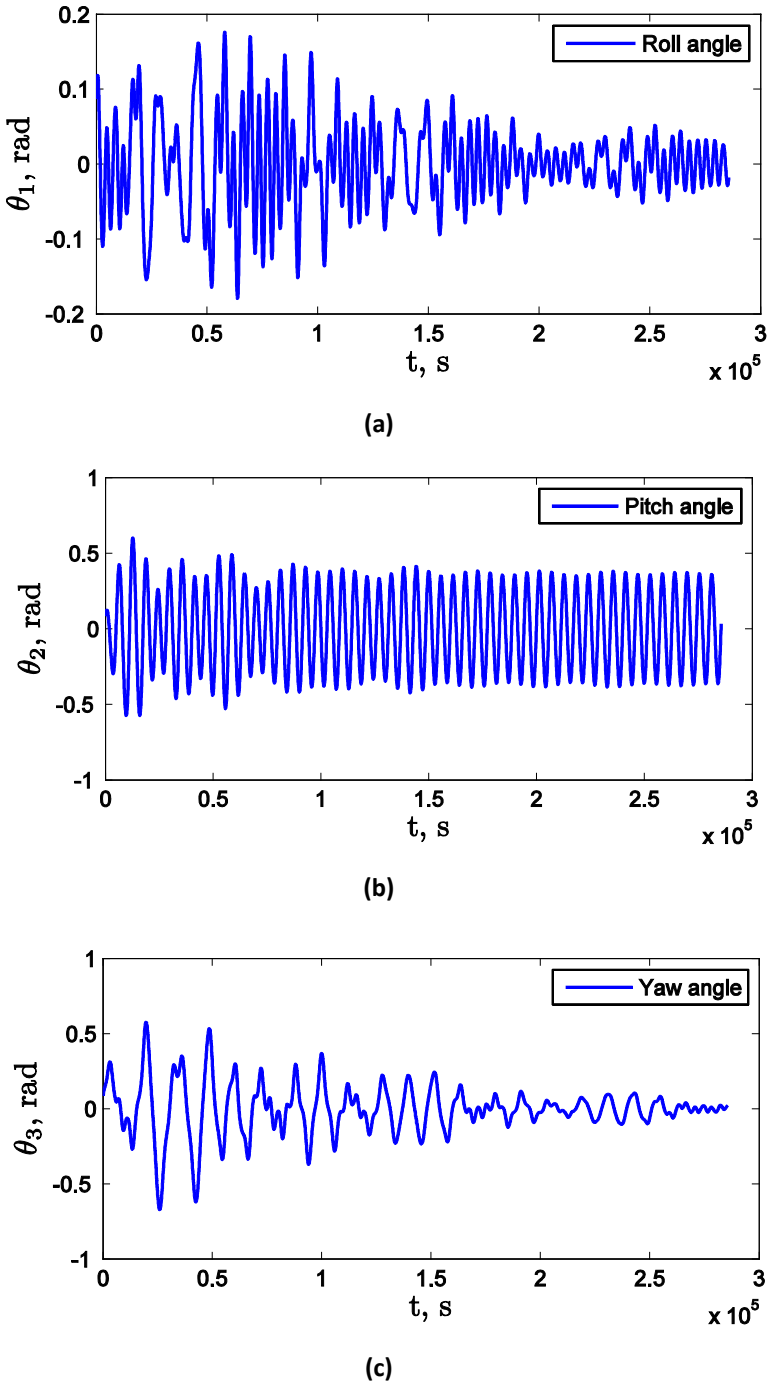

Figure 2.7: Attitude motion of a satellite in an elliptical orbit with the eccentricity of 0.05 **in the presence of damping torques of four fluid rings: (a) Roll angle; (b) Pitch angle; (c) Yaw angle**

The effect of the pyramidal configuration angles on the damping torque is investigated next. To this end, the angle γ is varied from a value slightly more than 0° to slightly less than 90°. Figures 2.6-2.8 correspond to the cases where the angle α is 45°, and the angle γ being chosen as

5°, 45°, and 85°. It can be seen that upon increasing the angle γ, a larger damping torque can be obtained. However, the damping effect is still not fast enough (the reduction of the satellite attitude angles is about 70% of their initial values in 50 orbits) even for large values of γ. Therefore, a controller is required for both circular and elliptical cases.

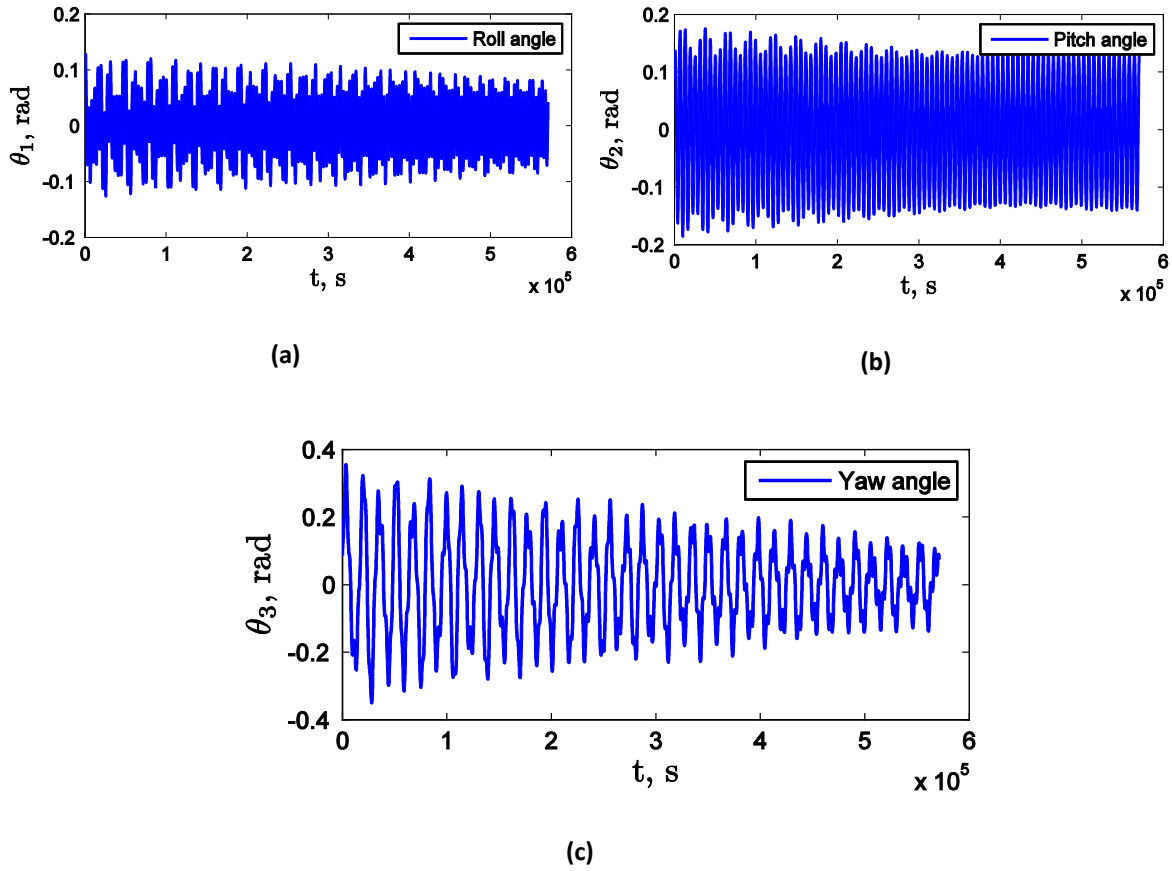

Figure 2.8: Attitude angles for the pyramidal angle $\gamma = 5°$: (a) Roll angle; (b) Pitch angle; (c) Yaw angle

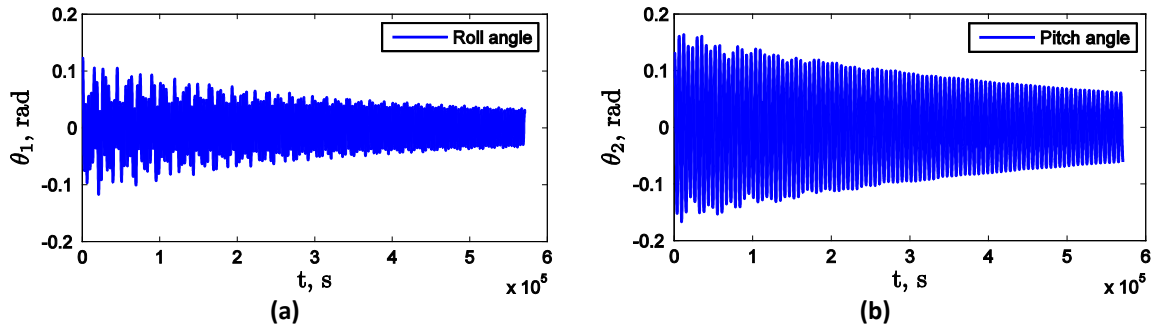

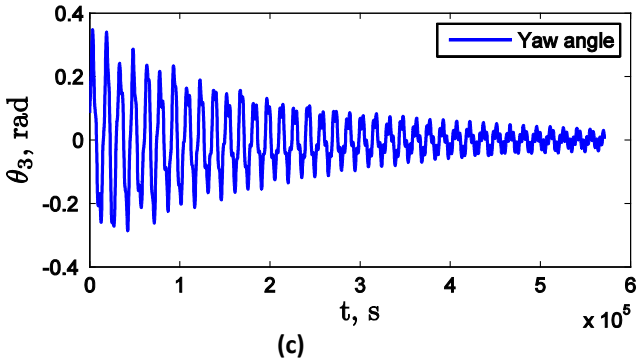

Figure 2.9: Attitude angles for the pyramidal angle $\gamma = 45°$: (a) Roll angle; (b) Pitch angle; (c) Yaw angle

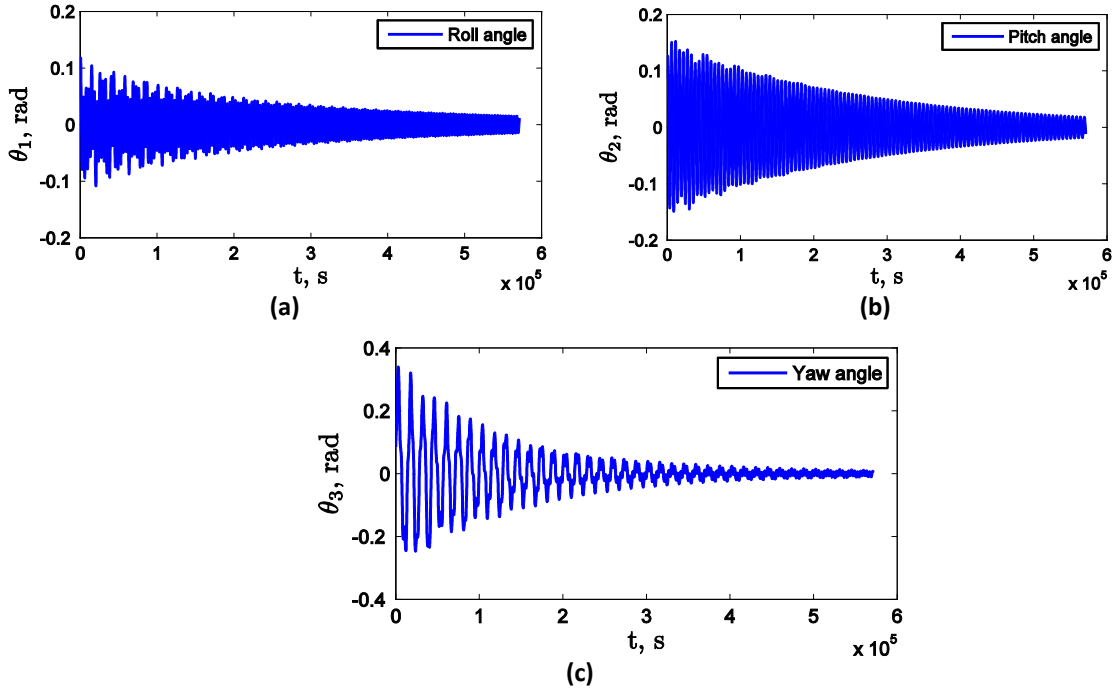

Figure 2.10: Attitude angles for the pyramidal angle$\gamma = 85°$: (a) Roll angle; (b) Pitch angle; (c) Yaw angle

Finally, for the reader's quick reference, the results of analyzing the stability condition of satellites in both circular and elliptical orbits, with and without fluid rings, are summarized in Tables 2.1 and 2.2.

Table 2.1: Stability condition of a satellite in a circular orbit

Attitude angle	Without fluid rings		With passive fluid rings	
	Stability condition	Stabilization time	Stability condition	Stabilization time
Roll	Stable (limit cycle)	N/A	Asymptotically stable	More than 50 orbits
Pitch	Stable (limit cycle)	N/A	Asymptotically stable	More than 50 orbits
Yaw	Stable (limit cycle)	N/A	Asymptotically stable	More than 50 orbits

Table 2.2: Stability condition of a satellite in an elliptical orbit with the eccentricity of 0.05

Attitude angle	Without fluid rings		With passive fluid rings	
	Stability condition	Stabilization time	Stability condition	Stabilization time
Roll	Stable (limit cycle)	N/A	Asymptotically stable	More than 50 orbits
Pitch	Stable (limit cycle)	N/A	Stable (limit cycle)	N/A
Yaw	Stable (limit cycle)	N/A	Asymptotically stable	More than 50 orbits

2.4 Summary

In this chapter, the dynamical model of a rigid satellite with fluid ring actuators was developed. The model is obtained for two satellites: one with three orthogonal fluid rings; the other with four in a pyramidal configuration. The passive damping effect of the fluid rings on the satellite attitude angles was examined. It was noted that the damping torque of the fluid rings was neither large enough to eliminate the oscillations of the satellite within a short period of time, nor could asymptotically stabilize the pitch angle of a satellite in an elliptical orbit. Further, the effect of the pyramidal configuration angle on the damping torque was investigated. The result showed that, although a larger pyramidal configuration angle increases the damping effect, the decay process is still quite slow. Hence, designing an active controller is necessary.

Chapter 3

DESIGNING OF CONTROLLERS FOR SATELLITES WITH FLUID RINGS

The dynamical model of a satellite with fluid ring actuators was developed in Chapter 2. The results obtained from this model showed that designing an active controller for fast asymptotic stabilization of the attitude motion is essential; this is thoroughly discussed in this chapter.

In this vein, as the first attempt, a PID controller is designed to examine the behaviour of the fluidic actuators. The case of failure of one fluid ring is also studied so as to test the redundancy of the system with four fluid rings in a pyramidal configuration.

A PID controller, whose gains are adjusted offline, relies heavily on the accuracy of the dynamical model. However, there are always uncertainties in a dynamical model associated with different components, such as sensors, actuators, etc. In fact, a robust controller is required to cope with the inevitable error in the fluid model as well as the uncertainties in the system parameters. A sliding mode controller, which can be applied to nonlinear systems, is an appropriate candidate. Therefore, a sliding mode controller is designed in this chapter, whose performance is found to be quite promising.

3.1 PID Controller

Deriving the equations of motion of the satellite with fluid rings actuators, the objective here is to stabilize the system at its equilibrium state, where we have:

$$\hat{\boldsymbol{\omega}} = [0 \quad -1 \quad 0]^{\mathrm{T}}, \qquad \beta_i' = 0, \qquad \boldsymbol{\theta} = \mathbf{0} \tag{3. 1}$$

in which $\boldsymbol{\theta} = [\theta_1 \quad \theta_2 \quad \theta_3]^T$, θ_i for $i = 1, \dots, 3$ being the roll, pitch, and yaw angles, respectively[1]. Adding the control input to the equations of motion of the satellite and the fluid rings, Eqs. (2.21) and (2.22), yields

$$\hat{\boldsymbol{I}}_{\boldsymbol{s}}\hat{\boldsymbol{\omega}}' + \hat{\boldsymbol{\omega}} \times \hat{\boldsymbol{I}}_{\boldsymbol{s}}\hat{\boldsymbol{\omega}} = \hat{\boldsymbol{\tau}}_{\boldsymbol{gg}} + \sum_{\boldsymbol{i=1}}^{\boldsymbol{k}} \boldsymbol{R}_{\boldsymbol{i}}\hat{\boldsymbol{\tau}}_{\boldsymbol{r_i}} + \hat{\boldsymbol{\tau}}^{\boldsymbol{c}} \quad \text{for } k = 3 \text{ or } 4 \tag{3. 2}$$

$$\hat{\boldsymbol{I}}_{\boldsymbol{fi}}\left(\boldsymbol{R}_{\boldsymbol{i}}^{\boldsymbol{T}}\hat{\boldsymbol{\omega}}' + \boldsymbol{\beta}_{\boldsymbol{i}}'' + \boldsymbol{R}_{\boldsymbol{i}}^{\boldsymbol{T}}\hat{\boldsymbol{\omega}} \times \boldsymbol{\beta}_{\boldsymbol{i}}'\right) + \boldsymbol{R}_{\boldsymbol{i}}^{\boldsymbol{T}}\hat{\boldsymbol{\omega}} \times \hat{\boldsymbol{I}}_{fi}\left(\boldsymbol{R}_{\boldsymbol{i}}^{\boldsymbol{T}}\hat{\boldsymbol{\omega}} + \boldsymbol{\beta}_{\boldsymbol{i}}'\right) = \boldsymbol{R}_{\boldsymbol{i}}^{\boldsymbol{T}}\hat{\boldsymbol{\tau}}_{\boldsymbol{gg_{fi}}} - \hat{\boldsymbol{\tau}}_{\boldsymbol{r_i}} - \hat{\boldsymbol{\tau}}_{\mathrm{i}}^{\boldsymbol{c}} \tag{3. 3}$$

where $\hat{\boldsymbol{\tau}}^{\boldsymbol{c}}$ is produced by the pumps that pressurize the fluid inside the rings, $\hat{\boldsymbol{\tau}}_{\mathrm{i}}^{\boldsymbol{c}}$ being the component of $\hat{\boldsymbol{\tau}}^{\boldsymbol{c}}$ that has to be produced by the ith fluid ring.

To apply a PID controller, in Eqs. (3. 2) and (3. 3), $\hat{\boldsymbol{\tau}}^{\boldsymbol{c}}$ is replaced by the PID control law given below:

$$\hat{\boldsymbol{\tau}}^{\boldsymbol{c}} = K_p(\boldsymbol{\theta} - \boldsymbol{\theta_d}) + K_d(\boldsymbol{\theta}' - \boldsymbol{\theta'_d}) + K_i\left(\int_0^T \boldsymbol{\theta}\, d\Gamma - \int_0^T \boldsymbol{\theta_d}\, d\Gamma\right) \tag{3. 4}$$

where T and Γ are the non-dimensional time variables. Figures 3.1−3.3 show the simulation results obtained after implementing the PID controller in a satellite with four fluid rings in a pyramidal configuration. The non-dimensional system parameters and initial conditions are chosen identical to the ones introduced in Section 2.3. Also, the satellite is assumed to be in a circular orbit with the radius of 7000 km as in Chapter 2. Figure 3.1 shows that the satellite attitude angles are asymptotically stabilized at their equilibrium state in less than five minutes. As

[1] The notation used throughout the whole thesis is uniform. A nomenclature section is added at page xi for quick reference.

can be seen in Figure 3.2, the maximum torque required is less than 0.015 N. m. To produce this torque, the maximum fluid angular velocity required is 7 rad/s (Figure 3.3).

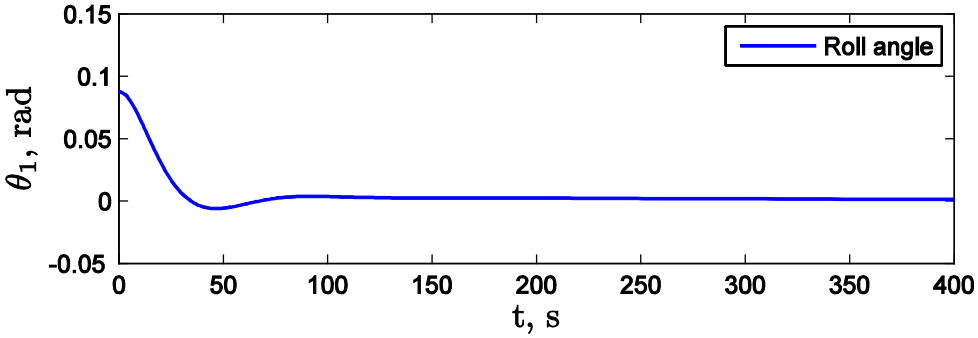

(a)

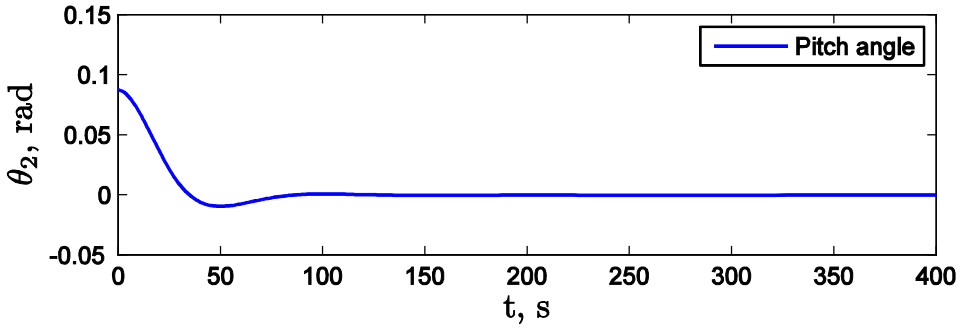

(b)

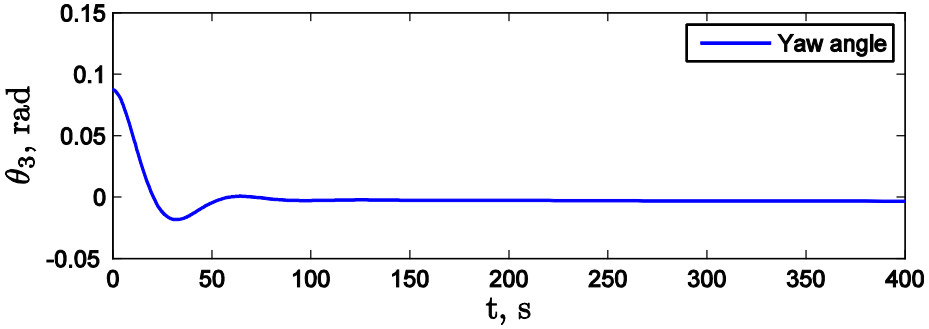

(c)

Figure 3.1: Attitude angles of the controlled system with PID gains $K_p = 5000$, $K_d = 10$, and $K_i = 0.5$ (circular orbit): (a) Roll angle; (b) Pitch angle; (c) Yaw angle

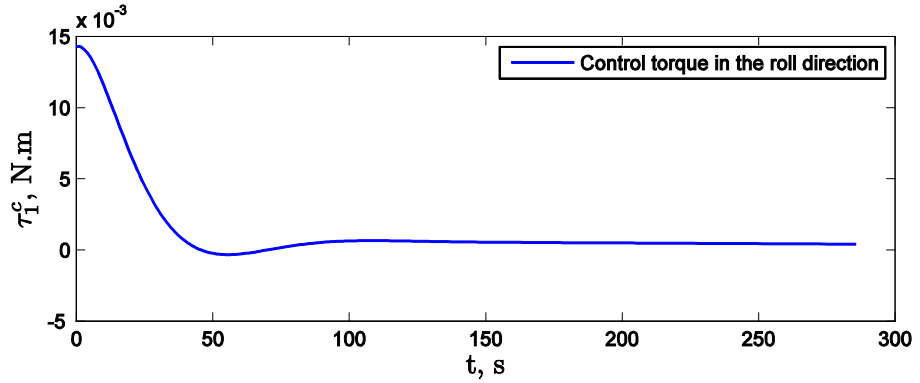

(a)

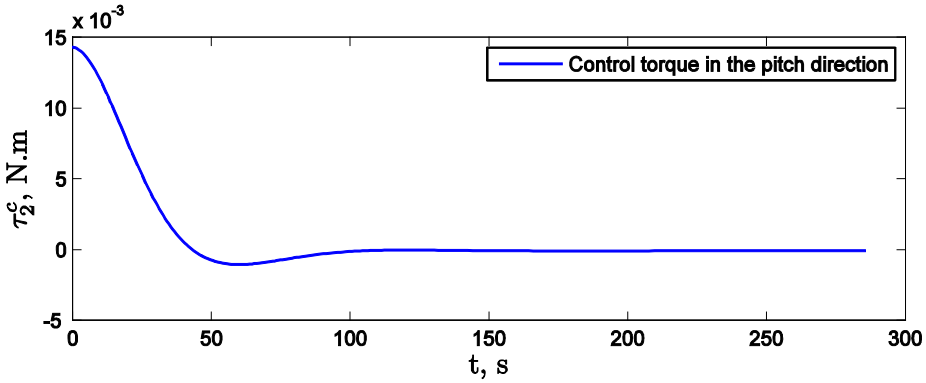

(b)

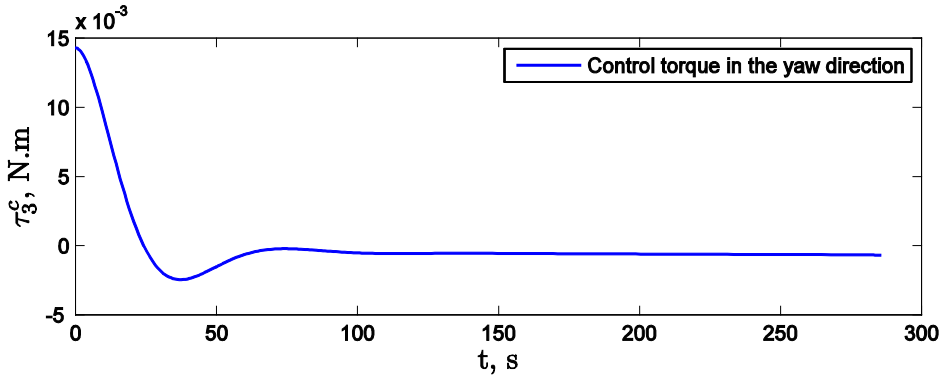

(c)

Figure 3.2: Control torque components with PID gains $K_p = 5000,\ K_d = 10,$ and $K_i = 0.5$ (circular orbit case); (a) Roll angle; (b) Pitch angle; (c) Yaw angle

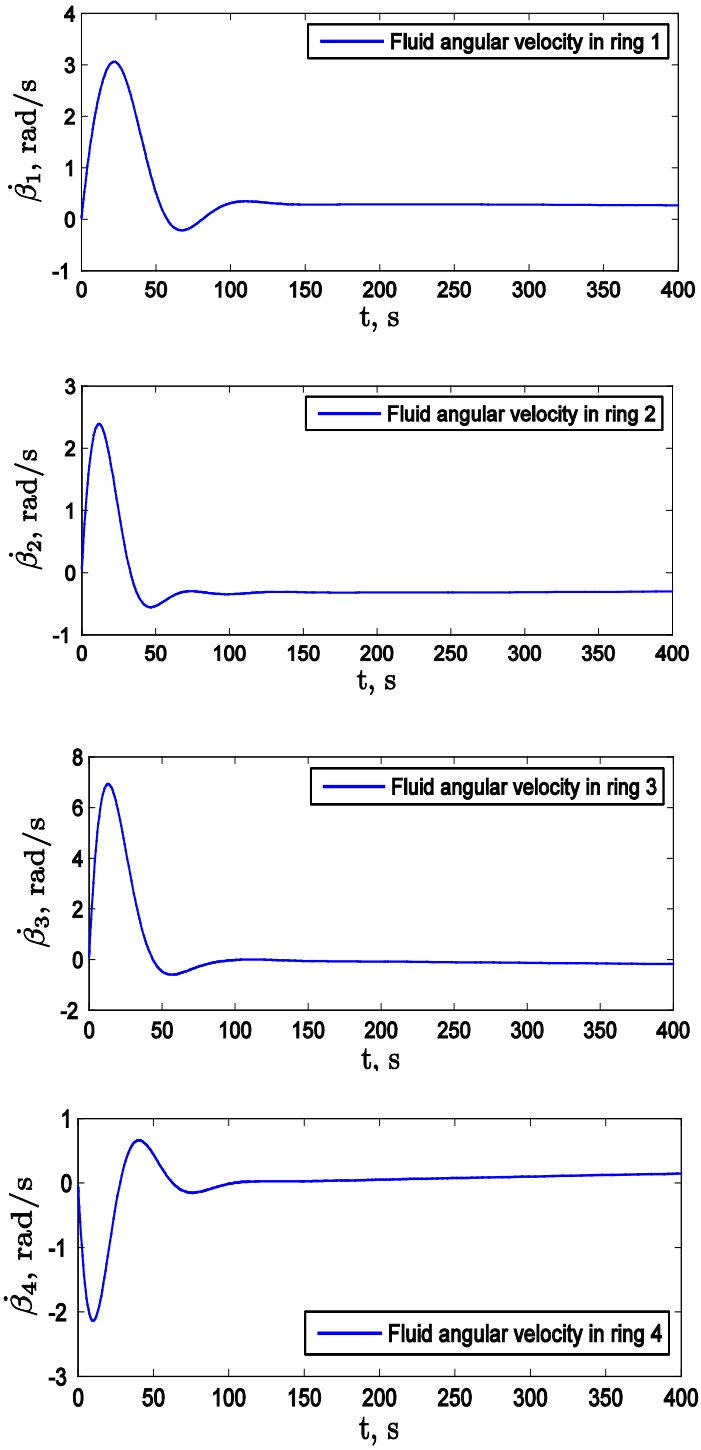

Figure 3.3: Fluid angular velocity with PID gains $K_p = 5000$, $K_d = 10$, and $K_i = 0.5$ (circular orbit case)

It is also interesting to determine the effect of varying the angle γ shown in Figure 2.2, on the performance of the active controller. To this end, simulation was carried out by considering different values of γ, let say 5°, 45°, and 85°, respectively. The results are presented in Figures 3.4 and 3.5.

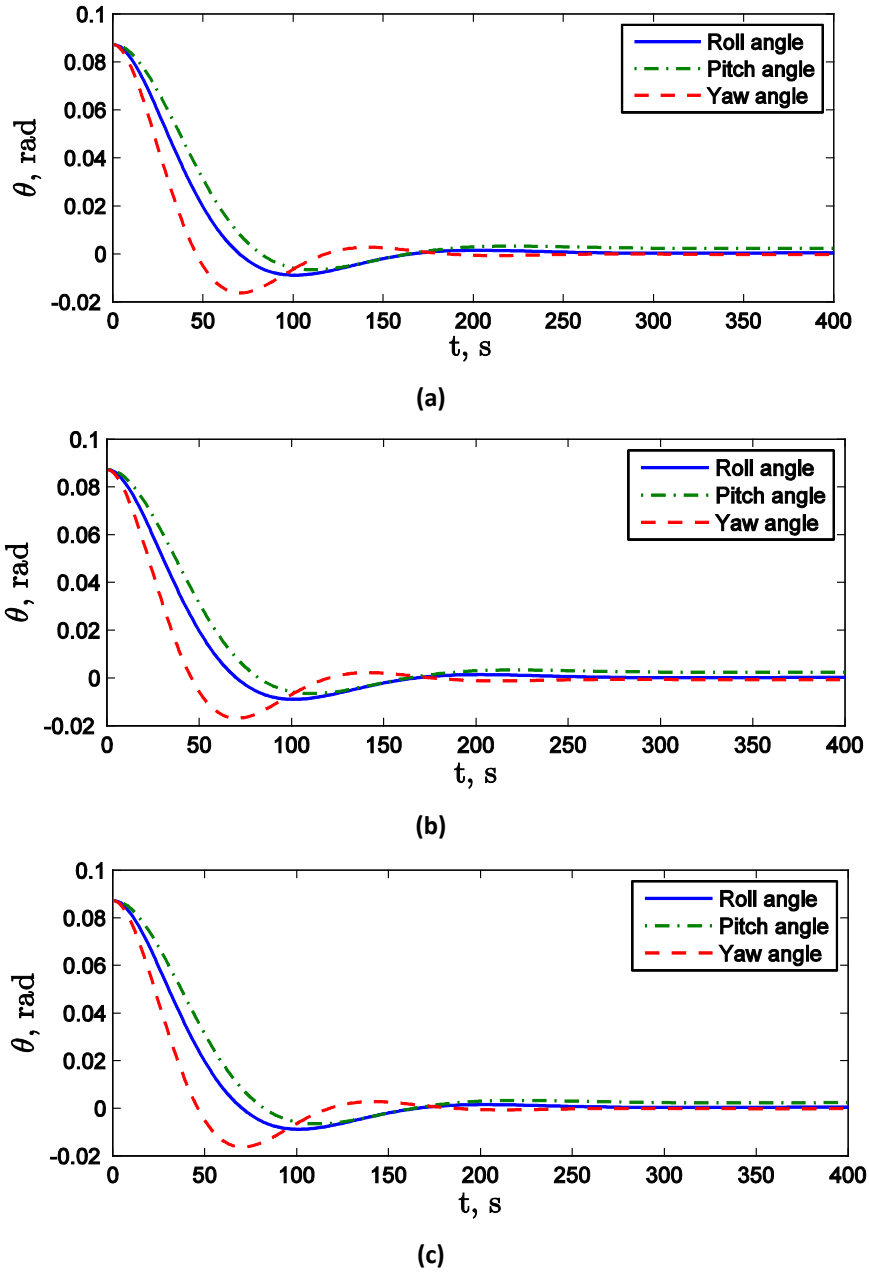

Figure 3.4: Attitude angles of the controlled system with various pyramidal angles using PID gains $K_p = 5000$, $K_d = 10$, and $K_i = 0.5$ (circular orbit case): (a) $\gamma = 5°$; (b) $\gamma = 45°$; (c) $\gamma = 85°$

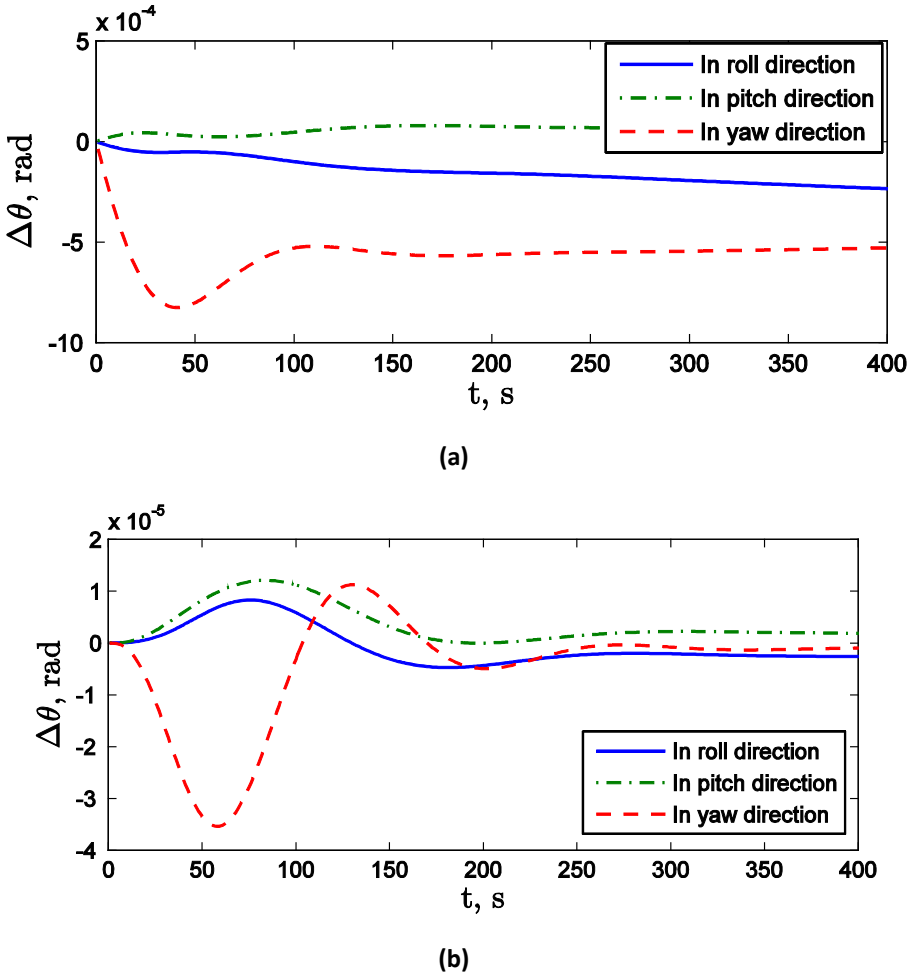

Figure 3.5: Attitude angle differences upon varying the pyramidal angle γ with PID gains $\mathrm{K_p} = 5000$, $\mathrm{K_d} = 10$, and $K_i = 0.5$: (a) Difference of attitude angles between $\gamma = 5°$ and $45°$; (b) Difference of attitude angles between $\gamma = 45°$ and $85°$ (circular orbit case)

As can be seen in Figures 3.4 and 3.5, the effect of varying the angle γ on the controlled motion is very small. In fact, it is difficult to observe any difference between Figures 3.4 (a), (b), and (c). Figure 3.5 establishes that the differences between the system attitude angles are quite small (4×10^{-5}). Therefore, it can be concluded that the angle γ neither has a significant effect on the natural damping of the satellite nor can justify an optimization process in the case of using an active controller.

3.2. Failure Analysis

Due to the sensitivity of satellite operations, the possibility of failure of control actuators cannot be neglected. Accordingly, for the control system proposed, the case of failure of one fluid ring is examined here. In fact, having four fluid rings adds redundancy to the system. Thus, with one fluid ring failed, while the other three are functional, the satellite attitude angles can still be stabilized at its equilibrium state upon re-tuning the PID gains. The simulation is done for four different cases associated with the failure of each of the four fluid rings. Based on the results obtained, two main points are concluded: (i) the fact that which fluid ring has failed does not make a significant difference in the attitude motion of the satellite. Thus, for the sake of brevity in Figure 3.6, a fluid ring is arbitrarily selected to be considered as failed; (ii) it was noted that the fluid flow inside the rings, as shown in Figure 3.6 (b) and (c), does not eventually vanish, although the total torque produced is zero. This implies that

$$\sum_{j=1}^{4} \boldsymbol{\tau_j^c} = 0, \quad \boldsymbol{\tau_j} \neq \mathbf{0} \qquad \text{for } i = 1, \dots, 4 \tag{3. 5}$$

In fact, Figure 3.6 (b) shows that the angular velocity of the fluid continuously increases, however with a quite small rate. This is not acceptable since pumping fluid consumes the valuable power resources. Further, the fluid rings will finally be saturated, meaning that, at some point, the pumps will reach their limits and cannot increase the fluid angular velocity any further because of the existing friction. Once the saturation of the fluid rings occurs, the satellite attitude motion cannot be stabilized. To cope with this problem, the original PID controller is modified, as per the equation below, by adding a weighted summation of the fluid angular velocity terms:

$$\begin{aligned} \hat{\boldsymbol{\tau}}^{\boldsymbol{c}} = K_p(\boldsymbol{\theta} - \boldsymbol{\theta_d}) + K_d(\boldsymbol{\theta'} - \boldsymbol{\theta'_d}) + K_i\left(\int_0^T \boldsymbol{\theta}\, d\Gamma - \int_0^T \boldsymbol{\theta_d}\, d\Gamma\right) \\ + K_v(\boldsymbol{R_1^T\beta_1'} + \boldsymbol{R_2^T\beta_2'} + \boldsymbol{R_3^T\beta_3'} + \boldsymbol{R_4^T\beta_4'}) \end{aligned} \tag{3. 6}$$

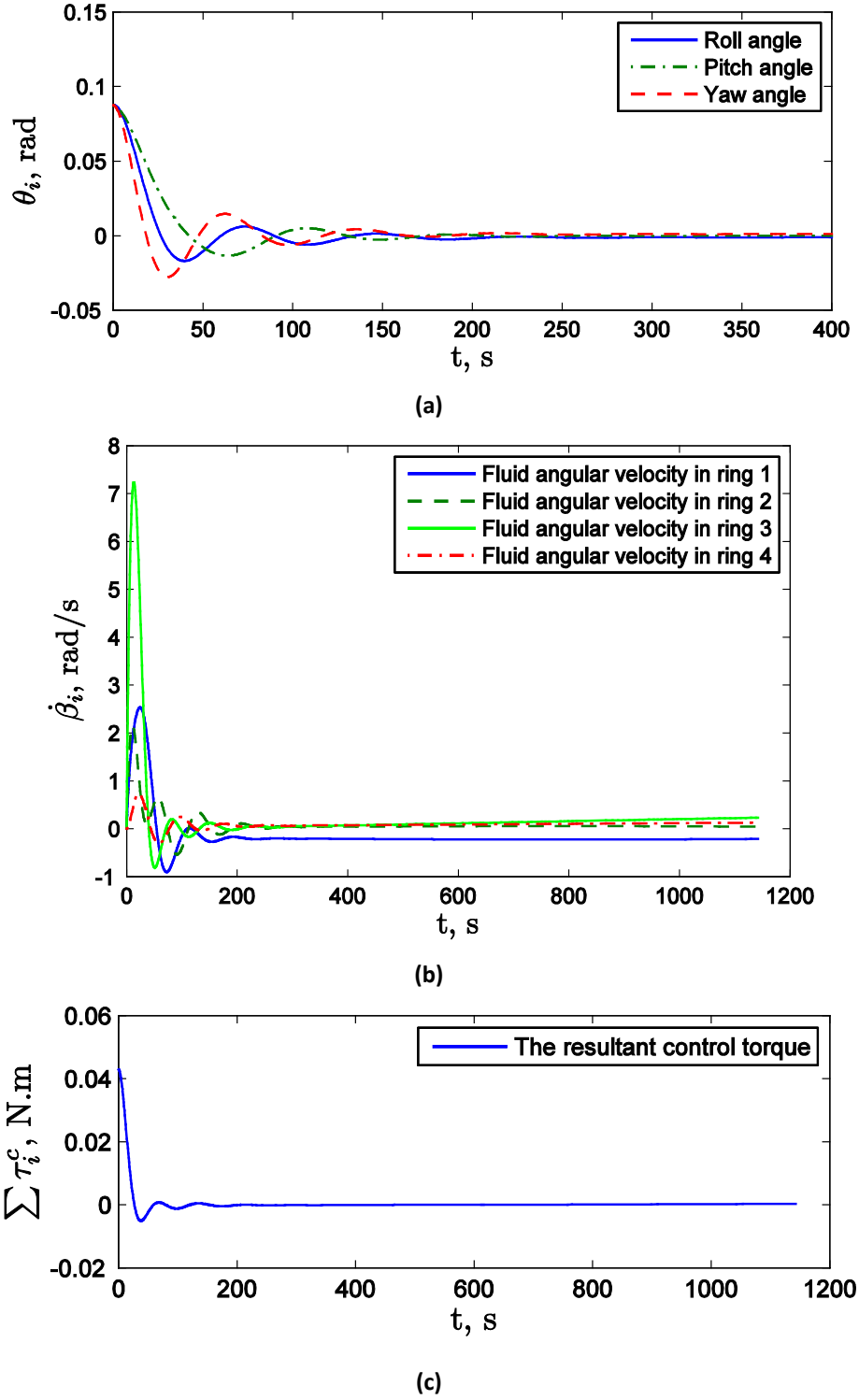

Figure 3.6: Response of the system subject to the failure of one fluid ring with using PID gains $K_p = 5000$, $K_d = 10$, and $K_i = 0.5$ (circular orbit case): (a) Satellite attitude angles; (b) Fluid angular velocity in the rings; (c) Resultant control torque

Choosing an appropriate value for the gain K_v in Eq. (3. 6), the response of the system is plotted in Figure 3.7. Given this provision, not only the satellite attitude angles are stabilized in a short time period, about 300 s, but also the fluid angular velocities vanish in the steady response. It is noteworthy that the maximum torque produced is about 0.01 N. m; to produce this amount of torque, the fluid angular velocity required is less than 7 rad/s.

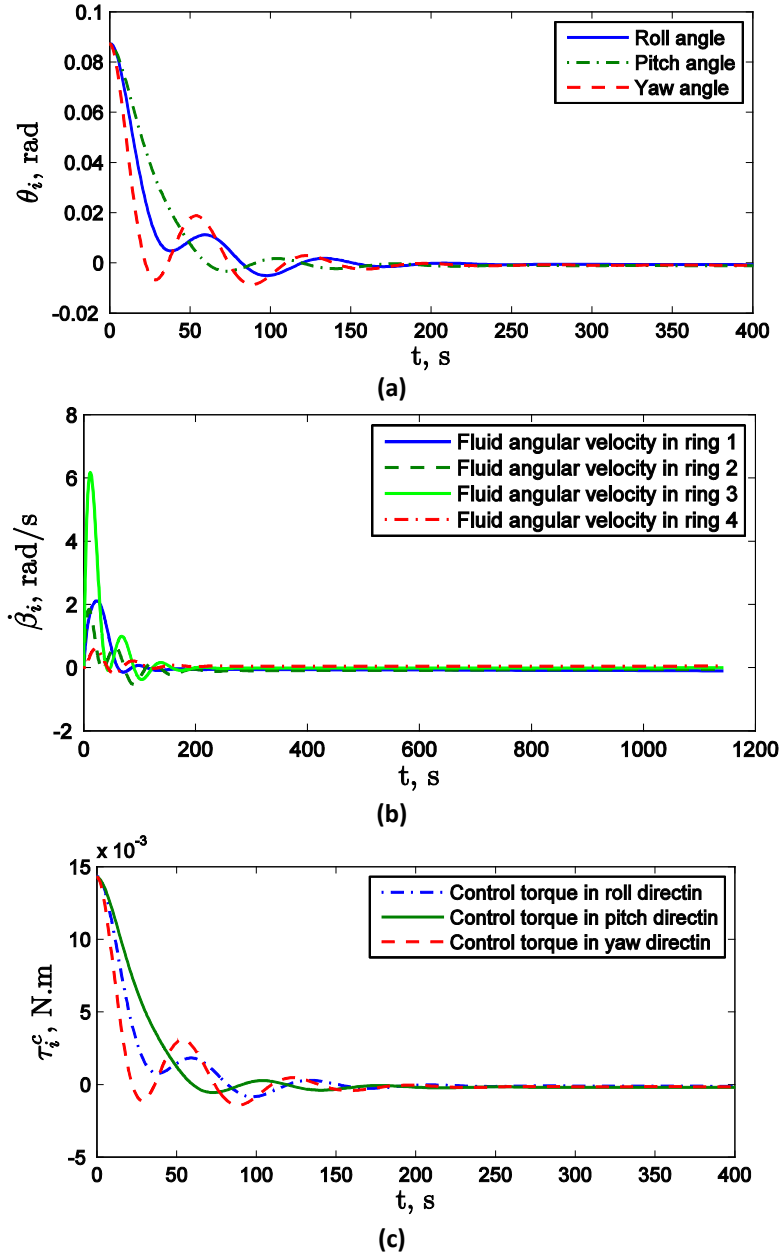

Figure 3.7: Response of the system associated with the failure of one fluid ring using the gains $K_p = 5000$, $K_d = 10$, $K_i = 0.5$, and $K_v = -0.5$ (circular orbit case): (a) Satellite attitude angles; (b) Fluid angular velocity in the rings; (c) Control torque

3.3. Designing a Sliding Mode Controller

One important factor to consider in designing a controller is its robustness. The importance of this factor becomes more apparent, if the uncertainty in the model itself and also in the system parameters is recalled. A sliding mode controller, which is applicable to nonlinear models, is robust against parametric uncertainties. There is an extensive literature on attitude control of satellites using sliding mode controllers, but only a few focuses on attitude stabilization using reaction/momentum wheels, which closely resemble the fluid ring actuators. For instance, for a satellite equipped with thrusters and reaction wheels, Topland and Gravdahl (2004) compared a sliding mode controller to three other alternatives. They concluded that the sliding mode controller, although not the optimum option, is capable of tolerating high levels of model uncertainties. Terui et al. (2005) designed a sliding mode controller for a moon-tracking satellite. The system considered included two momentum wheels for three-dimensional attitude stabilization. Ashrafiuon and Erwin (2005) studied a satellite with a single reaction wheel. They proposed a scheme to change the moment of inertia and angular velocity of the wheel to conserve the angular momentum of the system. They chose a sliding mode controller to cope with the nonlinearity of the system and also to add robustness to its performance. Kowalchuk and Hall (2008) proposed a new method to develop a sliding mode control law for a satellite with reaction wheels; the performance of the controller was tested via a hardware-in-the-loop experiment. Recently, Huo et al. (2011) implemented a sliding mode controller in a tracking satellite with reaction wheels; an adaptive controller was also used to estimate the upper bound of external disturbances.

Our aim here is to develop a sliding mode controller to stabilize the satellite attitude angles using the nonlinear model developed. In this case, because the goal is to stabilize the system on zero attitude angles, the following *sliding hypersurface* [1] is assumed (Slotine and Weiping, 1991):

$$s_i = \theta_i' + \lambda\theta_i \qquad \text{for } i = 1, \dots, 3 \tag{3.7}$$

[1] In sliding mode control design, the command should force the states of the system to move (slide) along the boundaries of a specific control structure, which is called the sliding hypersurface (Slotine and Weiping, 1991).

where s_i is the sliding surface for the ith angle, and θ_i' is the non-dimensional attitude angle derivative. The parameter λ is the slope of the line chosen as the hypersurface here. Large values of λ result in a faster stabilization at the cost of consuming more power. The attitude stabilization can be achieved when θ_i' and θ_i are zero, which in turn implies that at the equilibrium s_i is required to vanish. As an instance, the sliding line used for controlling the roll angle of the satellite understudy is shown in Figure 3.8.

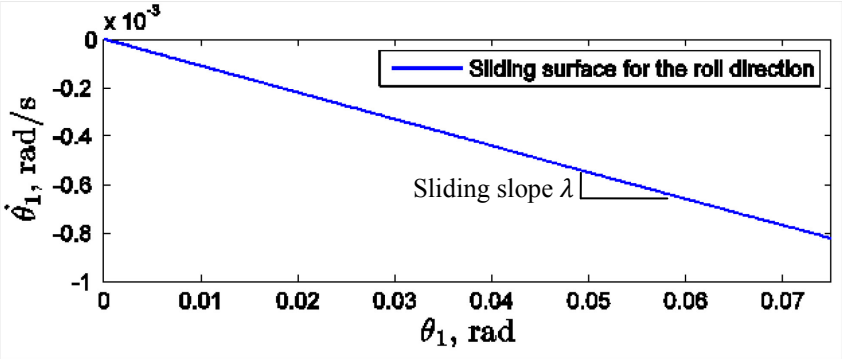

Figure 3.8: Sliding hypersurface for the roll direction

In order to proceed, an initial estimate of the parameters of the system, henceforth referred to as their nominal values, is required. Prior to designing the sliding mode controller, a notation convention needs to be established here: a parameter with an overhead bar denotes its nominal value, while without an overhead bar designates its actual value.

Generally speaking, the sliding mode control law has the following form (Slotine and Weiping, 1991):

$$\hat{\boldsymbol{\tau}}^c = \bar{\boldsymbol{J}}(\bar{\boldsymbol{u}} - \boldsymbol{k}\, sgn(s)) \tag{3. 8}$$

where $\bar{\boldsymbol{J}}$ is a modified inertia matrix, $\boldsymbol{k}$ being a design parameter vector; these two terms will be discussed shortly. Further, $\bar{\boldsymbol{u}}$ is a vector resulting from the addition of the derivative of the sliding surfaces vector with respect to time to a vector denoted by $\bar{\boldsymbol{g}}$, whose components are the variables of interest to be controlled. In attitude stabilization problem, $\bar{\boldsymbol{u}}$ can be expressed as:

$$\bar{\boldsymbol{u}} = \bar{\boldsymbol{g}} + [\mathrm{s}_1' \quad \mathrm{s}_2' \quad \mathrm{s}_3']^{\mathrm{T}} \tag{3. 9}$$

where $\bar{\boldsymbol{g}} \equiv \boldsymbol{\omega}'$. Substituting s_i from Eq. (3.7) into Eq. (3. 9), $\bar{\boldsymbol{u}}$ can be found as:

$$\bar{\boldsymbol{u}} = \bar{\boldsymbol{g}} + \boldsymbol{\theta}_{\boldsymbol{d}}'' - \lambda\boldsymbol{\theta}' \tag{3.10}$$

To find $\bar{\boldsymbol{g}}$, first, Eqs. (2.11) and (2.12) should be substituted into Eq. (2.2) in order to find the equation of motion of the satellite free of the fluid angular acceleration terms:

$$\begin{aligned}\left(\hat{\boldsymbol{I}}_{\boldsymbol{s}} + \sum_{i=1}^{k} \boldsymbol{R_i E \hat{I}_{fi} R_i^T}\right)\boldsymbol{\omega}' + \hat{\boldsymbol{\omega}} \times \hat{\boldsymbol{I}}_{\boldsymbol{s}}\hat{\boldsymbol{\omega}} = \boldsymbol{\tau_{gg}} + \sum_{i=1}^{k} \boldsymbol{R_i E R_i^T \tau_{gg_{fi}}} \\ - \sum_{i=1}^{k} \boldsymbol{R_i E}\{\hat{\boldsymbol{I}}_{\boldsymbol{fi}}(\boldsymbol{R_i^T}\hat{\boldsymbol{\omega}} \times \boldsymbol{\beta_i'}) + \boldsymbol{R_i^T}\hat{\boldsymbol{\omega}} \times \hat{\boldsymbol{I}}_{\boldsymbol{fi}}(\boldsymbol{R_i^T}\hat{\boldsymbol{\omega}} + \boldsymbol{\beta_i'})\} + \sum_{i=1}^{k} \boldsymbol{R_i}[0 \quad 0 \quad \tau_{fi}]^T\end{aligned} \tag{3.11}$$

Here, $\boldsymbol{E} = [\boldsymbol{e_1} \quad \boldsymbol{e_2} \quad \boldsymbol{0}]^{\boldsymbol{T}}$ with $\boldsymbol{e_1} = [1 \quad 0 \quad 0]^T$, $\boldsymbol{e_2} = [0 \quad 1 \quad 0]^T$. Now, $\bar{\boldsymbol{g}}$ is defined as:

$$\begin{aligned}\bar{\boldsymbol{g}} \equiv \boldsymbol{\omega}' = \boldsymbol{J^{-1}}(-\hat{\boldsymbol{\omega}} \times \bar{\boldsymbol{I}}_{\boldsymbol{s}}\hat{\boldsymbol{\omega}} + \bar{\boldsymbol{\tau}}_{\boldsymbol{gg}} + \sum_{i=1}^{k} \bar{\boldsymbol{R}}_{\boldsymbol{i}}\boldsymbol{E}\bar{\boldsymbol{R}}_{\boldsymbol{i}}^{\boldsymbol{T}}\bar{\boldsymbol{\tau}}_{\boldsymbol{gg_{fi}}} \\ - \sum_{i=1}^{k} \bar{\boldsymbol{R}}_{\boldsymbol{i}}\boldsymbol{E}\{\bar{\boldsymbol{I}}_{\boldsymbol{fi}}(\bar{\boldsymbol{R}}_{\boldsymbol{i}}^{\boldsymbol{T}}\hat{\boldsymbol{\omega}} \times \boldsymbol{\beta}_{\boldsymbol{i}}') + \bar{\boldsymbol{R}}_{\boldsymbol{i}}^{\boldsymbol{T}}\hat{\boldsymbol{\omega}} \times \bar{\boldsymbol{I}}_{\boldsymbol{fi}}(\bar{\boldsymbol{R}}_{\boldsymbol{i}}^{\boldsymbol{T}}\hat{\boldsymbol{\omega}} + \boldsymbol{\beta}_{\boldsymbol{i}}')\} + \sum_{i=1}^{k} \bar{\boldsymbol{R}}_{\boldsymbol{i}}[0 \quad 0 \quad \bar{\tau}_{fi}]^T)\end{aligned} \tag{3.12}$$

The term $\bar{\boldsymbol{J}}$ is the modified inertia matrix that also appeared in Eq. (3.8). This matrix is indeed the coefficient of $\boldsymbol{\omega}'$ in Eq. (3.11):

$$\bar{\boldsymbol{J}} = \bar{\boldsymbol{I}}_{\boldsymbol{s}} + \sum_{i=1}^{4} \bar{\boldsymbol{R}}_{\boldsymbol{i}}\boldsymbol{E}\bar{\boldsymbol{I}}_{\boldsymbol{fi}}\bar{\boldsymbol{R}}_{\boldsymbol{i}}^{\boldsymbol{T}} \tag{3.13}$$

The only term remaining in Eq. (3.8) to be defined is the vector $\boldsymbol{k}$. According to Slotine and Weiping (1991),

$$\boldsymbol{k} = \begin{bmatrix} F_1 + \eta_1 \\ F_2 + \eta_2 \\ F_3 + \eta_3 \end{bmatrix} \tag{3.14}$$

where η_i for $i = 1, \dots, 3$ are the control design variables to be tuned. In order to introduce F_i for $i = 1, \dots, 3$, first, the inequality below is recalled from (Slotine and Weiping, 1991):

$$\|\bar{\boldsymbol{g}} - \boldsymbol{g}\| \leq \left\|[\mathrm{F}_1 \quad \mathrm{F}_2 \quad \mathrm{F}_3]^{\mathrm{T}}\right\| \tag{3.15}$$

where $\|.\|$ denotes the 2-norm of a vector. Equation (3.15) states that $\boldsymbol{F} = [\mathrm{F}_1 \quad \mathrm{F}_2 \quad \mathrm{F}_3]^{\mathrm{T}}$ is a vector to be defined such that its 2-norm is greater than that of the vector $(\bar{\boldsymbol{g}} - \boldsymbol{g})$, which measures the difference between the nominal and actual angular accelerations of the satellite in the problem at hand. Here, F_i is chosen as:

$$F_i = 16\pi \bar{a}_1 \bar{a}_2 \bar{d} \left(\sum_{i=1}^{\mathrm{k}} \beta_i'^2 \right)^{1/2} \tag{3.16}$$

The reason behind this choice is that, in sliding mode control design, it is advised to select a physically meaningful quantity to be used as F_i variable; the non-dimensional fluid friction torque is hence chosen in Eq. (3.16). To investigate the performance of the sliding mode controller on the system, simulations are performed; the results are presented in the next subsection.

3.3.1. Dynamical behaviour of the system with the sliding mode controller

To study the performance of the sliding mode controller designed in the preceding section, a satellite with the nominal parameters identical to the non-dimensional parameters of the satellite introduced in Section 2.3 is considered; the parameters are assumed to have an uncertainty of $\pm 15\%$. Using the same initial conditions and orbital radius as those given in Section 2.3, the attitude angle variations of the satellite are plotted versus time in Figure 3.9. It can be concluded that despite the quite large uncertainty in the system parameters, the controller can satisfactorily stabilize the satellite attitude angles in about $500\ s$.

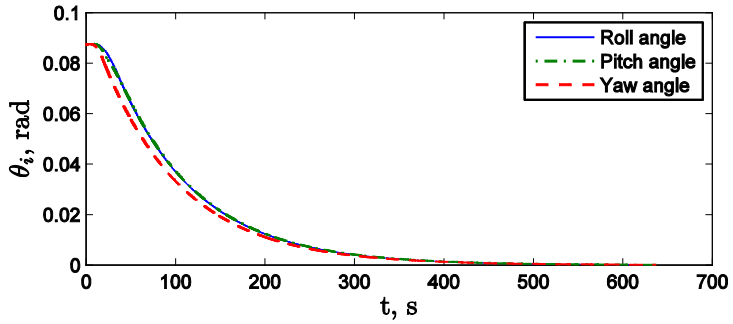

Figure 3.9: Attitude angles after applying the sliding mode controller (circular orbit case)

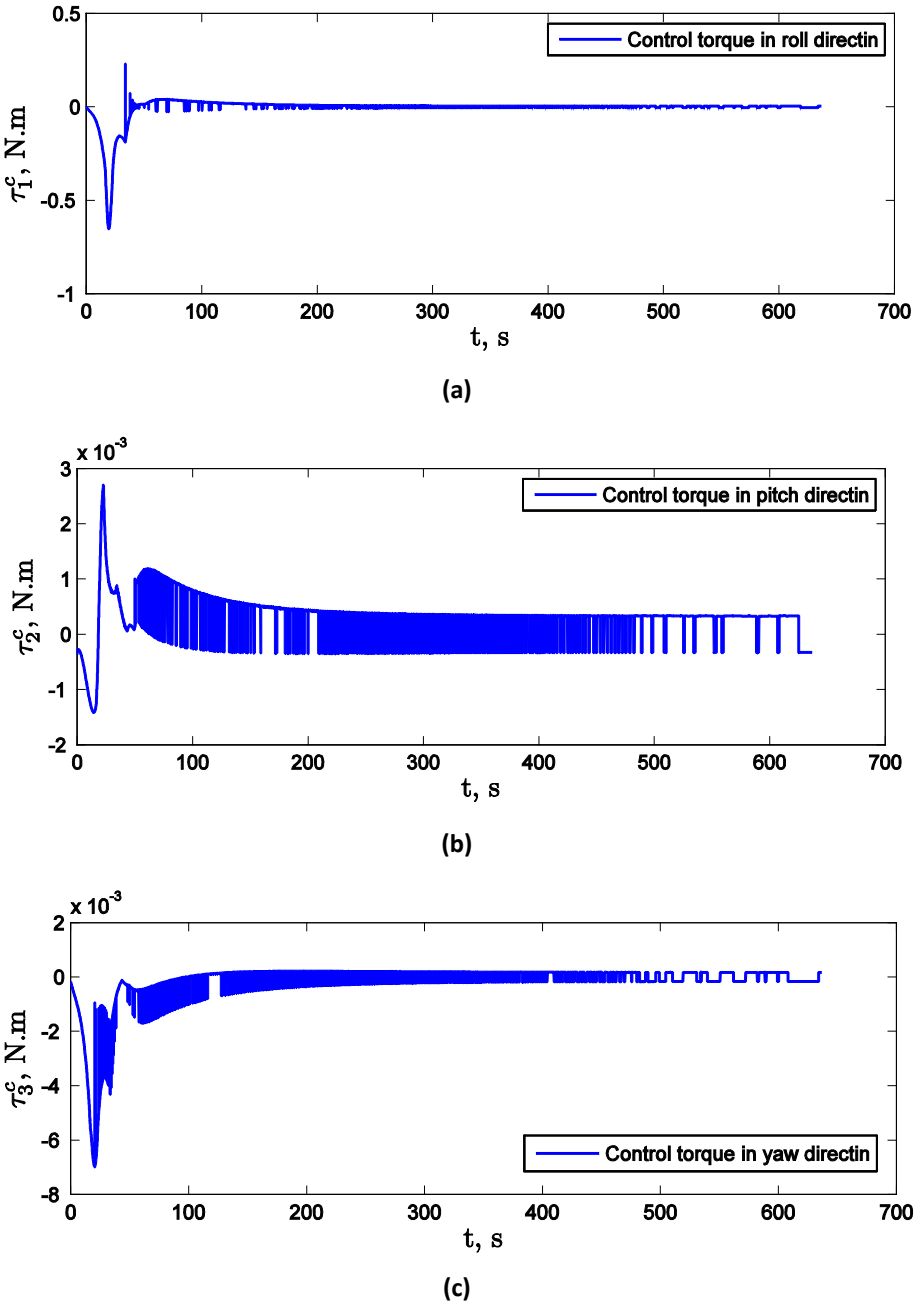

Figure 3.10: Components of the control torque resulting from the sliding mode controller: (a) Roll direction; (b) Pitch direction; (c) Yaw direction (circular orbit case)

Figure 3.10 shows the three components of the control torque produced by the sliding mode controller in the roll, pitch, and yaw directions. As can be seen, a high-frequency chattering exists after the transient response has been eliminated; this phenomenon is a well known characteristic of sliding mode controllers. Several methods have been proposed in the literature to modify the

control law to reduce this effect. In the next section, a switching control law is proposed to eliminate the chattering effect.

3.4. Switching Control Law

In order to eliminate the chattering in the response of the sliding mode controller designed in the foregoing section, a switching controller combining a PID with the sliding mode controller is set forth. The idea is to use the sliding mode controller until the error, $\delta = \|\boldsymbol{\theta} - \boldsymbol{\theta_d}\|$ becomes small enough, i.e., $\delta \leq \varepsilon$, where ε is a small number; at this point, the sliding mode control law is replaced by a PID controller to asymptotically stabilize the satellite attitude angles. In the general form, the control law for the switching controller can be written as:

$$\begin{cases} \hat{\boldsymbol{\tau}}^c = \bar{\boldsymbol{J}}\left(\bar{\boldsymbol{u}} - \boldsymbol{k}\, sgn(s)\right) & \delta > \varepsilon \\ \hat{\boldsymbol{\tau}}^c = K_p(\boldsymbol{\theta} - \boldsymbol{\theta_d}) + K_d(\boldsymbol{\theta}' - \boldsymbol{\theta}'_{\boldsymbol{d}}) + K_i\left(\int_0^T \boldsymbol{\theta}\, d\Gamma - \int_0^T \boldsymbol{\theta_d}\, d\Gamma\right) & \delta \leq \varepsilon \end{cases} \tag{3. 17}$$

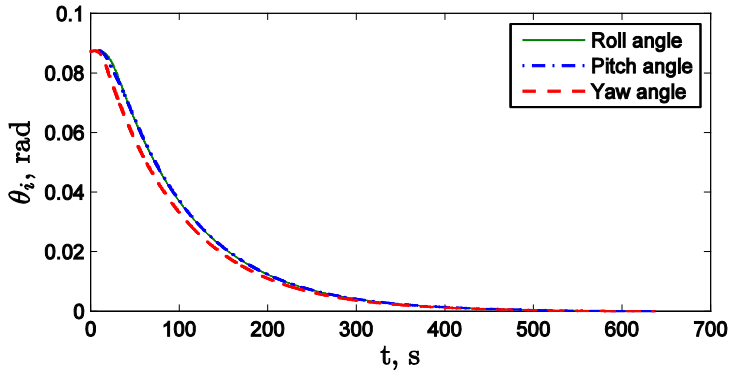

Figure 3.11: Attitude angles after applying the switching controller (circular orbit case)

Designing the switching controller for the satellite studied in Subsection 3.3.1, the variation of the attitude angles are illustrated in Figure 3.11, the control torque components being shown in Figure 3.12. At $t = 578$ s, the switching controller switches to the PID controller; the value of ε used here is 5×10^{-3}. As can be noticed in Figure 3.12, the chattering in the control input has been eliminated after this time step. The maximum control torque required is about 0.6 N. m in the roll direction, which is fairly high.

It is also interesting to compare these results to the case, in which a PID controller is only used. To this end, a PID controller is tuned for the satellite with the nominal parameter values. The attitude motion of this system is shown in Figure 3.13. Further, using the same PID gains, the

attitude angle variations are plotted in Figure 3.14, this time considering the 15% uncertainty of the parameters. It can be concluded from the two figures that the PID controller is not robust enough to be capable of properly handling a $\pm 15\%$ uncertainty in the parameter values. Despite this fact, for the purpose of the feasibility analysis of using fluid ring actuator in satellites, PID controllers will be designed in the forthcoming chapters.

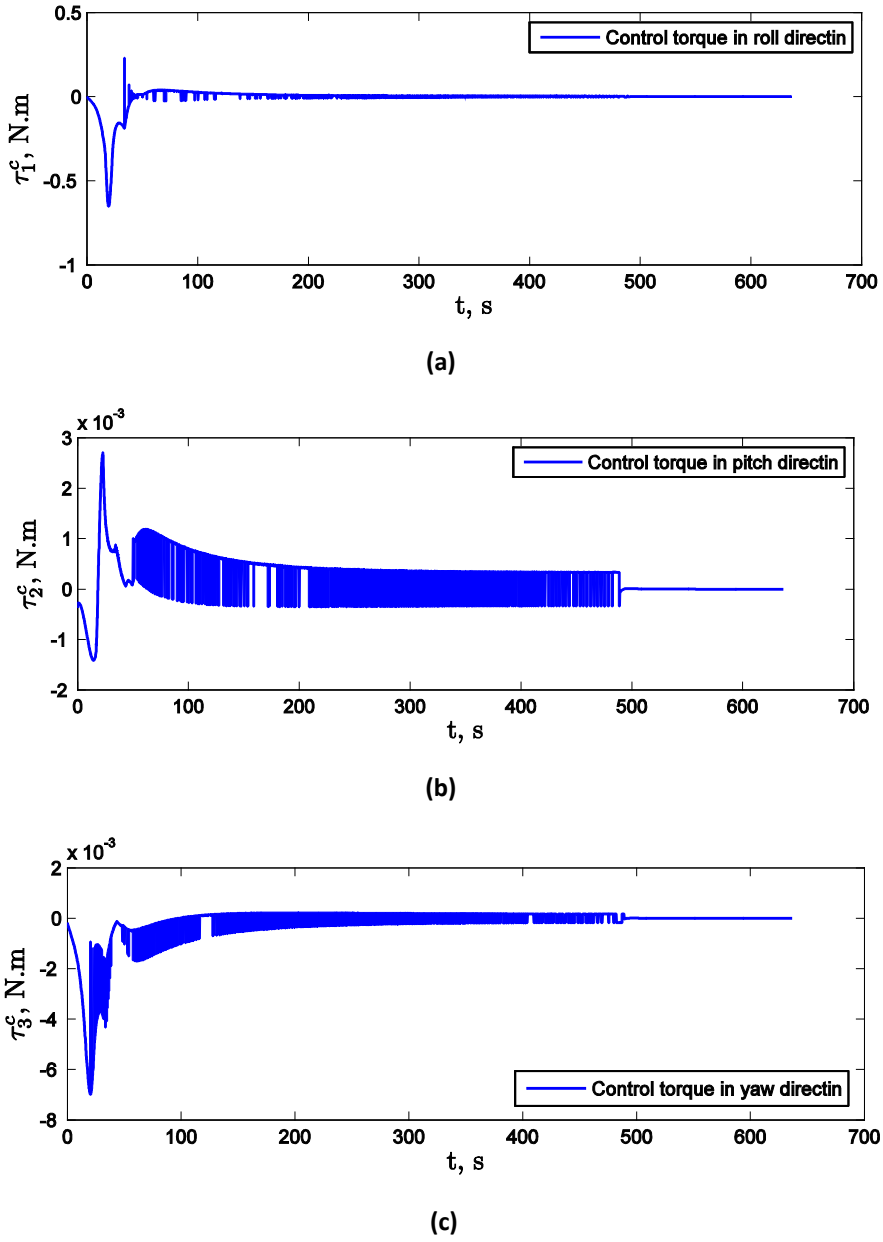

Figure 3.12: Control torque resulting from the switching controller; (a) Roll direction; (b) Pitch direction; (c) Yaw direction (circular orbit case)

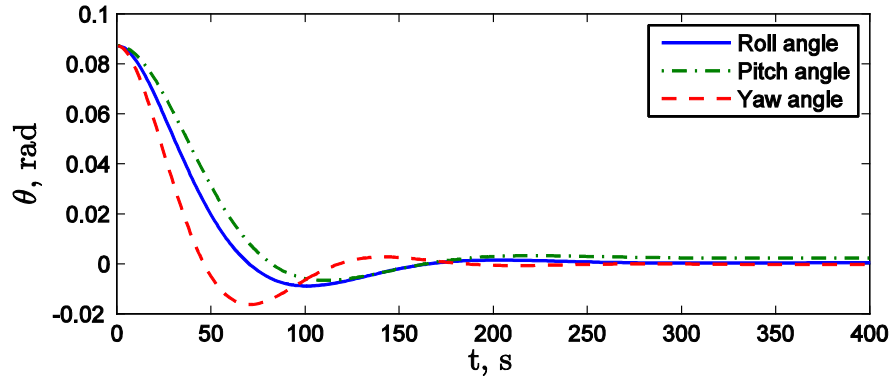

Figure 3.13: Satellite attitude angles using a PID controller with the nominal parameter values

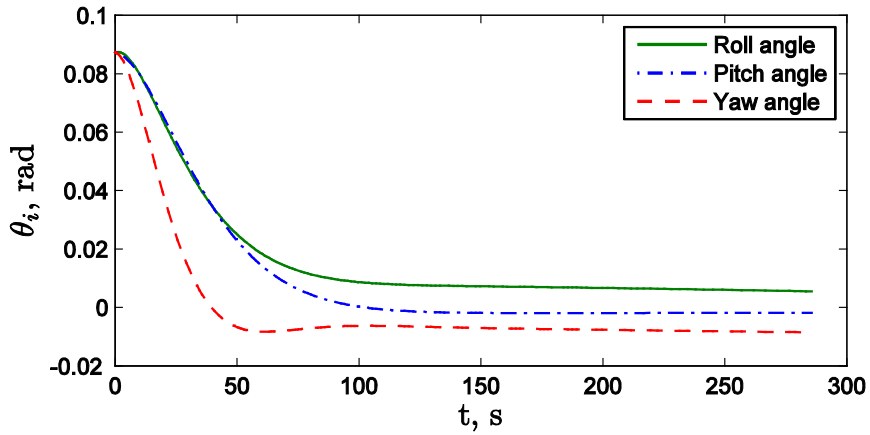

Figure 3.14: Satellite attitude angles using a PID controller subject to the $\pm 15\%$ uncertainty in the nominal parameter values

3.5. Summary

In this chapter, a PID controller was designed to demonstrate the feasibility of attitude stabilization of a satellite with fluid rings. The advantage of using a redundant set of fluid rings was also discussed by performing a failure analysis. To cope with the uncertainty of the dynamical model parameters, a sliding mode control law was also developed. The chattering in the steady response of the system, that is a well-known characteristic of sliding mode controllers, was eliminated via designing a switching controller consisting of a sliding mode and a PID controller. The simulation results showed that the attitude angles were asymptotically stabilized in less than $500\ s$, although a fairly high control torque, about 0.6 N. m, was required.

Chapter 4

EXPERIMENTAL RESULTS

In this chapter, the theoretical results reported in Chapters 2 and 3 are validated by conducting several experiments. To this end, initially, a setup with one fluid ring is designed and built. A few preliminary tests are then conducted to find a relation between the input voltage and the fluid angular velocity. Next, experiments are conducted to verify if the fluid ring is capable of producing a large enough torque to control the attitude of a satellite. A setup consisting of three orthogonal fluid rings is then used to evaluate the three-dimensional control algorithm. The experiments reported in this chapter are done in collaboration with a team from Ryerson University. The setup used in the experiments, reported in this chapter, was designed and built at Ryerson University. However, the design of the experiments, data processing and the analysis of the experimental results are solely performed by the author in her course of doctoral research.

4.1. Design of the Experimental Setup

The main component of the experimental setup is the fluid ring. Here, the selection of an appropriate fluid, a material for the structure of the ring, and a pump are among the major issues,

which are to be discussed in more detail. It is noteworthy that the preference is to choose the components and materials, which are space qualified. However, this is not a concern for the experimental setup meant to validate the feasibility of using fluid ring actuators.

4.1.1. Material selection

Metals are suitable candidates for the structure of the rings, as opposed to plastics, which are not durable enough in the low and high temperature and low pressure of the space. The ease of machining and soldering, electrical insulation, and low mass density are the most significant properties to be considered while choosing a proper metal. Among these, the machining simplicity is highly important, since the size of the rings is quite small. With this regard, copper and aluminum are appropriate options. Comparing the two, an aluminum ring has a smaller mass with lower electrical conductivity, but cannot be soldered easily. Therefore, to build a circular ring, the aluminum tube should be shrink-fitted, a process that is quite costly, at least, for the experimental stage. Knowing this fact and also taking a hint from the condenser systems in satellites, copper is chosen as the superior alternative to build the loop of the fluid ring setup in the experiments.

4.1.2. Fluid selection

To select an appropriate fluid, the properties such as the boiling and freezing points, viscosity, density, and toxicity should be taken into account. The importance of each property is described below.

i. *Boiling and freezing points:* the variation of temperature is quite significant in space. Hence, the number of possible choices for a fluid type is limited, since it is essential that the fluid maintains its state during the whole operation.
ii. *Viscosity:* in Chapter 2, it was shown that the friction torque resulting from the viscosity can damp out the attitude oscillations of a gravity gradient stabilized satellite. However, if the fluid is highly viscous, the pump cannot easily produce the flow. Indeed, the high friction torque reduces the efficiency of the active fluidic actuator. This is due to the fact that the torque produced by the pump is in opposite direction to the friction torque produced by the viscosity.

iii. *Density:* the higher the moment of inertia of the fluid, the larger the torque that the fluid ring produces. Indeed, the moment of inertia of the fluid is directly proportional to its density.

iv. *Toxicity:* the fluid should not impose any risk to the health of the researchers.

v. *Corrosive:* the fluid chosen should not be corrosive; otherwise it can damage the pump.

The first item above eliminates many fluid types from the selection list. Indeed, antifreezes and refrigerators' working fluids are good options considering the thermal variations, which is common in space. Of these types, *Freon* and *Ammonia* are commonly utilized in capillary pumped loops; also, *Ethylene* and *Propylene glycol* are antifreeze fluids in vehicles. The properties of these fluids are summarized in Table 4.1. From the table, it can be understood that the glycols maintain their liquid phase in a larger thermal interval. Comparing ethylene glycol and propylene glycol, the former is finally chosen for its higher density.

Table 4.1: Fluid properties

Fluid	Viscosity, P$a.s$ At 20℃	Density, Kg/m^3 At 20℃	Pressure, Atm At 20℃	Freezing point, ℃	Boiling point, ℃
Water	0.823	997	1	0	100
Ammonia	1.5×10^{-4}	600	8.39	-78	-33.5
Freon-11	0.004	1494	1	-111.1	23.8
Freon-12	0.002	1329	5.58	-157.7	-29.75
Ethylene Glycol	0.060	1095	1	-46.63	187.4
Propylene Glycol	0.090	1045	1	-45.5	197.1

4.1.3. Pump selection

The requirements of the system affecting the pump selection are categorized into two groups of primary and secondary. The primary requirements relate to the capacity of the pumps in order to produce a high flow rate in low pressure conditions, while operating with a DC voltage. On the other hand, the mass and the size of the pump, its compatibility with the metal loop, and its operation life are among the secondary requirements.

Among various types available, reciprocating pumps have pulsed operation and cannot thus produce a continuous flow. Hence, they are not appropriate for our application. Diaphragm pumps can operate in low pressure but cannot produce a high flow rate. Centrifugal pumps produce continuous high flow rates, even at low pressure. As centrifugal pumps, which can operate with a DC voltage exist, this type of pumps is chosen to be used in the experimental setup. Considering the secondary requirements, like the size of the pump, TCS-M400 which is designed and manufactured by *TCS Micro Pumps*, is chosen. This pump is a small, low mass centrifugal pump, which is available in the market.

Figure 4.1 shows a fluid ring built for the experiments. The ring is made of copper and equipped with a TCS-M400 centrifugal pump. The cross-sectional diameter of the ring is 9 mm, its radius is 8 cm so as to fit within a 20 cm cube. The ring is filled with ethylene glycol, as discussed earlier; the moment of inertia of the fluid about the axis of symmetry of the ring is 4.54×10^{-4} kgm^2. Further, the plastic base holder has a moment of inertia of 5.37×10^{-2} kgm^2 about the same axis.

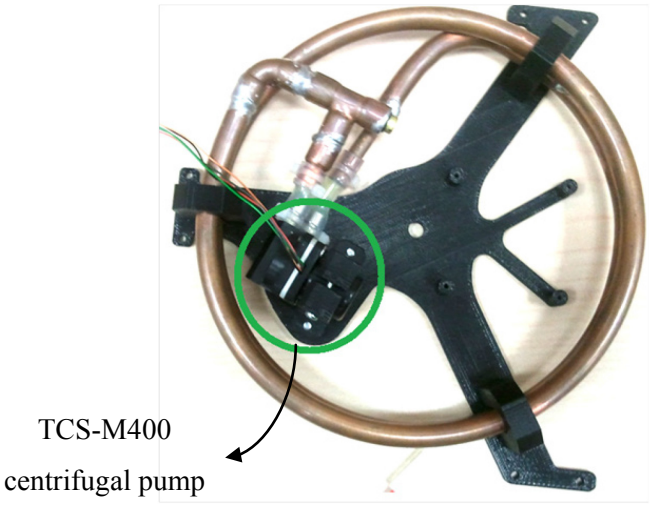

Figure 4.1: The fluid ring used in the experimental validation phase

4.2. Preliminary Analysis

To perform the experiments, first, a relation between the fluid rate and the voltage applied to the pump is required. To this end, the angular velocity of the impeller ω_{imp} is measured versus

the applied voltage V_{app}; the resulting data are plotted in Figure 4.2. Using the least square fit, the equation below is found between ω_{imp} and V_{app}:

$$\omega_{imp} = 0.682\ \mathrm{V_{app}} + 1.836 \tag{4.1}$$

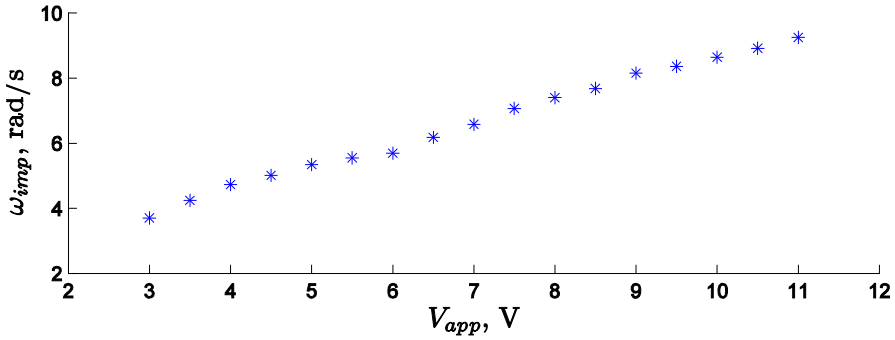

Figure 4.2: Angular velocity of the impeller versus the applied voltage

Next, before finding the relation between the input voltage and the angular velocity of the fluid $\dot{\beta}$ inside the ring, a relation between the latter and the angular velocity of the impeller is obtained. To this end, an experiment is conducted in which one fluid ring is mounted on a simulator that maintains the fluid ring floating in the air (Figure 4.3). The simulator is equipped with a gyroscope to find the angular velocity of the setup.

In the experiment, the following sinusoidal voltage was applied to the pump:

$$V_{app} = \begin{cases} 8 & t < 30s \\ 8 + 3\sin(0.1\pi t) & t \geq 30s \end{cases} \tag{4.2}$$

where t denotes the time. According to Eq. (4.2), a voltage of 8 V is applied at the first 30 s of the experiment so as to allow the operator to initialize the angular velocity of the setup at $0\ \mathrm{rad/s}$. After $t = 30$ s, the sinusoidal input voltage is applied; the angular velocity of the base and the ring are measured using the gyroscope, while the impeller angular velocity was found using an encoder. The angular velocity of the fluid versus the angular velocity of the impeller is plotted in Figure 4.4.

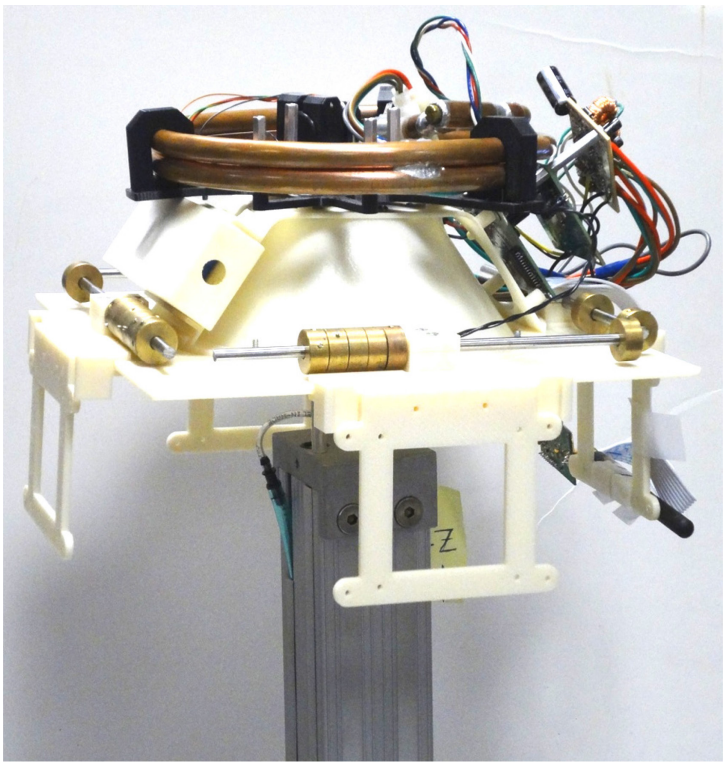

Figure 4.3: Fluid ring with its base mounted on the simulator

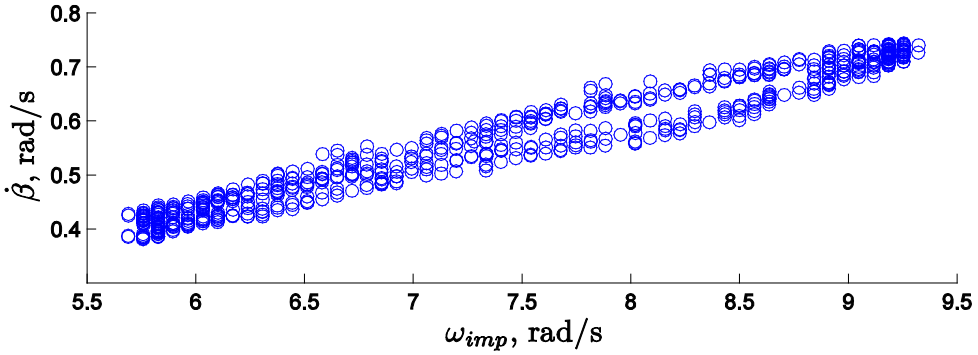

Figure 4.4: Fluid angular velocity $\dot{\beta}$ versus the impeller angular velocity ω_{imp} using a sinusoidal input voltage

Using the least square fit, the following relation between $\dot{\beta}$ and ω_{imp} can be found:

$$\dot{\beta} = 0.11\omega_{imp} - 0.11 \tag{4.3}$$

Combining Eqs. (4.1) and (4.3), the relation sought between the input voltage and the fluid angular velocity $\dot{\beta}$ is obtained as:

$$\dot{\beta} = 0.08\mathrm{V}_{\mathrm{app}} + 0.10 \tag{4.4}$$

Using this equation, the voltage required to produce the desired fluid angular velocity can be calculated.

4.3. Experiment with a Single Fluid Ring System

In this experiment, the target is to verify if:

i. the system with a fluid ring is controllable.
ii. the theoretical model represents the real fluid ring behaviour within acceptable precision.
iii. a fluid ring is capable of producing a large enough control torque.

To this end, the equations of motion of the system, i.e., a single fluid ring mounted on its base, as shown in Figure 4.3, are first derived.

$$I_b\ddot{\theta} = \tau_a\,, \qquad I_f\left(\ddot{\theta} + \ddot{\beta_d}\right) = -\tau_a \tag{4.5}$$

Here, θ is the attitude angle of the disk about its axis of symmetry; $\ddot{\beta}_d$ is the desired fluid angular acceleration; I_b and I_f are the moments of inertia of the base and the fluid inside the ring about the axis of symmetry of the disk. Further, τ_a is the torque that the fluid ring applies on the base. In fact, the torque τ_a has two components:

$$\tau_a = \tau_f + \tau_p \tag{4.6}$$

where τ_f and τ_p are the fluid friction torque and the torque resulting from the pump pressure, respectively. To control the system, the pump pressure torque is found using a PD control law:

$$\tau_p = K_p(\theta - \theta_d) + K_d\left(\dot{\theta} - \dot{\theta}_d\right) \tag{4.7}$$

where θ_d is the desired attitude angle chosen arbitrarily. To better demonstrate the different components involved in the control of the system at hand and their relations, a block diagram of the whole process is illustrated in Figure 4.5. In fact, in order to stabilize the system at the attitude angle θ_d, the PD control law (4.7) is substituted into Eq. (4.5), thereby the desired fluid angular

velocity $\dot{\beta}_d$ and acceleration $\ddot{\beta}_d$ are obtained. Since the actual control input is the voltage V^c to be supplied to the pump, a PD control law is designed below so as to produce the flow rate $\dot{\beta}_d$.

$$V^c = V_{app} + K_p\left(\omega_{imp} - \omega_{imp_d}\right) + K_d\left(\dot{\omega}_{imp} - \dot{\omega}_{imp_d}\right) \tag{4.8}$$

In the preceding equation, V_{app} can be obtained upon substituting $\dot{\beta}_d$ into Eq. (4.4), ω_{imp_d} and $\dot{\omega}_{imp_d}$ being the desired angular velocity and acceleration of the impeller.

In our experimental setup, the data and the control commands are transmitted between the system and the computer via radio signals. Therefore, for a more reliable performance, a filter is required to eliminate the noise from the measured data; this is discussed next.

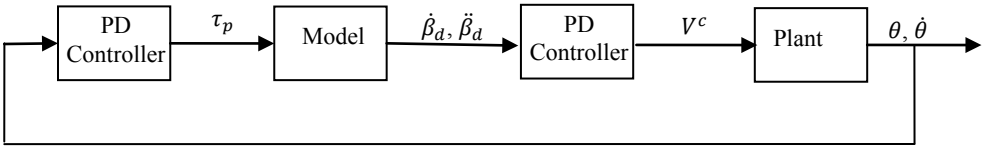

Figure 4.5: The block diagram of the controllers used between the model and the plant

4.3.1. Designing a Kalman filter

A discrete Kalman filter uses the data measured by sensors from the physical system as well as the theoretical data obtained from the mathematical model to estimate the signals of the next step (Kalman, 1960). A Kalman filter includes a state estimation and a state covariance step to predict the future signal. The block diagram below shows the application of the Kalman filter to a plant controlled by a PD controller.

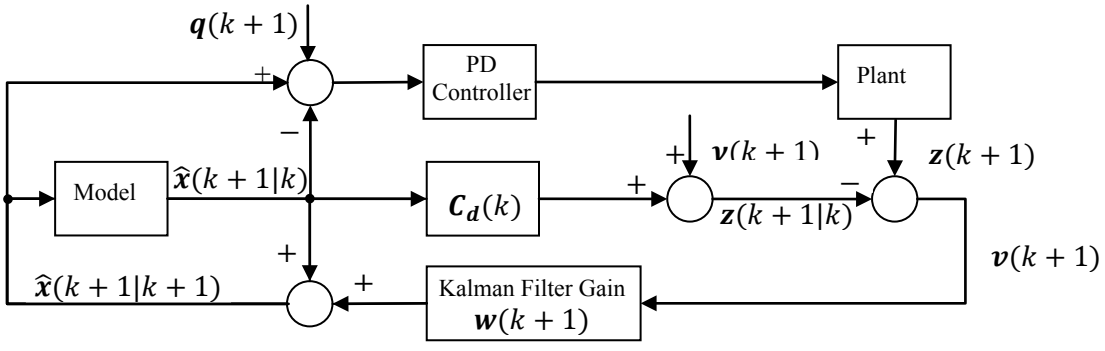

Figure 4.6: The block diagram of a system with a Kalman filter

In Figure 4.6, $\hat{\boldsymbol{x}}(k+1|k)$ is the state vector predicted for the $(k+1)$st time step using the theoretical model and the data at time step k. The vector $\hat{\boldsymbol{x}}(k+1|k+1)$ is the state estimated at the $(k+1)$st time step using $\hat{\boldsymbol{x}}(k+1|k)$ and the sensor measurement data vector denoted by $\boldsymbol{z}(k+1)$. Designating the observation model matrix by $\boldsymbol{C_d}(k)$, we have

$$\boldsymbol{z}(k+1|k) = \boldsymbol{C_d}(k)\hat{\boldsymbol{x}}(k+1|k) + \boldsymbol{v}(k+1) \tag{4.9}$$

where $\boldsymbol{z}(k+1|k)$ is the measurement data predicted using $\hat{\boldsymbol{x}}(k+1|k)$, and $\boldsymbol{v}(k+1)$ is the observation noise. In Figure 4.6, $\boldsymbol{v}(k+1)$ is the measurement residual vector obtained such that $\boldsymbol{v}(k+1) = \boldsymbol{z}(k+1) - \boldsymbol{z}(k+1|k)$. The Kalman filter gain $\boldsymbol{w}(k+1)$ can be obtained using the observation model matrix $\boldsymbol{C_d}(k)$ and the *error covariance matrix* $\boldsymbol{P}$, whose elements p_{ij} with $i \neq j$ represent the variance of the ith with respect to the jth state, p_{ii}being the variance of the ith state. The matrix $\boldsymbol{P}$ can be predicted using the data at time k as follows:

$$\boldsymbol{P}(k+1|k) = \boldsymbol{A_d}(k)\boldsymbol{P}(k|k)\boldsymbol{A_d}(k)^T + \boldsymbol{Q}(k+1) \tag{4.10}$$

where $\boldsymbol{Q}(k+1)$ is the covariance matrix of the process noise, $\boldsymbol{A_d}$ is the state transition matrix in the state-space model of the system: $\boldsymbol{x}(k+1) = \boldsymbol{A_d}\boldsymbol{x}(k) + \boldsymbol{B_d}\boldsymbol{u}(k)$. Finally, the Kalman filter gains vector $\boldsymbol{w}(k+1)$ can be calculated as:

$$\boldsymbol{w}(k+1) = \boldsymbol{P}(k+1|k)\boldsymbol{C_d}(k+1)^T\boldsymbol{s}(k+1)^{-1} \tag{4.11}$$

where $\boldsymbol{s}(k+1)$=$\boldsymbol{C_d}(k+1)\boldsymbol{P}(k+1|k)\boldsymbol{C_d}(k+1) + \boldsymbol{R}(k+1)$, with $\boldsymbol{R}(k+1)$ being covariance matrix of the observation noise. The error covariance matrix $\boldsymbol{P}$ can be updated at the $(k+1)$st step using the equation below:

$$\boldsymbol{P}(k+1|k+1) = \boldsymbol{P}(k+1|k) - \boldsymbol{w}(k+1)\boldsymbol{s}(k+1)\boldsymbol{w}(k+1)^T \tag{4.12}$$

To design a Kalman filter for our specific application, the dynamical equations of the system (4.5), expressed below for quick reference, are required to be discretized.

$$I_d\ddot{\theta} = 16\pi^2 r^3 \mu\dot{\beta} + \tau_p$$
$$I_f\left(\ddot{\theta} + \ddot{\beta}\right) = -16\pi^2 r^3 \mu\dot{\beta} - \tau_p \tag{4.13}$$

The terms τ_f of Eq. (4.5) are expanded here using Eq. (2.16). Casting Eq. (4.13) in the state-space form, we obtain:

$$\dot{\boldsymbol{s}} = \boldsymbol{A}\boldsymbol{s} + \boldsymbol{B}\tau_p$$
$$\boldsymbol{A} = \begin{bmatrix} 0 & 1 & 0 & 0 \\ 0 & 0 & 0 & q/I_d \\ 0 & 0 & 0 & 1 \\ 0 & 0 & 0 & -q/(I_d\, I_f\,)(I_d + I_f) \end{bmatrix}, \quad \boldsymbol{B} = \begin{bmatrix} 0 \\ 1/I_d \\ 0 \\ -1/(I_d\, I_f\,)(I_d + I_f) \end{bmatrix}, \boldsymbol{s} = \begin{bmatrix} \theta \\ \dot{\theta} \\ \beta \\ \dot{\beta} \end{bmatrix} \tag{4.14}$$

where $q = 16\pi^2 r^3 \mu$ and τ_p is the control torque obtained from the PD control law below:

$$\tau_p = K_p(\theta - \theta_d) + K_d\left(\dot{\theta} - \dot{\theta}_d\right) \tag{4.15}$$

Discretizing Eq. (4.14) leads to

$$\begin{bmatrix} \theta(k+1) \\ \dot{\theta}(k+1) \\ \beta(k+1) \\ \dot{\beta}(k+1) \end{bmatrix} = \boldsymbol{A_d} \begin{bmatrix} \theta(k) \\ \dot{\theta}(k) \\ \beta(k) \\ \dot{\beta}(k) \end{bmatrix} + \boldsymbol{B_d}\tau_{p_d} \tag{4.16}$$

where $\boldsymbol{A_d} = e^{T\boldsymbol{A}} \cong \boldsymbol{I} + T\boldsymbol{A}$ and $\boldsymbol{B}_d = \left(\int_0^T e^{\boldsymbol{A}\nu} d\nu\right)\boldsymbol{B} \cong (T\boldsymbol{1} + 1/2T^2\boldsymbol{A}\,)\boldsymbol{B}$ (Slotine and Weiping, 1991), the parameter T being the sample time. Expanding Eq. (4.16) yields

$$\begin{bmatrix}\theta(k+1)\\ \dot{\theta}(k+1)\\ \beta(k+1)\\ \dot{\beta}(k+1)\end{bmatrix}=\begin{bmatrix}1 & 1 & 0 & 0\\ 0 & 1 & 0 & q/I_d\\ 0 & 0 & 1 & 1\\ 0 & 0 & 0 & 1-q/(I_d\,I_f\,)(I_d+I_f)\end{bmatrix}\begin{bmatrix}\theta(k)\\ \dot{\theta}(k)\\ \beta(k)\\ \dot{\beta}(k)\end{bmatrix}$$
$$+\begin{bmatrix}1/(2I_d)\\ 1/I_d\ -q(I_d+I_f)/(2I_d^2I_f)\\ -q/(2I_d\,I_f\,)(I_d+I_f)\\ -q/(I_d\,I_f\,)(I_d+I_f)(1-q/(I_d\,I_f\,)(I_d+I_f))\end{bmatrix}\tau_{p_d} \quad (4.17)$$

where τ_{p_d} is a discrete PD controller:

$$\tau_{p_d}=[K_p \quad K_d \quad 0 \quad 0]\begin{bmatrix}\theta(k)-\theta_d(k)\\ \dot{\theta}(k)-\dot{\theta}_d(k)\\ \beta(k)\\ \dot{\beta}(k)\end{bmatrix} \quad (4.18)$$

Finally,

$$\begin{bmatrix}\theta(k+1)\\ \dot{\theta}(k+1)\\ \beta(k+1)\\ \dot{\beta}(k+1)\end{bmatrix}$$
$$=\begin{bmatrix}1 & 1 & 0 & 0\\ K_p/I_d & 1+K_p/I_d & 0 & q/I_d\\ 0 & 0 & 1 & 1\\ -K_p/(I_d\,I_f\,)(I_d+I_f) & -K_d/(I_d\,I_f\,)(I_d+I_f) & 0 & 1-q/(I_d\,I_f\,)(I_d+I_f)\end{bmatrix}\begin{bmatrix}\theta(k)\\ \dot{\theta}(k)\\ \beta(k)\\ \dot{\beta}(k)\end{bmatrix} \quad (4.19)$$
$$-\boldsymbol{B_d}[K_p \quad K_d \quad 0 \quad 0]\begin{bmatrix}\theta_d(k)\\ \dot{\theta}_d(k)\\ 0\\ 0\end{bmatrix}$$

In fact, Eq. (4.19**)** is the theoretical model block in the diagram illustrated in Figure 4.6.

4.3.2. Single fluid ring system experiment

In this experiment, the objective is to maintain the base of the setup, shown in Figure 4.3, at a specific angle, let us say 60°. This, indeed, resembles the one-dimensional attitude control of a

satellite, which is achievable using only one fluid ring actuator. To this end, $\theta_d = 60°$ and $\dot{\theta}_d = 0\ \mathrm{rad/s}$ are substituted into Eq. (4.19**)** to obtain the desired fluid angular velocity $\dot{\beta}_\mathrm{d}$, which produces the necessary control torque. The desired impeller speed, that leads to $\dot{\beta}_\mathrm{d}$ sought, is then found from Eq. (4.2**)**, which is modified as per the equation below:

$$\begin{cases} \omega_{imp} = 7 & t < 30\ s \\ \omega_{imp} = 1/0.11(\dot{\beta}_\mathrm{d} + 0.11) + 7 & t \geq 30\ s \end{cases} \tag{4.20}$$

The reason for this modification lies in the fact that the setup does not operate properly for the impeller speeds of less than $4\ \mathrm{rad/s}$ due to the friction and inertial effects. In Eq. (4.20**)**, the value of $7\ \mathrm{rad/s}$ is assigned to the first 30 seconds of the experiment so as to allow the operator to initialize the attitude angle of the setup, let say at zero degree. The same offset is applied after $t = 30\ \mathrm{s}$ in Eq. (4.20**)** to compensate the internal friction of the system. The input voltage to the pump is finally calculated using Eq. (4.8**)**. Here, the angular velocity of the base is measured by a gyroscope and transmitted to a computer using radio signals. Although a Kalman filter was used to cancel out the noises existing in the signals, limitations in the computational speed of the computer used did not allow for a real time filter. Therefore, the Kalman filter was only used offline at the data processing stage. Here, a word of caution is in order: since the Kalman filter is implemented offline, the measurement data already contain the effect of the observation noise and its covariance matrix, $\nu(\mathrm{k}+1)$ and $\mathrm{R}(\mathrm{k}+1)$, introduced in the equations pertaining to the design of the Kalman filter. With this regard, indeed, there is no need to consider $\mathrm{Q}(\mathrm{k}+1)$ that denotes the covariance matrix of the process noise.

Figures 4.7−4.11 present the variation of various important quantities versus time obtained from the theory and the experiment. From Figure 4.7, it can be concluded that the difference between the impeller angular velocity obtained from the theory and the experiment is small; this is slightly higher in the first 10 seconds but diminishes over time. The same effect can be observed in the rotation angle and angular velocity plots of the disk shown in Figures 4.8 and 4.9, respectively. The reason for this difference lies in the Coulomb friction forces existing inside the pump and also the time delay in the communication of the control input. At $\mathrm{t} = 25\ s$, a jump is observed in the actual impeller angular velocity plot in Figure 4.7. This is due to either the instantaneous malfunction of the impeller caused by air pockets or the loss of data sent by the

controller. This jump could not be avoided in any trials of the experiment, though the time of its occurrence varied.

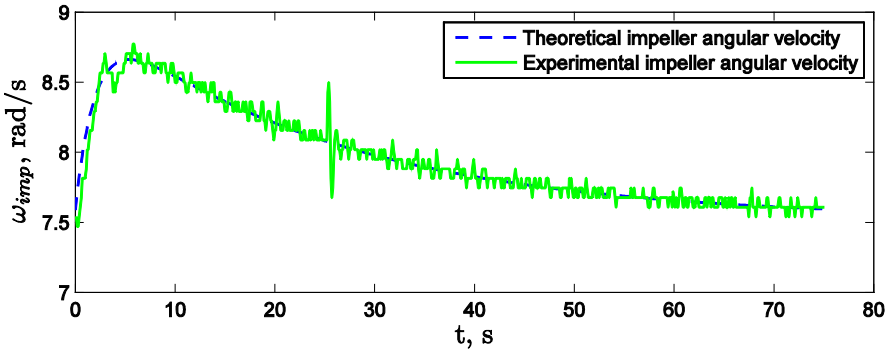

Figure 4.7: Theoretical and experimental plots of the impeller angular velocity versus time

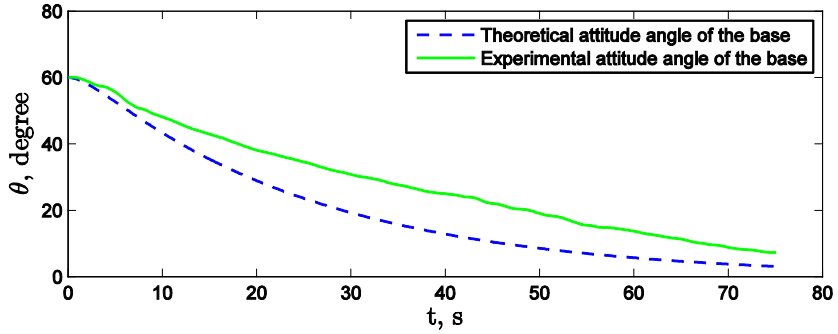

Figure 4.8: Theoretical and experimental plots of the attitude angle of the disk versus time

Another observation in Figure 4.8 is that, in the experiment, the slope of the plot of the attitude angle of the base versus time is less than what is expected from the theory. The reason behind is that the impeller has an initial error in tracking the input control command. This error has also affected the base angular velocity plotted in Figure 4.9; to correct this error, the PD controller has produced a quite large control command at $t = 6\,\mathrm{s}$. Despite the difference discussed in this section, the results of the theory and the experiment have trends, which are reasonably close.

Figures 4.10 and 4.11 show the control torque produced and the input voltage required by the pump, respectively. From the former, the maximum torque produced is about $0.007\,\mathrm{N.m}$, which is quite small. However, according to Figure 4.11, to produce this torque, the voltage

required is more than 10 V. This reveals the need for a high voltage to produce the required control torque.

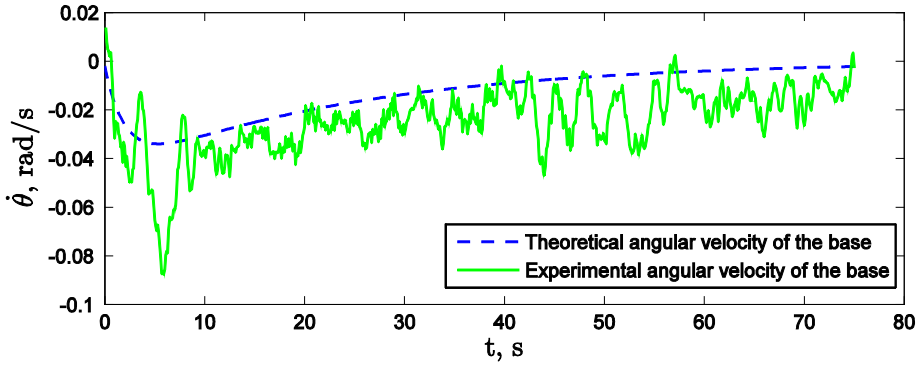

Figure 4.9: The theoretical and experimental plots of the disk angular velocity versus time

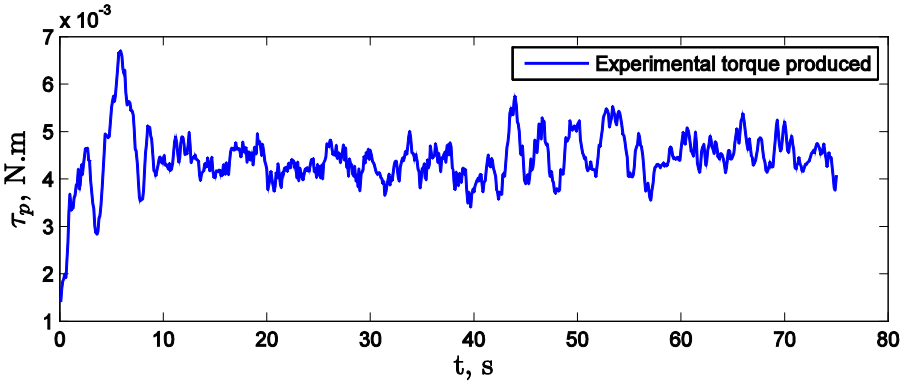

Figure 4.10: The experimental control torque versus time

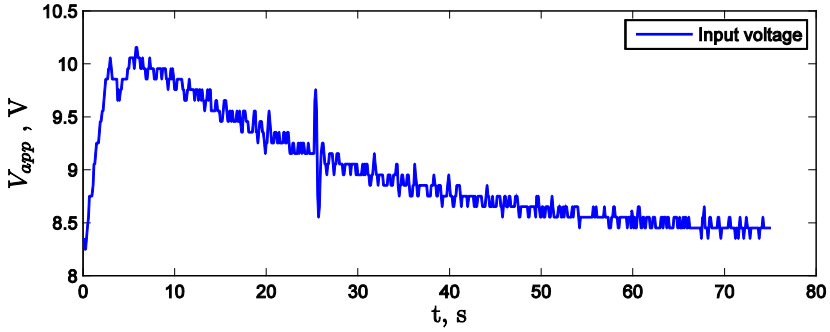

Figure 4.11: Input voltage which is applied to the fluid ring system

4.4. Three Dimensional (3D) Control Experiment

For the three dimensional (3D) control experiment, a cubic satellite equipped with three fluid rings mounted orthogonally was built; the schematic of this system is shown in Figure 2.1. The cubic satellite was then installed on the simulator to make a free floating condition. Due to various reasons, such as the malfunction of the pumps, the existence of air pockets in the fluid rings, limitation in the computational speed, and data loss during radio communication, this was performed as a hardware-in-the-loop experiment; the setup is shown in Figure 4.12. with this provision, issues, such as the malfunction of the pumps and the existence of air pockets in the rings are not significant.

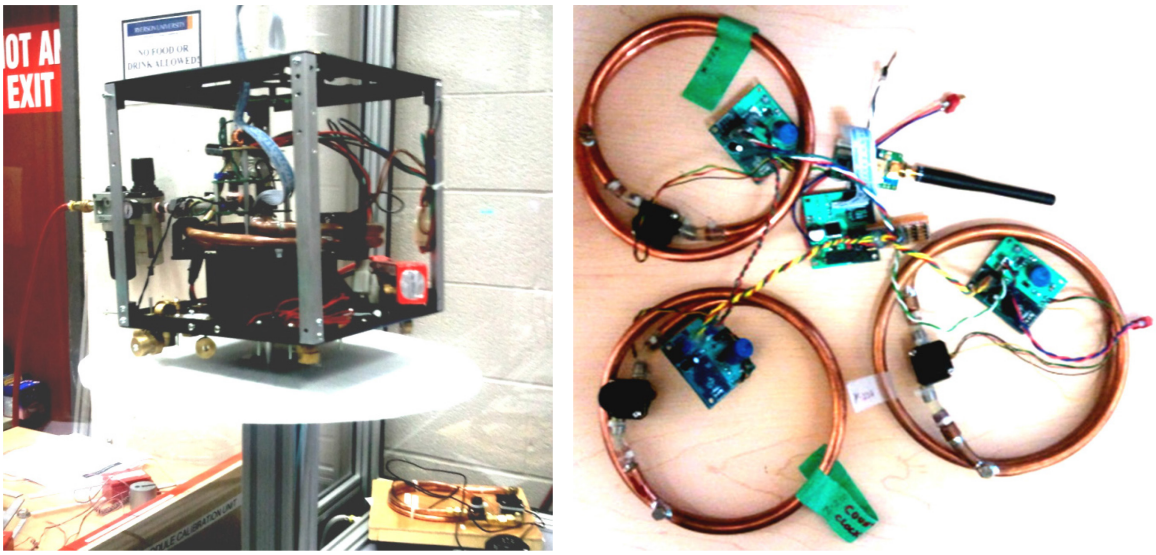

(a) (b)

Figure 4.12: (a) Cubic satellite floating on the simulator; (b) Hardware-in-the-loop experimental setup

Figure 4.13 shows the attitude angles of the system obtained from the theory reported in Section 2.1. Figures 4.14−4.16 compare the experimental and theoretical angular velocities found for the impellers of the pumps installed on the rings whose axes of symmetry are along the roll, pitch, and yaw directions. As can be seen, the maximum impeller speed is fairly small, less than 14 rad/s.

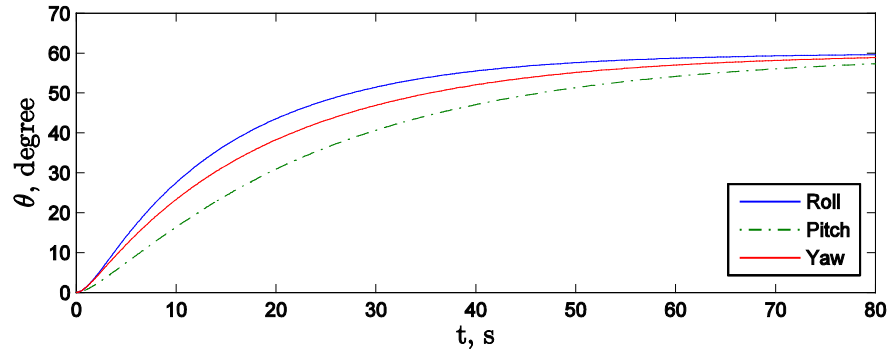

Figure 4.13: Attitude angles found from the theoretical model

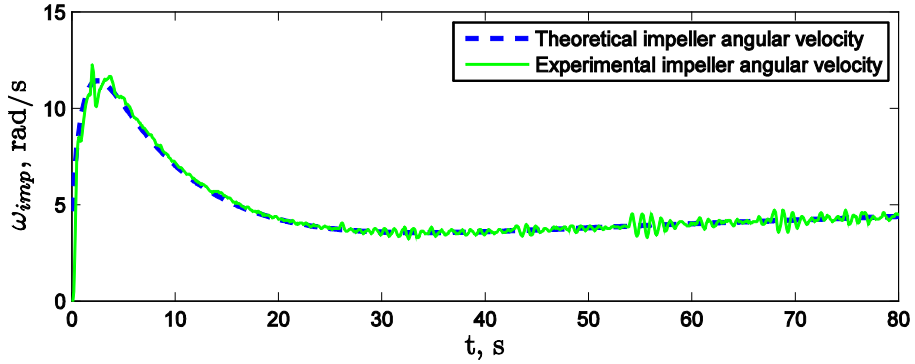

Figure 4.14: Theoretical and Experimental angular velocities of the roll-axis impeller

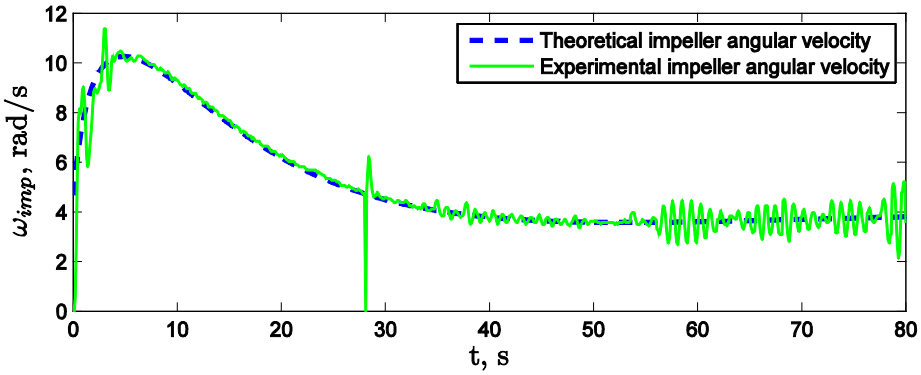

Figure 4.15: Theoretical and Experimental angular velocities of the pitch-axis impeller

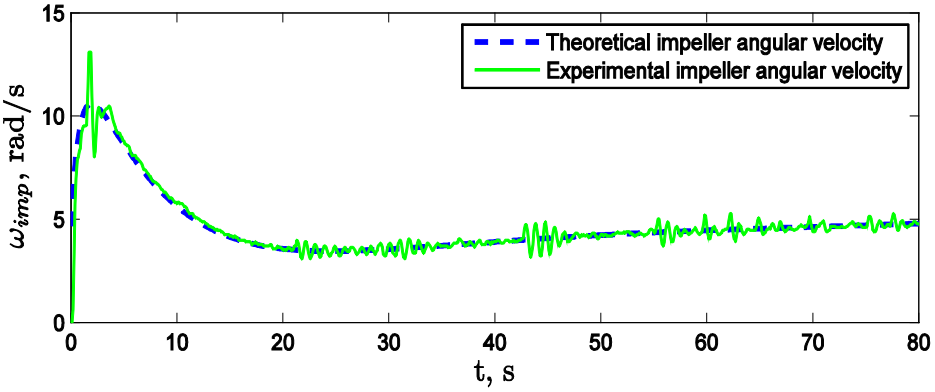

Figure 4.16: Theoretical and Experimental angular velocities of the yaw-axis impeller

Figure 4.17 shows the desired fluid angular velocity found upon substituting the desired impeller angular velocities of Figures 4.14-4.16 into Eq. (4.20**)**. As can be noticed, the maximum angular velocity of the fluid, that is 1.4 rad/s, occurs in the first 20 seconds of the experiment. As time progresses, the fluid angular velocity in different rings reduces to 0.5 rad/s, as expected from the bias angular velocity existing in Eq. (4.20**)** .

Figure 4.18 shows the applied voltage to produce the fluid angular velocity, and hence, the torque required. Accordingly, to produce the maximum fluid angular velocity of 1.4 rad/s, the voltage required is about 13 V, which is quite high. Considering the light structure of the cubic satellite used in this experiment, one can readily conclude that the application of fluid ring actuators in typical satellites requires high input voltages of more than 12 V. This in turns reveals the necessity of using massive batteries; more fuel is then required to launch the satellite to its orbit. Therefore, the application of fluid rings as primary means of stabilizing the attitude of satellites is not really a practical option. Nevertheless, fluid ring actuators bring interesting advantages to either satellites requiring small-magnitude torque for attitude stabilization, or as auxiliary attitude control actuators; the latter is discussed in detail in Chapters 5 and 6.

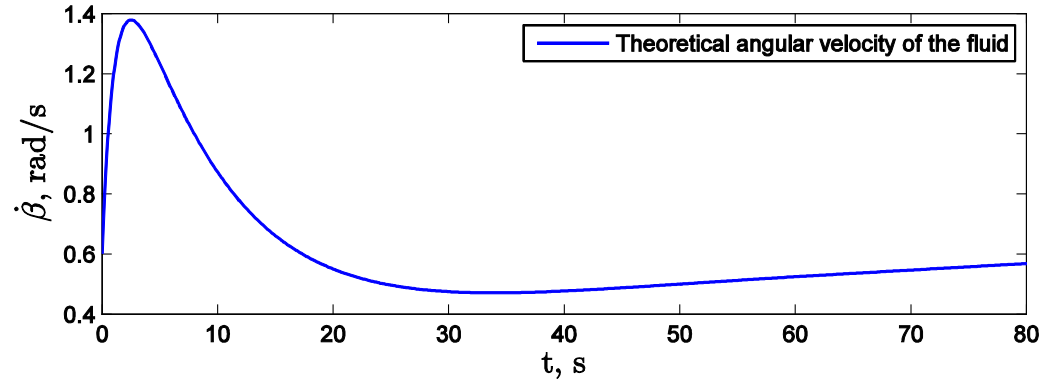

(a)

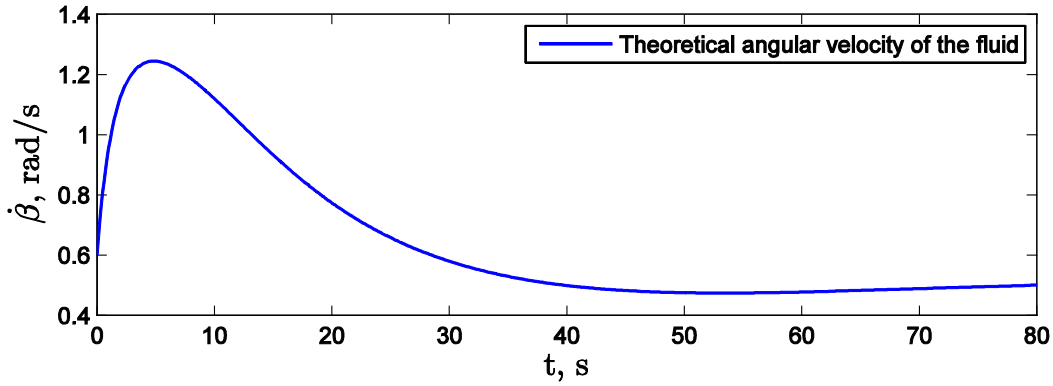

(b)

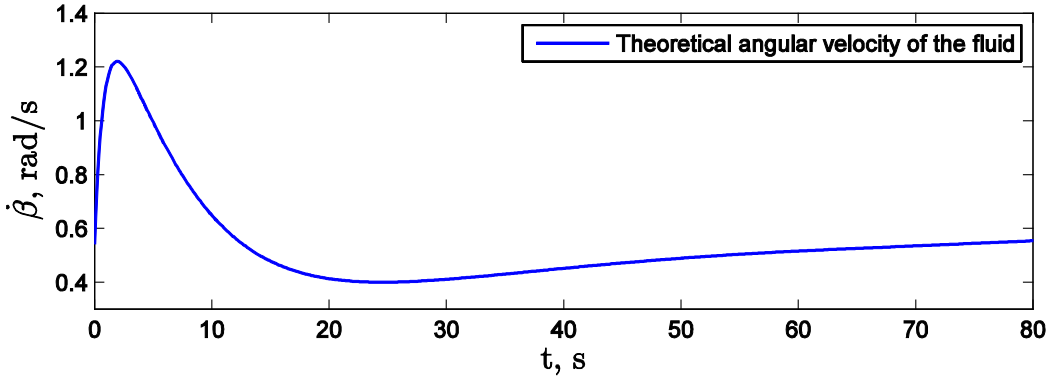

(c)

Figure 4.17: Desired fluid angular velocity in the: (a) Roll-axis ring; (b) Pitch-axis ring; (c) Yaw-axis ring

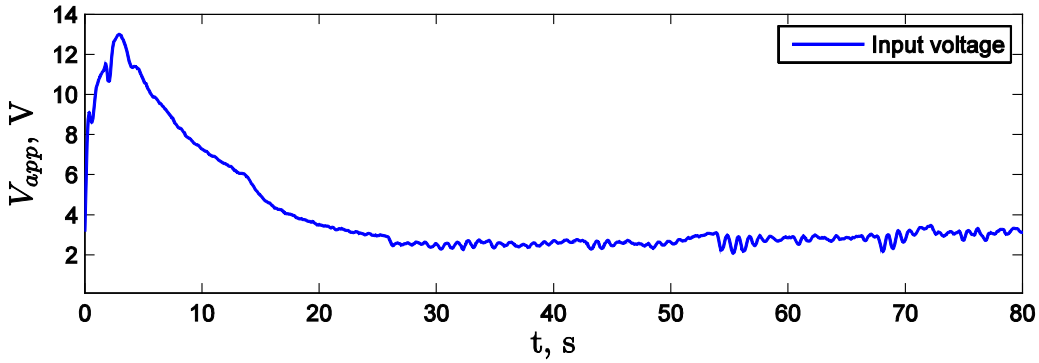

(a)

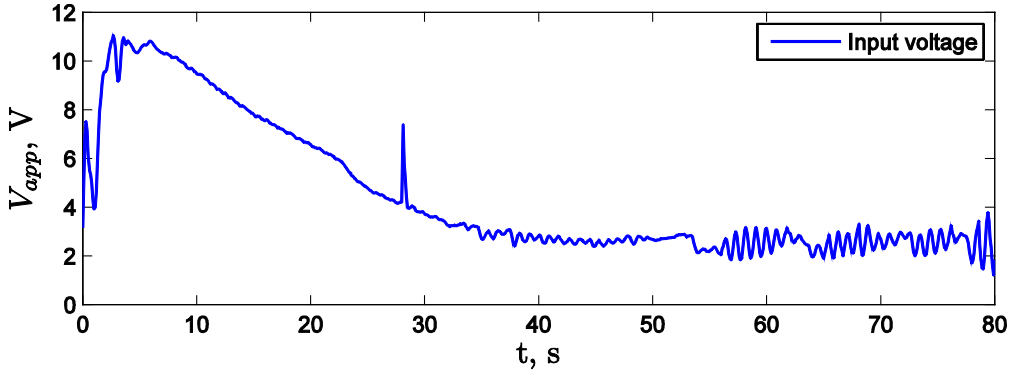

(b)

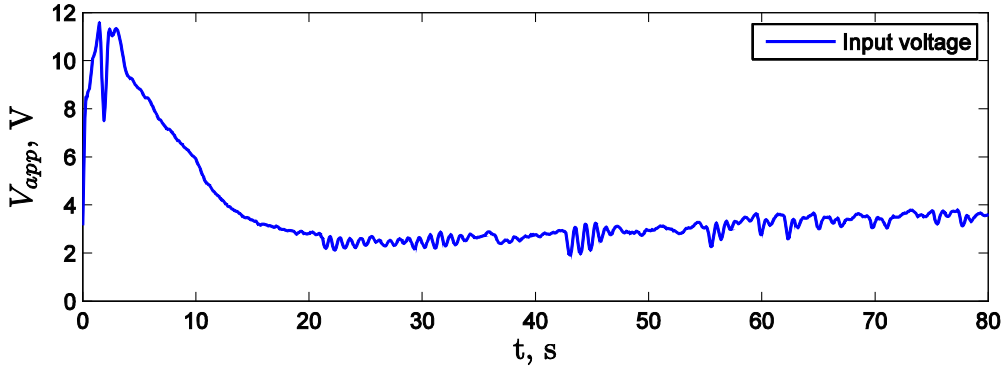

(c)

Figure 4.18: Applied voltage to the pumps on different rings versus time: (a) roll-axis; (b) pitch-axis; (c) yaw axis

4.5. Summary

In this chapter, a few experiments were conducted to validate the concept of utilizing fluid ring actuators. To this end, first, the selection of the material for the fabrication of the ring, the type of the pump, and the fluid were discussed. A copper ring which is equipped with a small centrifugal pump was built. The ring was filled with ethylene glycol, which is an antifreeze liquid and has appropriate characteristics for space applications. To perform the experiments, the empirical relation between the input voltage of the pump and the fluid angular velocity was found. Next, an experiment with a single fluid ring mounted on the simulator was conducted. The input voltage was applied to this system using a PD controller. The results achieved from the single fluid ring system were satisfactory, thus proving the concept of using fluid ring actuators. Next, a three dimensional attitude stabilization experiment was presented. Due to various imperfections, such as the malfunction of the pumps, the existence of air pockets in the fluid rings, and data loss during radio communication, this was performed as a hardware-in-the-loop experiment. Despite the pertinence of the results, it was concluded that, to produce a small fluid angular velocity of $1.5\ \mathrm{rad/s}$, a quite high voltage of about $13\ \mathrm{V}$ is required. Indeed, this fact limits the applications of the fluid rings as auxiliary actuators.

Chapter 5

SPINNING SATELLITES WITH FLUID RING ACTUATORS

The results of the experiments, reported in Chapter 4, showed that the fluid rings require a quite high voltage (above $12\ \mathrm{V}$) to produce a fluid angular velocity that is greater than $2\ \mathrm{rad/s}$. To produce this voltage, large-size batteries are required, which increase the overall mass of the satellite, and thus the total cost of the mission. Despite this drawback, the low mass of the fluid rings and their easy implementation justify the search for other applications, such as auxiliary attitude stabilization actuators. In this chapter, the use of fluid rings in spinning satellites is studied. A spinning satellite resists any variation of its orientation because of the bias momentum resulting from spinning about one of its axes. However, natural disturbances, such as solar radiation pressure, adversely affect the orientation of spinning satellites. The error resulting from such disturbance can be eliminated using a relatively small control torque. The application of fluid rings to pursue this objective is discussed in this chapter.

5.1. Development of the Dynamical Model

The system considered here is a symmetric spinning satellite consisting of two fluid rings whose axes of symmetry are aligned with the roll and yaw axes, as depicted in Figure 5.1.

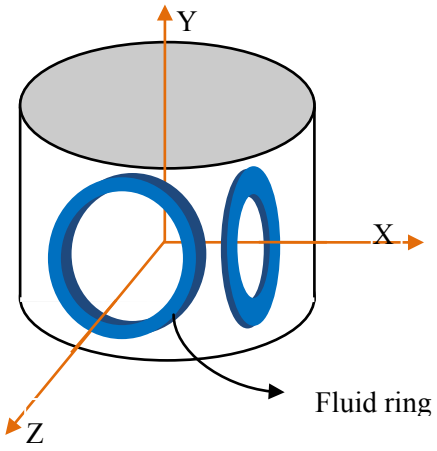

Figure 5.1: A cylindrical satellite with two fluid rings

The center of mass of each of the two fluid rings is assumed to coincide with that of the satellite. A local vertical and local horizontal (LVLH) reference frame with its origin located at the center of mass of the satellite is defined as follows: X_0 is along the local horizontal; Y_0 is perpendicular to the orbital plane; and Z_0 is directed towards the center of the Earth (Wie, 1998). The LVLH frame rotates about the Earth at the orbital rate of n. A spinning frame is defined that initially coincides with the LVLH reference frame; this frame spins about the Y_0-axis with respect to the LVLH frame with the angular velocity Ω. The third reference frame defined is the body fixed frame of the satellite whose axes coincide with the principal axes of the satellite; this frame is identical to the spinning frame, if the satellite does not tilt. Figure 5.2 shows the three coordinate frames introduced; for better visualization, the origin of the frames are shown non-coincident. The orientation of the satellite at any instant is described by three rotation angles, θ_1, θ_2, and θ_3, respectively, about the X, Y, and Z axes of the body fixed frame with respect to the LVLH frame. Also, Θ_1, Θ_2, and Θ_3 denote another set of rotation angles which describes the rotation of the body fixed frame with respect to the spinning frame. The relations between the attitude angles, θ_1, θ_2, and θ_3, and the set of rotation angles Θ_1, Θ_2, and Θ_3 are

$$\theta_1 = \Theta_1, \qquad \theta_2 = \Theta_2 + \Omega t, \qquad \theta_3 = \Theta_3 \tag{5.1}$$

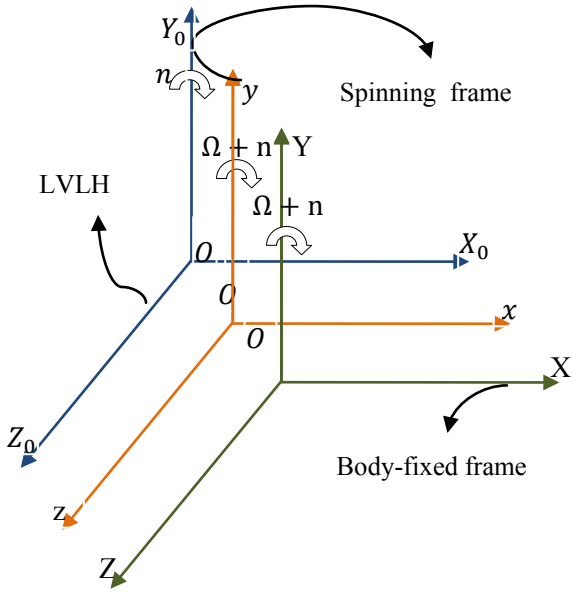

Figure 5.2: Three coordinates frames used in dynamical modeling

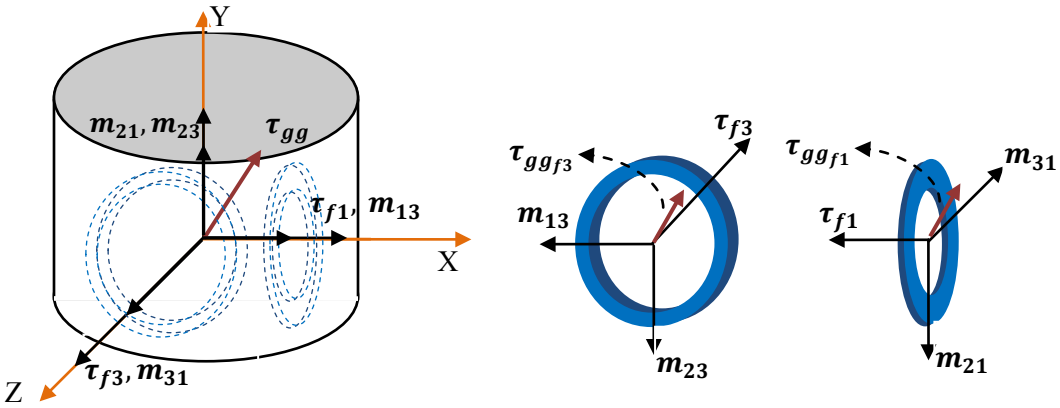

Figure 5.3: Free body diagrams of the satellite and two fluid rings (only moment vectors are shown)

The equations of motion of a spinning satellite with two fluid rings are derived using Eqs. (2.2) and (2.10) from Chapter 2. To this end, the term $\sum_{i=1}^{2} \boldsymbol{R_i \tau_{r_i}}$ is expanded, the rotation matrices $\boldsymbol{R_1}$ and $\boldsymbol{R_2}$ being recalled from Eq. (2.3).

$$\boldsymbol{I_s \dot{\omega} + \omega \times I_s \omega = \tau_{gg} + \tau_{r_1} + \tau_{r_3}} \tag{5.2}$$

$$\boldsymbol{I_{f1}\left(\dot{\omega} + \ddot{\beta}_1 + \omega \times \dot{\beta}_1\right) + \omega \times I_{f1}\left(\omega + \dot{\beta}_1\right) = -\tau_{r_1} + \tau_{gg_{f1}}} \tag{5.3}$$

$$\boldsymbol{I_{f3}\left(\dot{\omega} + \ddot{\beta}_3 + \omega \times \dot{\beta}_3\right) + \omega \times I_{f3}\left(\omega + \dot{\beta}_3\right) = -\tau_{r_3} + \tau_{gg_{f3}}} \tag{5.4}$$

where $\boldsymbol{\tau_{r_1}} = [\tau_{f1} \quad m_{21} \quad m_{31}]^T$ and $\boldsymbol{\tau_{r_3}} = [m_{13} \quad m_{23} \quad \tau_{f3}]^T$. Equations (5.2)-(5.4) are written in the body fixed frame of the satellite. The inertia matrix of the satellite, without considering the fluid itself, is denoted by $\boldsymbol{I_s}$. Let us assume here that $\boldsymbol{I_s}$ is diagonal with non-zero entries of I_t, I_a, I_t in the roll, pitch, and yaw directions, respectively; the y-axis is the axis of symmetry of the cylindrical satellite as per Figure 5.1. The axes of symmetry of the fluid rings are aligned with the roll and yaw axes; the inertia matrices of the fluid rings are as expressed below:

$$\boldsymbol{I_{f1}} = \begin{bmatrix} I_f & 0 & 0 \\ 0 & I_f/2 & 0 \\ 0 & 0 & I_f/2 \end{bmatrix}, \quad \boldsymbol{I_{f3}} = \begin{bmatrix} I_f/2 & 0 & 0 \\ 0 & I_f/2 & 0 \\ 0 & 0 & I_f \end{bmatrix}, \quad I_f = 2\pi\rho A r^3 \tag{5.5}$$

where ρ, A, and r denote the fluid density, the fluid ring cross-sectional area, and the fluid ring radius, respectively. Further, $\boldsymbol{\tau_{gg}}$, $\boldsymbol{\tau_{gg_{f1}}}$, and $\boldsymbol{\tau_{gg_{f3}}}$ are gravity gradient torques exerted on the satellite and the fluid rings. The terms $\dot{\boldsymbol{\beta}}_{\boldsymbol{1}} = [\dot{\beta}_1 \quad 0 \quad 0]^T$ and $\dot{\boldsymbol{\beta}}_{\boldsymbol{3}} = [0 \quad 0 \quad \dot{\beta}_3]^T$ are the angular velocity vectors of the fluid relative to the fluid loops. The free body diagrams of the satellite and each fluid rings are depicted in Figure 5.3. In this figure, m_{ij} for $i = 1, 2$ and $j = 1, 3$ is the reaction moment in the ith direction exerted by the jth fluid ring on the satellite. The reaction moments m_{ij} can be found from Eqs. (5.3) and (5.4) as:

$$m_{21} = -\boldsymbol{e_2^T}[\boldsymbol{I_{f1}}(\dot{\boldsymbol{\omega}} + \ddot{\boldsymbol{\beta}}_{\boldsymbol{1}} + \boldsymbol{\omega} \times \dot{\boldsymbol{\beta}}_{\boldsymbol{1}}) + \boldsymbol{\omega} \times \boldsymbol{I_{f1}}(\boldsymbol{\omega} + \dot{\boldsymbol{\beta}}_{\boldsymbol{1}}) - \boldsymbol{\tau_{gg_{f1}}}] \tag{5.6}$$

$$m_{31} = -\boldsymbol{e_3^T}[\boldsymbol{I_{f1}}(\dot{\boldsymbol{\omega}} + \ddot{\boldsymbol{\beta}}_{\boldsymbol{1}} + \boldsymbol{\omega} \times \dot{\boldsymbol{\beta}}_{\boldsymbol{1}}) + \boldsymbol{\omega} \times \boldsymbol{I_{f1}}(\boldsymbol{\omega} + \dot{\boldsymbol{\beta}}_{\boldsymbol{1}}) - \boldsymbol{\tau_{gg_{f1}}}] \tag{5.7}$$

$$m_{13} = -\boldsymbol{e_1^T}[\boldsymbol{I_{f3}}(\dot{\boldsymbol{\omega}} + \ddot{\boldsymbol{\beta}}_{\boldsymbol{3}} + \boldsymbol{\omega} \times \dot{\boldsymbol{\beta}}_{\boldsymbol{3}}) + \boldsymbol{\omega} \times \boldsymbol{I_{f3}}(\boldsymbol{\omega} + \dot{\boldsymbol{\beta}}_{\boldsymbol{3}}) - \boldsymbol{\tau_{gg_{f3}}}] \tag{5.8}$$

$$m_{23} = -\boldsymbol{e_2^T}[\boldsymbol{I_{f3}}(\dot{\boldsymbol{\omega}} + \ddot{\boldsymbol{\beta}}_{\boldsymbol{3}} + \boldsymbol{\omega} \times \dot{\boldsymbol{\beta}}_{\boldsymbol{3}}) + \boldsymbol{\omega} \times \boldsymbol{I_{f3}}(\boldsymbol{\omega} + \dot{\boldsymbol{\beta}}_{\boldsymbol{3}}) - \boldsymbol{\tau_{gg_{f3}}}] \tag{5.9}$$

where $\boldsymbol{e_1} = [1 \quad 0 \quad 0]^T$, $\boldsymbol{e_2} = [0 \quad 1 \quad 0]^T$, and $\boldsymbol{e_3} = [0 \quad 0 \quad 1]^T$. Since $\boldsymbol{e_i^T}\ddot{\boldsymbol{\beta}}_{\boldsymbol{j}}$ vanishes identically, Eqs. (5.6)−(5.9) can be used to replace m_{ij} in Eq. (5.2). Hence, the equations of motion of the satellite are obtained free of the fluid angular acceleration terms which can then be solved using a stable numerical integrator. In fact, the fluid acceleration terms only appear in the equations below, which are the first row of Eq. (5.3) and the third row of Eq. (5.4).

$$I_f\ddot{\beta}_1 + \boldsymbol{e_1^T}\left[\boldsymbol{I_{f1}}(\dot{\boldsymbol{\omega}} + \boldsymbol{\omega}\times\dot{\boldsymbol{\beta}}_{\boldsymbol{1}}) + \boldsymbol{\omega}\times\boldsymbol{I_{f1}}(\boldsymbol{\omega}+\dot{\boldsymbol{\beta}}_{\boldsymbol{1}}) - \boldsymbol{\tau_{gg_{f1}}}\right] + \tau_{f1} = 0 \tag{5.10}$$

$$I_f\ddot{\beta}_i + \boldsymbol{e_3^T}\left[\boldsymbol{I_{f3}}(\dot{\boldsymbol{\omega}} + \boldsymbol{\omega}\times\dot{\boldsymbol{\beta}}_{\boldsymbol{3}}) + \boldsymbol{\omega}\times\boldsymbol{I_{f3}}(\boldsymbol{\omega}+\dot{\boldsymbol{\beta}}_{\boldsymbol{3}}) - \boldsymbol{\tau_{gg_{f3}}}\right] + \tau_{f3} = 0 \tag{5.11}$$

The solution of Eqs. (5.10) and (5.11) yields the angular acceleration of the fluid.

5.2. Small Angle Approximation

Designing a controller for the system with the nonlinear mathematical model expressed in Eqs. (5.2), (5.10), and (5.11) is not straightforward. Therefore, to obtain some insight into the system dynamics, it is necessary to first approach the problem with a simplifying assumption on the magnitude of the attitude angles: the angles in question are small enough to allow simplification expressed hereafter. Before adopting the assumption on the magnitude of the angles in the mathematical model of the system, it is required to express these equations in terms of Θ_1, Θ_2, and Θ_3. In fact, the attitude angle θ_2, which is the rotation angle of the satellite about the spin axis, continuously grows, thus cannot be assumed small. However, the small angle assumption can be applied to θ_1 and θ_3. As mentioned earlier, the nominal spin rate of the satellite is denoted by Ω. Therefore, the absolute angular rate of the spinning frame is $\nu = \Omega + n$, as the satellite is considered to be in a circular orbit. The equations below relate the satellite angular velocity to the angles Θ_1, Θ_2, and Θ_3 and their derivatives using the small angle approximation (Hughes, 1986).

$$\begin{gathered}\omega_1 = \dot{\Theta}_1 - \nu\Theta_3 \rightarrow \dot{\omega}_1 = \ddot{\Theta}_1 - \nu\dot{\Theta}_3 \\ \omega_2 = \dot{\Theta}_2 - \nu \rightarrow \dot{\omega}_2 = \ddot{\Theta}_2 \\ \omega_3 = \dot{\Theta}_3 + \nu\Theta_1 \rightarrow \dot{\omega}_3 = \ddot{\Theta}_3 + \nu\dot{\Theta}_1\end{gathered} \tag{5.12}$$

The gravity gradient torque exerted on the satellite can be obtained as (Schaub and Junkins, 2003):

$$\boldsymbol{\tau_{gg}} = -3n^2\hat{\boldsymbol{a}}_{\boldsymbol{3}}\times\boldsymbol{J}.\hat{\boldsymbol{a}}_{\boldsymbol{3}} \tag{5.13}$$

where $\hat{\boldsymbol{a}}_{\boldsymbol{3}} \equiv \boldsymbol{r_c}/\|\boldsymbol{r_c}\|$, $\boldsymbol{r_c}$ being the position vector of the center of mass of the satellite with respect to the Earth center, described in the LVLH frame. To evaluate $\boldsymbol{\tau_{gg}}$ in the body fixed frame of the satellite, $\hat{\boldsymbol{a}}_{\boldsymbol{3}}$ is required to be expressed in this frame; this is possible upon applying the rotation matrix $\boldsymbol{C}$ defined below:

$$\boldsymbol{C} = \boldsymbol{C_1}(\Theta_1)\boldsymbol{C_2}(\Theta_2)\boldsymbol{C_3}(\Theta_3)\boldsymbol{C_2}(-\Omega \mathrm{t}) \tag{5.14}$$

where $\boldsymbol{C_i}(\Theta_j)$ is the matrix associated with the rotation of the angle Θ_j about the ith axis. Using Eq. (5.14), under the assumption of infinitesimal attitude angles, the gravity gradient torque can be obtained in the satellite body-fixed frame as:

$$\boldsymbol{\tau_{gg}} = -3n^2 \begin{bmatrix} (I_{yy} - I_{zz})(\Theta_3 \sin \Omega t \cos \Omega t + \Theta_1 \cos^2 \Omega t) \\ (I_{zz} - I_{xx})(\Theta_2 \sin^2 \Omega t - \Theta_2 \sin \Omega t \cos \Omega t - \Theta_2 \cos^2 \Omega t) \\ (I_{xx} - I_{yy})(-\Theta_3 \sin^2 \Omega t - \Theta_1 \cos \Omega t \sin \Omega t) \end{bmatrix} \tag{5.15}$$

In order to obtain the equation of motion of the satellite, Eqs. (5.2)−(5.4) are rewritten considering Eqs. (5.12) and (5.15). As mentioned before, the diagonal moment of inertia matrix of the satellite is $\boldsymbol{I_s}$= diag($I_{xx} = I_t,\ I_{yy} = I_a,\ I_{zz} = I_t$); therefore, the gravity gradient torque is zero in the Y direction. The equation describing the satellite rotation about the Y axis is not included, as it has the simple form: $I_a \ddot{\Theta}_2 = 0$. Moreover, as stated in Eq. (5.1), $\Theta_1 = \theta_1$ and $\Theta_3 = \theta_3$; thus, we have

$$\begin{gathered} (I_t + I_f/2)\ddot{\theta}_1 - (2I_t - I_a + I_f)\nu\dot{\theta}_3 \\ +(I_a - I_t - I_f/2)[\nu^2\theta_1 + 3n^2(\theta_1 c + \theta_3 s)c] - \tau_{f1} - I_f\nu\dot{\beta}_3 = 0 \end{gathered} \tag{5.16}$$

$$\begin{gathered} (I_t + I_f/2)\ddot{\theta}_3 + (2I_t - I_a + I_f)\nu\dot{\theta}_1 \\ +(I_a - I_t - I_f/2)[\nu^2\theta_3 + 3n^2(\theta_1 c + \theta_3 s)s] - \tau_{f3} + I_f\nu\dot{\beta}_1 = 0 \end{gathered} \tag{5.17}$$

$$I_f(\ddot{\beta}_1 + \ddot{\theta}_1) + \tau_{f1} - I_f\nu\dot{\theta}_3 = 0 \tag{5.18}$$

$$I_f(\ddot{\beta}_3 + \ddot{\theta}_3) + \tau_{f3} + I_f\nu\dot{\theta}_1 = 0 \tag{5.19}$$

Here, s and c denote $\sin \Omega t$ and $\cos \Omega t$, respectively. Next, a new set of variables γ_1 and γ_3 are defined in order to eliminate the periodic coefficients of s and c from Eqs. (5.16) and (5.17) (Hughes, 1986):

$$\begin{bmatrix}\theta_1\\ \theta_3\end{bmatrix} = \begin{bmatrix}\cos\Omega\, t & \sin\Omega t\\ -\sin\Omega t & \cos\Omega t\end{bmatrix}\begin{bmatrix}\gamma_1\\ \gamma_3\end{bmatrix} \tag{5.20}$$

Upon introducing this new set of variables, the abovementioned equations of motion of the spinning satellite become

$$\begin{gathered}\left(I_t + I_f/2\right)(\ddot{\gamma}_1 c - \ddot{\gamma}_3 s) + \left(2I_t n + I_a \nu + I_f n\right)(\dot{\gamma}_1 s + \dot{\gamma}_3 c)\\ -[I_a(n\nu - 3n^2) + 4I_t n^2 + 2I_f n^2]\gamma_1 c + \left(I_a n\nu + I_t n^2 + I_f/2n^2\right)\gamma_3 s\\ -\tau_{f1} - I_R \nu \dot{\beta}_3 = 0\end{gathered} \tag{5.21}$$

$$\begin{gathered}\left(I_t + I_f/2\right)(\ddot{\gamma}_1 s + \ddot{\gamma}_3 c) - \left(2I_t n + I_a \nu + I_f n\right)(\dot{\gamma}_1 c - \dot{\gamma}_3 s)\\ -[I_a(n\nu - 3n^2) + 4I_t n^2 + 2I_f n^2]\gamma_1 s - \left(I_a n\nu + I_t n^2 + I_f/2n^2\right)\gamma_3 c\\ -\tau_{f3} + I_f \nu \dot{\beta}_1 = 0\end{gathered} \tag{5.22}$$

$$\begin{gathered}I_f(\ddot{\beta}_1 + \ddot{\gamma}_1 c - \ddot{\gamma}_3 s) + \left(2I_f n + I_f \nu\right)\dot{\gamma}_1 s + \left(2I_f n + I_f \nu\right)\dot{\gamma}_3 c\\ -\left(I_f n\nu + I_f n^2\right)\gamma_1 c + \left(I_f n\nu + I_f n^2\right)\gamma_3 s + \tau_{f1} = 0\end{gathered} \tag{5.23}$$

$$\begin{gathered}I_f(\ddot{\beta}_3 + \ddot{\gamma}_1 s + \ddot{\gamma}_3 c) - \left(2I_f n + I_f \nu\right)\dot{\gamma}_1 c + \left(2I_f n + I_f \nu\right)\dot{\gamma}_3 s\\ -\left(I_f n\nu + I_f n^2\right)\gamma_1 s - \left(I_f n\nu + I_f n^2\right)\gamma_3 c + \tau_{f3} = 0\end{gathered} \tag{5.24}$$

In order to proceed to design a linear controller for the system, first, we need to eliminate the time-varying variables denoted by s and c from Eqs. (5.21) and (5.22). This is done in two steps: (i) The time-varying coefficient of the terms $\ddot{\gamma}_1$ and $\ddot{\gamma}_3$ are first eliminated by obtaining two new equations via forming the linear combination of the two equations in question, as per the relation below:

$$\begin{gathered}Eq.(5.21)\, c + Eq.(5.22)\, s = 0\\ -Eq.(5.21)\, s + Eq.(5.22)\, c = 0\end{gathered} \tag{5.25}$$

Expanding Eq. (5.25) yields:

$$\begin{aligned}\left(I_t + I_f/2\right)\ddot{\gamma}_1 + \left(2I_t n + I_a \nu + I_f n\right)\dot{\gamma}_3 - [I_a(n\nu - 3n^2) + 4I_t n^2 + 2I_f n^2]\gamma_1 \\ -\tau_{f1} c - I_f \nu \dot{\beta}_3 c - \tau_{f3} s + I_f \nu \dot{\beta}_1 s = 0\end{aligned} \tag{5.26}$$

$$\begin{aligned}\left(I_t + I_f/2\right)\ddot{\gamma}_3 - \left(2I_t n + I_a \nu + I_f n\right)\dot{\gamma}_1 - [I_a n\nu + I_t n^2 + I_f/(2n\text{^}2\ )]\gamma_3 \\ +\tau_{f1} s + I_f \nu \dot{\beta}_3 s - \tau_{f3} c + I_f \nu \dot{\beta}_1 c = 0\end{aligned} \tag{5.27}$$

(ii) The remaining terms with the time-varying coefficient s and c are handled by regrouping the variables. A control input can be defined that includes the terms having the time-varying coefficient. This control input simplifies the controller design. However, prior to this operation, the variables are non-dimensionalized.

5.2.1. Non-dimensionalization

In order to reduce the effect of computational errors and enhance the applicability of the results, equations obtained in the preceding section are non-dimensionalized. To this end, the non-dimensional time variable $T = nt$ is used, similar to Subsection 2.1.1. The non-dimensional angular velocity terms can then be defined as:

$$\gamma_1' \equiv \dot{\gamma}_1/n, \qquad \gamma_3' \equiv \dot{\gamma}_3/n, \qquad \beta_1' \equiv \dot{\beta}_1/n, \qquad \beta_3' \equiv \dot{\beta}_3/n, \qquad \hat{\nu} \equiv (\Omega/\mathrm{n}) + 1 \tag{5.28}$$

Hence, the non-dimensional form of Eqs. (5.23), (5.24), (5.26), and (5.27) are:

$$\begin{aligned}(K_t + K_R/2)\gamma_1'' + (2K_t + \hat{\nu} + K_R)\gamma_3' - [(\hat{\nu} - 3) + 4K_t + 2K_R]\gamma_1 \\ -\hat{\tau}_{f1} c - K_R \hat{\nu} \beta_3^{'} c - \hat{\tau}_{f3} s + K_R \hat{\nu} \beta_1^{'} s = 0\end{aligned} \tag{5.29}$$

$$\begin{aligned}(K_t + K_R/2)\gamma_1'' + (2K_t + \hat{\nu} + K_R)\gamma_3' - [(\hat{\nu} - 3) + 4K_t + 2K_R]\gamma_1 \\ -\hat{\tau}_{f1} c - K_R \hat{\nu} \beta_3^{'} c - \hat{\tau}_{f3} s + K_R \hat{\nu} \beta_1^{'} s = 0\end{aligned} \tag{5.30}$$

$$K_R[\beta_1'' + \gamma_1'' c - \gamma_3'' s + (2 + \hat{\nu})(\gamma_1' s + \gamma_3' c) - (1 + \hat{\nu})(\gamma_1 c - \gamma_3 s)] + \hat{\tau}_{f1} = 0 \tag{5.31}$$

$$K_R[\beta_3'' + \gamma_1'' s + \gamma_3'' c - (2 + \hat{\nu})(\gamma_1' c - \gamma_3' s) - (1 + \hat{\nu})(\gamma_1 s + \gamma_3 c)] + \hat{\tau}_{f3} = 0 \tag{5.32}$$

where K_t, K_R are the inertia ratios defined below:

$$K_t \equiv I_t/I_a\,, \quad K_R \equiv I_f/I_a \tag{5.33}$$

Moreover, $\hat{\tau}_{f1}$ and $\hat{\tau}_{f3}$ are non-dimensional form of the fluid friction torques, as defined earlier in Eq. (2.26):

$$\hat{\tau}_{fi} = -16\,\pi\, a_1 a_2 \hat{d}\beta_i', \qquad \text{for } i = 1, 3 \tag{5.34}$$

where $\hat{d}$, a_1, and a_2 are the non-dimensional parameters defined below:

$$\hat{d} \equiv d/r\,, \qquad a_1 \equiv (\rho\pi r^5)/I_a\,, \qquad a_2 \equiv \mu/(\rho r n D) \tag{5.35}$$

5.3. Design of a Controller for the Linear Model

To design a controller, the control input terms τ_1^c and τ_3^c are added to the right hand side of the equations of motion of the satellite (5.29) and (5.30). As discussed in Section 5.2, a regrouping of the variables is needed to eliminate the time-varying coefficients s and c from Eqs. (5.29) and (5.30); this leads to

$$(K_t + K_R/2)\gamma_1'' + (2K_t + \hat{v} + K_R)\gamma_3' - [(\hat{v} - 3) + 4K_t + 2K_R]\gamma_1 = v_1^c \tag{5.36}$$

$$(K_t + K_R/2)\gamma_3'' - (2K_t + \hat{v} + K_R n)\gamma_1' - (\hat{v} + K_t + K_R/2)\gamma_3 = v_3^c \tag{5.37}$$

where

$$v_1^c = \tau_1^c - (-\hat{\tau}_{f1}c - K_R\hat{v}\beta_3' c - \hat{\tau}_{f3}s + K_R\hat{v}\beta_1' s) \tag{5.38}$$

$$v_3^c = \tau_3^c - (\hat{\tau}_{f1}s + K_R\hat{v}\beta_3' s - \hat{\tau}_{f3}c + K_R\hat{v}\beta_1' c) \tag{5.39}$$

Since Eqs. (5.36) and (5.37) are linear, a controller can be designed using the pole placement method, which is simple to implement. To this end, the system equations are first expressed in the state-space form:

$$\dot{\boldsymbol{x}} = \boldsymbol{A}\boldsymbol{x} + \boldsymbol{B}\boldsymbol{v} \tag{5.40}$$

where $\boldsymbol{x} = [x_1 \quad x_2 \quad x_3 \quad x_4]^T$ is the state vector of the system with $x_1 = \gamma_1$, $x_2 = \gamma_1'$, $x_3 = \gamma_3$, and $x_4 = \gamma_3'$. The matrices $\boldsymbol{A}$ and $\boldsymbol{B}$ are

$$\boldsymbol{A} = \begin{bmatrix} 0 & 1 & 0 & 0 \\ q_1 & 0 & 0 & -q_2 \\ 0 & 0 & 0 & 1 \\ 0 & q_3 & q_4 & 0 \end{bmatrix}, \quad \boldsymbol{B} = \begin{bmatrix} 0 & 0 \\ 1 & 0 \\ 0 & 0 \\ 0 & 1 \end{bmatrix} \tag{5.41}$$

where

$$q_1 = [(\hat{v} - 3) + 4K_t + 2K_R]/(K_t + K_R/2); \quad q_2 = q_3 = (2K_t + \hat{v} + K_R)/(K_t + K_R/2)$$
$$q_4 = (\hat{v} + K_t + K_R/2)/(K_t + K_R/2) \tag{5.42}$$

The controllability of the system can be determined by finding the rank of the *controllability matrix* $\boldsymbol{M} = [\boldsymbol{B} \quad \boldsymbol{AB} \quad \boldsymbol{A^2B} \quad \boldsymbol{A^3B}]$ (Ogata, 2009). This matrix is full row rank, as in general, $q_1\, q_4$ is non-zero. The feedback control law applied to the system has the form $\boldsymbol{v} = \boldsymbol{Kx}$, where

$$\boldsymbol{K} = [\alpha_4 - a_4 \quad \alpha_3 - a_3 \quad \alpha_2 - a_2 \quad \alpha_1 - a_1]\boldsymbol{T}^{-1} \tag{5.43}$$

in which a_i, for $i = 1, \ldots, 4$ are the coefficients of the characteristic equation of the open-loop system:

$$a_1 = 0, \quad a_2 = q_2\, q_3 - q_1 - q_4, \quad a_3 = 0, \quad a_4 = q_1\, q_4 \tag{5.44}$$

Further, parameters α_i for $i = 1, \ldots, 4$ are the coefficients of the characteristic equation of the closed loop system. To find these, for each control input v_1^c and v_3^c, an appropriate set of poles p_1 to p_4 is chosen; here, for the sake of simplicity, identical values are chosen for different poles. In Eq. (5.43), matrix $\boldsymbol{T} = \boldsymbol{MW}$, while $\boldsymbol{W}$ is

$$\boldsymbol{W} = \begin{bmatrix} a_3 & a_2 & a_1 & 1 \\ a_2 & a_1 & 1 & 0 \\ a_1 & 1 & 0 & 0 \\ 1 & 0 & 0 & 0 \end{bmatrix} \tag{5.45}$$

What has been obtained so far are the artificial control inputs v_1^c and v_3^c. However, the objective is to find the angular velocity magnitudes of the fluid in the two rings which stabilize the system. To this end, upon adding the control inputs τ_1^c and τ_3^c, the ordinary differential equations (5.31)

and (5.32) should be solved simultaneously with the algebraic equations (5.38) and (5.39). The pertaining differential equations are repeated below for convenience. The solution process is that, at every step, the values of τ_1^c and τ_3^c are obtained from Eqs. (5.38) and (5.39) knowing β_1' and β_3' at the same step. Substituting τ_1^c and τ_3^c into Eqs. (5.31) and (5.32), the equations below are found from which the values of β_1' and β_3' can be obtained for the next step. The same process is repeated to complete the solution.

$$K_R[\beta_1'' + \gamma_1'' c - \gamma_3'' s + (2+\hat{v})(\gamma_1' s + \gamma_3' c) - (1+\hat{v})(\gamma_1 c - \gamma_3 s)] + \hat{\tau}_{f1} = -\tau_1^c \tag{5.46}$$

$$K_R[\beta_3'' + \gamma_1'' s + \gamma_3'' c - (2+\hat{v})(\gamma_1' c - \gamma_3' s) - (1+\hat{v})(\gamma_1 s + \gamma_3 c)] + \hat{\tau}_{f3} = -\tau_3^c \tag{5.47}$$

5.3.1. Numerical results for the linear model

The performance of the controller and the fluid rings is examined by considering a 50 kg cylindrical satellite with the radius and height of 0.3 m and 1 m, respectively. The principal moments of inertia of the satellite about its center of mass are $I_{xx} = 5.29\ \text{kgm}^2$, $I_{yy} = 2.25\ \text{kgm}^2$, and $I_{zz} = 5.29\ \text{kgm}^2$. Moreover, the same fluid rings and orbit are chosen as the case study introduced in Chapters 2 and 3. This implies that the two fluid rings in the roll and yaw directions are assumed to have a radius of 0.2 m and the cross-sectional diameter of 0.02 m, the satellite is in an orbit with an altitude of 700 km. The initial values of the attitude angles, their rates, and the relative angular velocity of the fluid in the fluid rings are chosen as $\pi/36$ rad, 10^{-4} rad/s, and zero, respectively. The spin rate of the satellite is considered to be $50n$, where $n = 1.1 \times 10^{-3}$ rad/s is the mean orbital rate.

For the sake of simplicity, all poles desired are assumed to coincide. In general, large negative poles result in a faster stabilization, but with more energy consumption. This implies that there is a trade off in choosing the poles. In our problem, there is an additional significant constraint in choosing the poles: they should not be too large not to violate the small-angle assumption. To comply with this constraint, the attitude angles are considered to be bounded below 0.25 rad, the poles being chosen as -10. Simulating the motion of the system, Figure 5.4 shows that the satellite is stabilized in both the roll and yaw directions in about 0.2 of an orbital period.

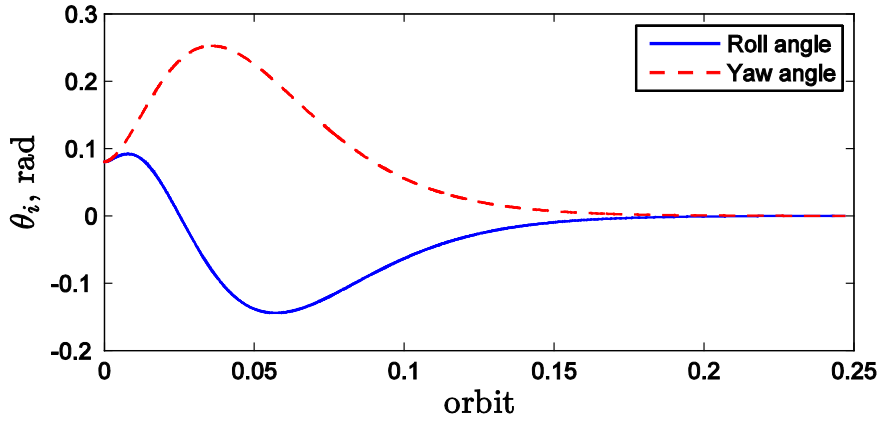

Figure 5.4: Roll and yaw angles using the linear controller with $p_i = -10$

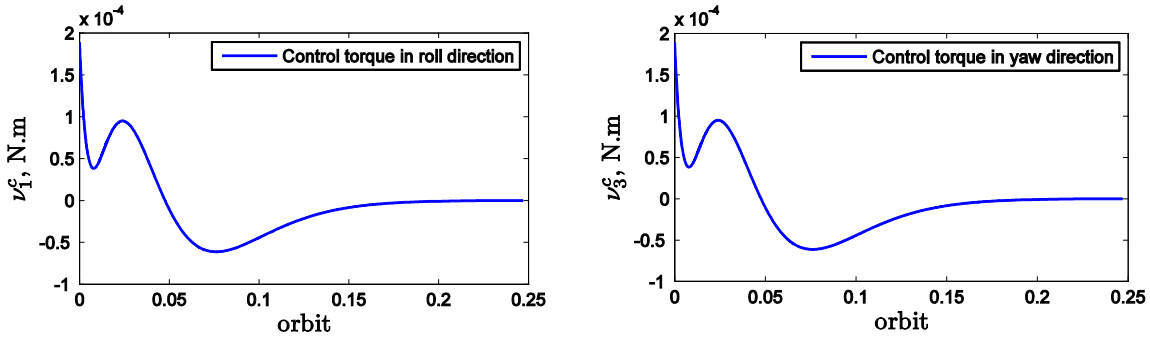

Figure 5.5: Control torque in the roll and yaw directions using the linear controller with $p_i = -10$

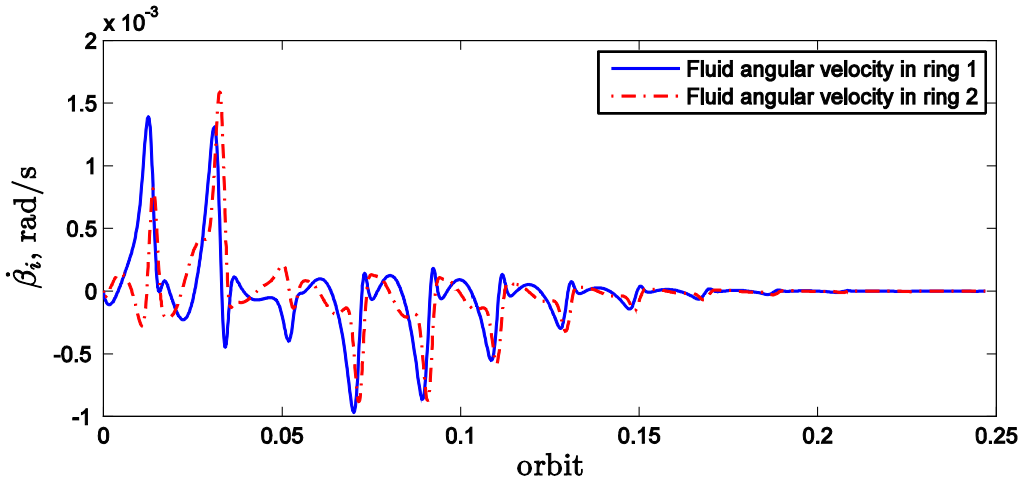

Figure 5.6: Fluid angular velocity using the linear controller with $p_i = -10$

The control torque required to stabilize the satellite is plotted in Figure 5.5. The maximum control torque required is less than 5×10^{-4} N. m, which is quite small. The variations of the fluid angular velocity producing this control torque are also illustrated in Figure 5.6, the maximum fluid angular velocity being about 1.5×10^{-3} rad/s.

5.4. Design of the Controller for the Nonlinear Model

In the light of the results obtained in the study of the linear model, in this section, a controller is designed for the complete nonlinear model. To this end, the same approach is taken: we resort to a modified control input vector $\boldsymbol{v^c} = [v_1^c \quad 0 \quad v_3^c]^T$, which includes all the terms with s and c coefficients; the equations of motion of the satellite (5.2) can thus be written as:

$$\boldsymbol{I_s\dot{\omega} + \omega \times I_s\omega = v^c} \tag{5.48}$$

$$v_i^c = \boldsymbol{e_i^T}(\boldsymbol{\tau_{gg}} + [\tau_{f1} \quad m_{21} \quad m_{31}]^T + [m_{13} \quad m_{23} \quad \tau_{f3}]^T) + \tilde{\tau}_i^c \qquad \text{for } i = 1, 3 \tag{5.49}$$

were $\boldsymbol{\tau^c} = [\tilde{\tau}_1^c \quad 0 \quad \tilde{\tau}_3^c]$, $\boldsymbol{e_1}$ and $\boldsymbol{e_3}$ being the unit vectors $[1 \quad 0 \quad 0]^T$ and $[0 \quad 0 \quad 1]^T$, respectively. The fluid angular velocity in the two rings can be obtained from Eqs. (5.3) and (5.4) reproduced below with the control input $\tilde{\tau}_i^c$ for $i = 1, 3$ implemented.

$$\ddot{\beta}_i = -\boldsymbol{e_i^T}\{\dot{\boldsymbol{\omega}} + \boldsymbol{\omega} \times \dot{\boldsymbol{\beta}}_{\boldsymbol{i}} + \boldsymbol{I_{fi}^{-1}}[\boldsymbol{\omega} \times \boldsymbol{I_{fi}}(\boldsymbol{\omega} + \dot{\boldsymbol{\beta}}_{\boldsymbol{i}})] + \boldsymbol{\tau_{gg_{fi}}}\} + \tau_{fi} - \tilde{\tau}_i^c, \quad \text{for i} = 1, 3 \tag{5.50}$$

Before designing a controller, Eqs. (5.48)−(5.50) are non-dimensionalized as:

$$\boldsymbol{\hat{I}_s\omega' + \hat{\omega} \times \hat{I}_s\hat{\omega} = \hat{v}^c} \tag{5.51}$$

$$\hat{v}_i^c = \boldsymbol{e_i^T}(\boldsymbol{\hat{\tau}_{gg}} + [\hat{\tau}_{f1} \quad \hat{m}_{21} \quad \hat{m}_{31}]^T + [\hat{m}_{13} \quad \hat{m}_{23} \quad \hat{\tau}_{f3}]^T) + \hat{\tau}_i^c \tag{5.52}$$

$$\beta_i'' = \boldsymbol{e_i^T}\{\boldsymbol{\omega'} + \hat{\boldsymbol{\omega}} \times \boldsymbol{\beta_i'} + \boldsymbol{\hat{I}_{fi}^{-1}}[\hat{\boldsymbol{\omega}} \times \boldsymbol{\hat{I}_{fi}}(\hat{\boldsymbol{\omega}} + \boldsymbol{\beta_i'})] + \boldsymbol{\hat{\tau}_{gg_{fi}}}\} + \hat{\tau}_{fi} - \hat{\tau}_i^c \tag{5.53}$$

for $i = 1$ and 3. Further, $\boldsymbol{\hat{I}_s}$, $\boldsymbol{\hat{I}_{f1}}$, and $\boldsymbol{\hat{I}_{f3}}$ are the non-dimensional inertia matrices as follows:

$$\hat{\boldsymbol{I}}_{\boldsymbol{s}} = \begin{bmatrix} K_t & 0 & 0 \\ 0 & 1 & 0 \\ 0 & 0 & K_t \end{bmatrix}, \hat{\boldsymbol{I}}_{\boldsymbol{f1}} = \begin{bmatrix} K_R & 0 & 0 \\ 0 & K_R/2 & 0 \\ 0 & 0 & K_R/2 \end{bmatrix}, \hat{\boldsymbol{I}}_{\boldsymbol{f3}} = \begin{bmatrix} K_R/2 & 0 & 0 \\ 0 & K_R/2 & 0 \\ 0 & 0 & K_R \end{bmatrix} \tag{5.54}$$

where K_t and K_R are given in Eq. (5.33). In the non-dimensional equations, $\hat{\boldsymbol{\omega}}$, $\hat{\boldsymbol{\tau}}_{\boldsymbol{gg}}$, $\hat{\boldsymbol{\tau}}_{\boldsymbol{gg_{fi}}}$ are

$$\hat{\boldsymbol{\omega}} \equiv \boldsymbol{\omega}/n, \quad \hat{\boldsymbol{\tau}}_{\boldsymbol{gg}} \equiv \boldsymbol{\tau}_{\boldsymbol{gg}}/(\boldsymbol{I}_{\boldsymbol{a}}\, n), \quad \hat{\boldsymbol{\tau}}_{\boldsymbol{gg_{fi}}} \equiv \boldsymbol{\tau}_{\boldsymbol{gg_{fi}}}/(\boldsymbol{I}_{\boldsymbol{a}} n) \tag{5.55}$$

Now, a modified PD controller is designed as:

$$\hat{v}_i^c = K_{p1_i}(\theta_1 - \theta_{1d}) + K_{d1_i}(\theta_1' - \theta_{1d}') + K_{p2_i}(\theta_2 - \theta_{2d}) + K_{d2_i}(\theta_2' - \theta_{2d}'), \text{ for } i = 1,3 \tag{5.56}$$

where the gains K_{p1_i}, K_{p2_i}, K_{d1_i}, and K_{d2_i} of the controller can be chosen from the feedback control matrix $\boldsymbol{K}$ obtained using the pole placement method in the linear analysis. This implies that the elements of the first and second row of the matrix $\boldsymbol{K}$ are to be used for the gains of the $\hat{v}_1^c$ and $\hat{v}_2^c$, respectively.

5.4.1. Numerical results for the nonlinear system

The performance of the fluid ring actuators in spinning satellites are discussed here when the nonlinear dynamical model is used. The numerical parameters chosen are identical to the ones introduced in Subsection 5.3.1. The gains of the modified PD control law are chosen from the feedback controller obtained using the poles chosen as -10. In Figures 5.7 and 5.8, the pitch, roll and yaw angles are plotted versus the number of orbits. The pitch angle linearly increases with time due to the constant spin rate of the satellite. However, the roll and yaw angles are stabilized in 0.2 of an orbit. This shows that the linearized model can represent the nonlinear system with a good approximation. Further, the oscillations of the roll and yaw angles about zero degree represents the need for higher control gains.

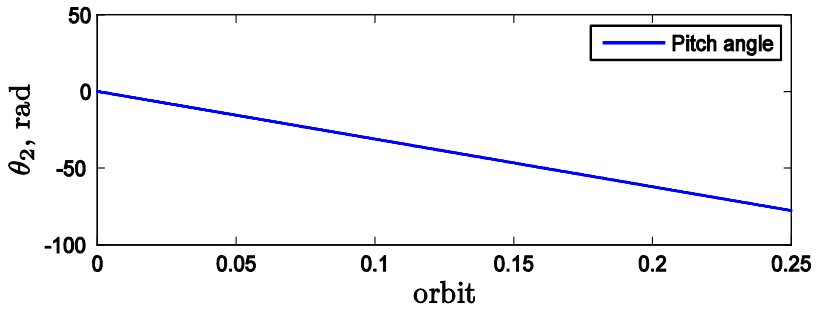

Figure 5.7: Pitch angle θ_2 while using the modified PD controller with the gains obtained from the linear controller: $K_{p1_i} = 364$; $K_{d1_i} = -25$; $K_{p2_i} = 140$; and $K_{d2_i} = -23$

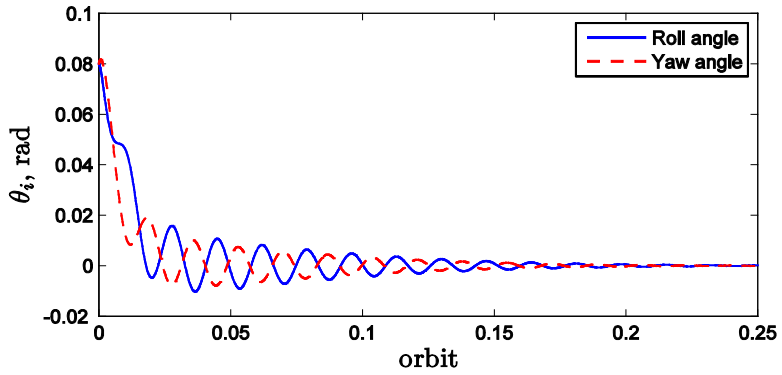

Figure 5.8: Roll and yaw angles (θ_1 and θ_3), while utilizing the modified PD controller with the gains obtained from the linear controller: $K_{p1_i} = 364$; $K_{d1_i} = -25$; $K_{p2_i} = 140$; and $K_{d2_i} = -23$

Shown in Figures 5.9 and 5.10, respectively, are the plots of the control torque values required in the roll and yaw directions and also the fluid angular velocities. Considering Figure 5.9, the maximum torque required is less than 5×10^{-4} N. m, which is fairly small torque. To produce this amount of control torque, the maximum angular velocity of the fluid is about 0.1 rad/s. Using Eqs. (4.1) and (4.20), the maximum voltage required is about 9 V, which is acceptable.

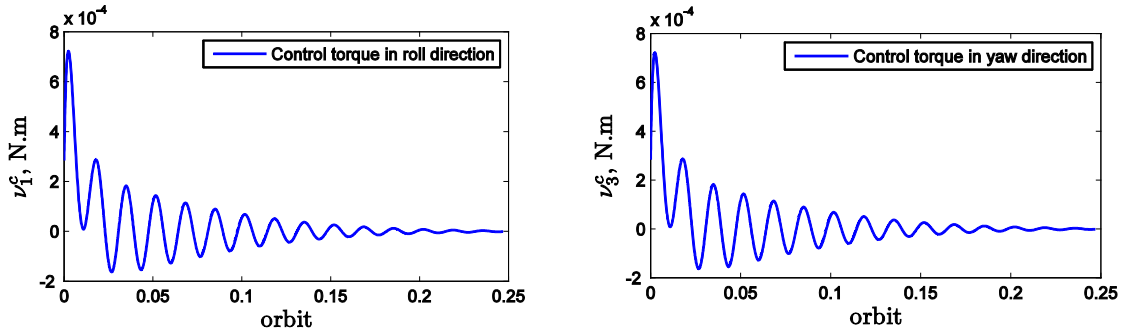

Figure 5.9: Control torque produced by the modified PD controller with the gains obtained from the linear controller: $K_{p1_i} = 364$; $K_{d1_i} = -25$; $K_{p2_i} = 140$; and $K_{d2_i} = -23$

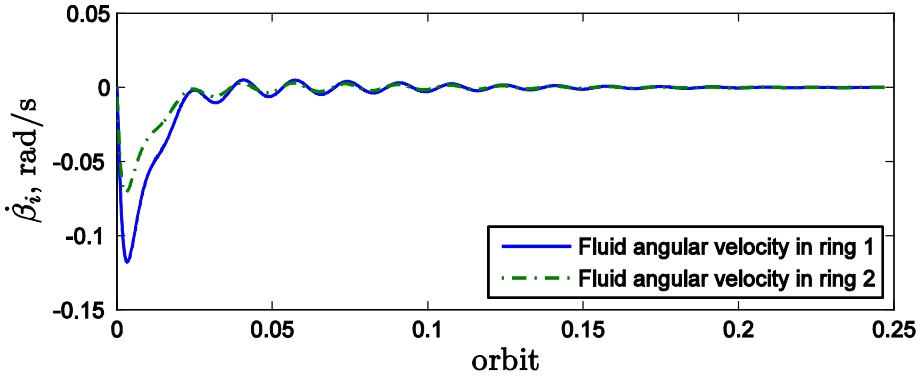

Figure 5.10: Angular velocity of the fluid, while using the modified PD controller with the gains obtained in the linear controller: $K_{p1_i} = 364$; $K_{d1_i} = -25$; $K_{p2_i} = 140$; **and** $K_{d2_i} = -23$

As mentioned previously, although the results are satisfactory, to eliminate the oscillations in the response of the attitude angles shown in Figures 5.7 and 5.8, the modified PD controller gains can be slightly changed as $= 350$; $K_{p2_i} = 140$; $K_{d1_1} = -25$; $K_{d2_1} = -5$; $K_{d1_2} = -5$; and $K_{d2_2} = -25$. Figures 5.11−5.13 show the variation of the satellite attitude angles, the control torque, and the fluid angular velocity, respectively, after applying this new set of gains to the modified PD controller. As can be seen, the satellite stabilization time is reduced by five times, while the maximum torque and the maximum fluid angular velocity required remain in the same range.

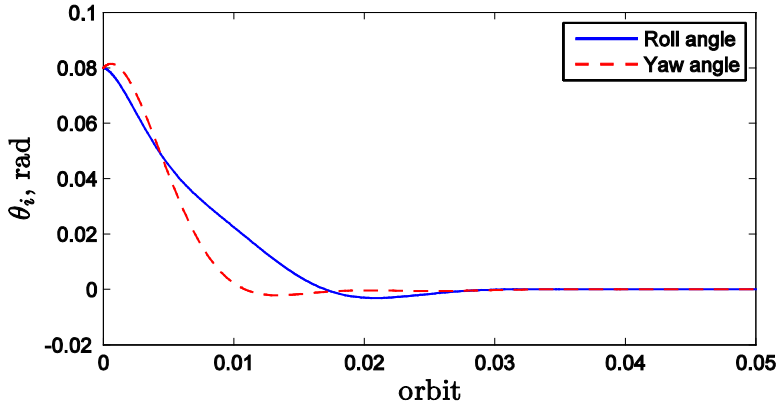

Figure 5.11: Roll and yaw angles (θ_1 and θ_3), while using the modified PD controller with the gains of $K_{p1_i} = 350$; $K_{p2_i} = 140$; $K_{d1_1} = -25$; $K_{d2_1} = -5$; $K_{d1_2} = -5$; **and** $K_{d2_2} = -25$

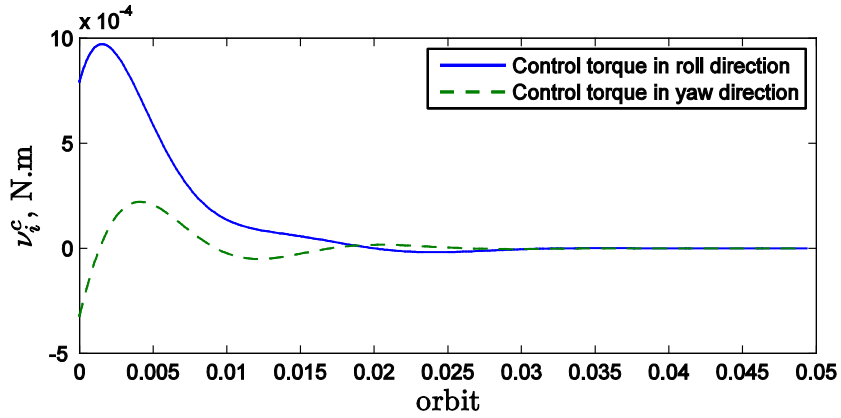

Figure 5.12: Control torque produced by the modified PD controller with the gains of $K_{p1_i} = 350$; $K_{p2_i} = 140$; $K_{d1_1} = -25$; $K_{d2_1} = -5$; $K_{d1_2} = -5$; **and** $K_{d2_2} = -25$

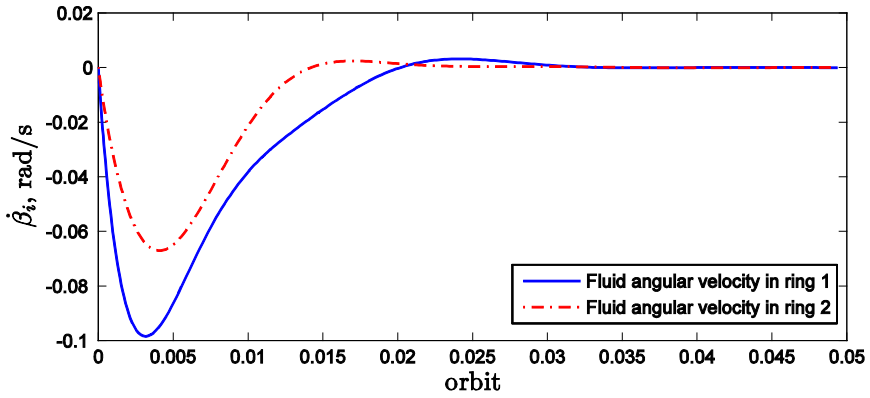

Figure 5.13: : Angular velocity of the fluid, while using the modified PD controller with the gains of $K_{p1_i} = 350$; $K_{p2_i} = 140$; $K_{d1_1} = -25$; $K_{d2_1} = -5$; $K_{d1_2} = -5$; **and** $K_{d2_2} = -25$

5.5. Summary

In this chapter, the attitude dynamics and control of a spinning satellite using two fluid rings as attitude actuators were investigated. To obtain a better understanding of the system's behaviour, first, a linear dynamical model of this satellite and the fluid rings was developed. Then, by applying the pole placement method, a controller was designed to asymptotically stabilize the attitude angles. A similar analysis was carried out using the nonlinear model, where a modified PD controller was designed to stabilize the satellite dynamics. The same gains as the ones obtained for the linear feedback controller were used in this modified PD controller. The performance of the fluid ring actuators was then improved by changing the controller's gains

slightly. The results achieved were satisfactory: the magnitude of the fluid angular velocity required was acceptably small, while the satellite was stabilized quite fast.

Chapter 6

A HYBRID ATTITUDE CONTROLLER CONSISTING OF ECTROMAGNETIC TORQUE RODS AND A FLUID RING

To select an appropriate attitude control actuator, one issue to consider is the size of the satellite. Small satellites are constrained by their mass and the power budget. Moreover, the stabilizing torque that small satellites require is not so large. Magnetic actuators are appropriate for the attitude control of small satellites, especially as these actuators are quite light. The downside of the electromagnetic actuators is that they cannot produce a general three-dimensional torque. Nevertheless, although slowly, a satellite can be completely stabilized by using two magnetic coils due to the strong dynamics coupling between the roll and yaw motions. It is shown in this chapter that adding an active fluid ring to the system of two magnetic actuators will lead to a faster stabilization.

6.1. Dynamics Modeling

To formulate the dynamics model, a LVLH reference frame located at the center of mass of the satellite is defined, as in Section 2.1 (Figure 2.3): Y_0 is perpendicular to the orbital plane; Z_0 is directed towards the center of the Earth; and X_0 is defined so as to obtain a right hand coordinate system. At the equilibrium configuration, the principal axes of the satellite are aligned with the LVLH reference frame. The orientation of the satellite at any instant is described by three rotation angles θ_1, θ_2, and θ_3 about X, Y, and Z axes of the body frame, respectively. Moreover, the satellite is considered to have two magnetic coils which produce torques along the roll and pitch axes as well as a fluid ring whose axis of symmetry is in the yaw direction, as depicted in Figure 6.1. The center of mass of each coil and the fluid ring is assumed to coincide with that of the satellite.

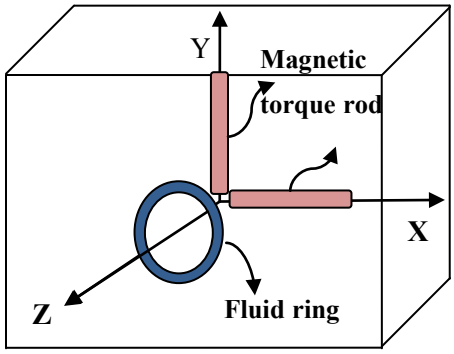

Figure 6.1: A satellite with two magnetic coils and one fluid ring

The equations governing the motion of the satellite and the fluid ring are

$$\boldsymbol{I_s\dot{\omega} + \omega \times I_s\omega = \tau_{gg} + \tau^c + \tau_r} \tag{6.1}$$

$$\boldsymbol{I_f\left(\dot{\omega} + \ddot{\beta} + \omega \times \dot{\beta}\right) + \omega \times I_f\left(\omega + \dot{\beta}\right) = \tau_{gg_f} - \tau_r - \tau_p} \tag{6.2}$$

Equations (6.1) and (6.2) are obtained from Eqs. (2.2) and (2.10) as per the explanation given hereafter: since there is only one fluid ring in this satellite, the terms $\sum_{i=1}^{k} \boldsymbol{R_i\tau_{r_i}}$ are replaced by $\boldsymbol{\tau_r} = [m_{11} \quad m_{21} \quad \tau_f]^T$, where m_{11} and m_{21} are the reaction moments exerted by the fluid ring along the roll and pitch directions, respectively. Further, τ_f is the fluid friction

torque which can be obtained using Eq. (2.16). In Eq. (6.1), the control torque $\boldsymbol{\tau^c}$ includes the torque $\boldsymbol{\tau_m}$ produced by the magnetic torquers as well as $\boldsymbol{\tau_p} = [0 \quad 0 \quad \tau_p]^T$ produced by the pump of the fluid ring. Further, in Eqs. (6.1) and (6.2), $\boldsymbol{\omega}$ is the angular velocity of the satellite, $\dot{\boldsymbol{\beta}} = [0 \quad 0 \quad \dot{\beta}\,]^T$, where $\dot{\beta}$ is the fluid angular velocity. The inertia matrices of the satellite and the fluid ring are denoted by $\boldsymbol{I_s}$ and $\boldsymbol{I_f}$, respectively. Further, $\boldsymbol{\tau_{gg}}$ and $\boldsymbol{\tau_{gg_f}}$ are the gravity gradient torques exerted on the satellite and the fluid ring, respectively.

As mentioned previously, the attitude control torque in this satellite is produced by two magnetic coils and one fluid ring. Since magnetic coils cannot produce torque in the direction of the Earth's geomagnetic field vector $\boldsymbol{b}$, the component of the control torque $\boldsymbol{\tau^c}$ parallel to $\boldsymbol{b}$ should be produced by the pump pressure; this decomposition method is indeed extracted from a previous work reported by Forbes and Damaren (2010) . On the other hand, the direction of the pump pressure torque $\boldsymbol{\tau_p}$ is fixed and aligned with the Z axis of the satellite body fixed frame. This indicates that only by changing the magnitude of $\boldsymbol{\tau_p}$, the parallel component of the control torque $\boldsymbol{\tau}_{\parallel}$ can be produced. This is illustrated in Figure 6.2, in which the plane P is perpendicular to the vector $\boldsymbol{b}$. The term $\boldsymbol{\tau_m}$ is the magnetic torque vector; $\boldsymbol{\tau^c} = \boldsymbol{\tau}_{\perp} + \boldsymbol{\tau}_{\parallel}$, where $\boldsymbol{\tau}_{\perp}$ being the component of the control torque perpendicular to vector $\boldsymbol{b}$.

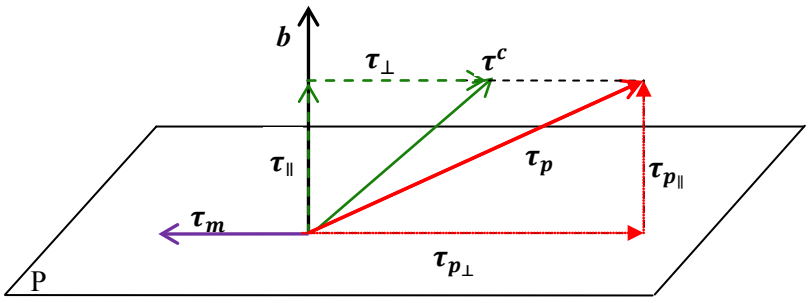

Figure 6.2: The control torque vector decomposition

The parallel component of the control torque is given by

$$\boldsymbol{\tau}_{\parallel} = \hat{\boldsymbol{b}}\hat{\boldsymbol{b}}^{\boldsymbol{T}}\boldsymbol{\tau^c} \tag{6.3}$$

where $\widehat{\boldsymbol{b}} = \boldsymbol{b}/\|\boldsymbol{b}\|$ is the unit vector along the Earth's geomagnetic field; this is worth mentioning that in numerical computations, this vector is expressed in the body frame of the satellite. Further, $\boldsymbol{\tau}_{\|} = \boldsymbol{\tau}_{\boldsymbol{p}_{\|}}$ and $\boldsymbol{\tau}_{\boldsymbol{p}_{\|}} = \widehat{\boldsymbol{b}}\widehat{\boldsymbol{b}}^{\boldsymbol{T}}\boldsymbol{\tau}_{\boldsymbol{p}}$; hence, Eq. (6.3) can be rewritten as below:

$$\widehat{\boldsymbol{b}}\widehat{\boldsymbol{b}}^{\boldsymbol{T}}\boldsymbol{\tau}^{\boldsymbol{c}} = \widehat{\boldsymbol{b}}\widehat{\boldsymbol{b}}^{\boldsymbol{T}}\boldsymbol{\tau}_{\boldsymbol{p}} \tag{6.4}$$

In the above equation, $\widehat{\boldsymbol{b}}^{\boldsymbol{T}}\boldsymbol{\tau}^{\boldsymbol{c}}$ and $\widehat{\boldsymbol{b}}^{\boldsymbol{T}}\boldsymbol{\tau}_{\boldsymbol{p}}$ are scalar. Since $\boldsymbol{\tau}_{\boldsymbol{p}} = [0 \quad 0 \quad \tau_p]^T$, we have $\widehat{\boldsymbol{b}}^{\boldsymbol{T}}\boldsymbol{\tau}_{\boldsymbol{p}} = \hat{b}_3\tau_p$. Therefore, the above equation can be simplified as:

$$\widehat{\boldsymbol{b}}^{\boldsymbol{T}}\boldsymbol{\tau}^{\boldsymbol{c}} = \hat{b}_3\tau_p \tag{6.5}$$

From Eq. (6.5), it can be readily concluded that $\tau_p = (1/\hat{b}_3)\widehat{\boldsymbol{b}}^{\boldsymbol{T}}\boldsymbol{\tau}^{\boldsymbol{c}}$; thus, the torque vector required to be produced by the pump pressure is:

$$\boldsymbol{\tau}_{\boldsymbol{p}} = 1/\hat{b}_3(\widehat{\boldsymbol{b}}^{\boldsymbol{T}}\boldsymbol{\tau}^{\boldsymbol{c}})[0 \quad 0 \quad 1]^T \tag{6.6}$$

Substituting Eq. (6.6) into Eq. (6.2) yields the equation of motion of the fluid ring:

$$\boldsymbol{I}_{\boldsymbol{f}}\left(\dot{\boldsymbol{\omega}} + \ddot{\boldsymbol{\beta}} + \boldsymbol{\omega} \times \dot{\boldsymbol{\beta}}\right) + \boldsymbol{\omega} \times \boldsymbol{I}_{\boldsymbol{f}}\left(\boldsymbol{\omega} + \dot{\boldsymbol{\beta}}\right) = \boldsymbol{\tau}_{\boldsymbol{gg_f}} - \boldsymbol{\tau}_{\boldsymbol{r}} - (1/\hat{b}_3)(\widehat{\boldsymbol{b}}^{\boldsymbol{T}}\boldsymbol{\tau}^{\boldsymbol{c}})[0 \quad 0 \quad 1]^T \tag{6.7}$$

Referring back to Figure 6.2, the normal component of the control torque $\boldsymbol{\tau}_{\perp}$ is produced by the coils and the fluid ring, as per the equation $\boldsymbol{\tau}_{\perp} = \boldsymbol{\tau}_{\boldsymbol{p}_{\perp}} + \boldsymbol{\tau}_{\boldsymbol{m}}$. Knowing that $\boldsymbol{\tau}_{\|} = \boldsymbol{\tau}_{\boldsymbol{p}_{\|}}$, we can obtain:

$$\boldsymbol{\tau}_{\boldsymbol{m}} = \boldsymbol{\tau}^{\boldsymbol{c}} - \boldsymbol{\tau}_{\boldsymbol{p}} \tag{6.8}$$

To determine the torque to be produced by each magnetic coil, an orthonormal set of base vectors $\widehat{\boldsymbol{q}}_{\boldsymbol{1}}$ and $\widehat{\boldsymbol{q}}_{\boldsymbol{2}}$, which spans the plane P, is chosen as follows (Das et al., 2010):

$$\widehat{\boldsymbol{q}}_{\boldsymbol{1}}^{\boldsymbol{T}} = [1 \quad 0 \quad -\hat{b}_1/\hat{b}_3], \qquad \widehat{\boldsymbol{q}}_{\boldsymbol{2}}^{\boldsymbol{T}} = [-\hat{b}_1\hat{b}_2/\hat{b}_3 \quad (\hat{b}_1^2 + \hat{b}_3^2)/\hat{b}_3^2 \quad -\hat{b}_2] \tag{6.9}$$

Defining the matrix $\widehat{\boldsymbol{Q}} = [\widehat{\boldsymbol{q}}_{\boldsymbol{1}} \; \widehat{\boldsymbol{q}}_{\boldsymbol{2}}]$, we have

$$\widehat{\boldsymbol{Q}}^{\boldsymbol{T}}\boldsymbol{\tau_m} = \widehat{\boldsymbol{Q}}^{\boldsymbol{T}}(\boldsymbol{\tau^c} - \boldsymbol{\tau_p}) \tag{6.10}$$

Now, the relation between $\boldsymbol{\tau_m}$ and the magnetic dipole moment vector $\boldsymbol{m_{coil}} = \begin{bmatrix} m_{coil_x} & m_{coil_y} & 0 \end{bmatrix}^T$ is recalled from (Wertz, 1999):

$$\boldsymbol{\tau_m} = \|\boldsymbol{b}\|\widehat{\boldsymbol{b}}^{\times}\boldsymbol{m_{coil}} \tag{6.11}$$

where $\widehat{\boldsymbol{b}}^{\times}$ is the cross product matrix of $\widehat{\boldsymbol{b}}$ defined below:

$$\widehat{\boldsymbol{b}}^{\times} = \begin{bmatrix} 0 & -\hat{b}_3 & \hat{b}_2 \\ \hat{b}_3 & 0 & -\hat{b}_1 \\ -\hat{b}_2 & \hat{b}_1 & 0 \end{bmatrix} \tag{6.12}$$

Since this system consists of only two coils, $\boldsymbol{m_{coil}}$ has only two non-zero components. Hence, Eq. (6.11) can be rewritten as:

$$\boldsymbol{\tau_m} = \|\boldsymbol{b}\|\widehat{\boldsymbol{b}}^{\times}\begin{bmatrix} m_{coil_x} & m_{coil_y} & 0 \end{bmatrix}^T \tag{6.13}$$

Therefore, from Eqs. (6.10) and (6.13), one obtains:

$$\|\boldsymbol{b}\|\begin{bmatrix} 1 & 0 & -\dfrac{\hat{b}_1}{\hat{b}_3} \\ -\dfrac{\hat{b}_1\hat{b}_2}{\hat{b}_3} & \dfrac{\hat{b}_1^2 + \hat{b}_3^2}{\hat{b}_3^2} & -\hat{b}_2 \end{bmatrix}\begin{bmatrix} 0 & \hat{b}_3 \\ -\hat{b}_3 & 0 \\ \hat{b}_2 & -\hat{b}_1 \end{bmatrix}\begin{bmatrix} m_{coil_x} \\ m_{coil_y} \end{bmatrix} = \widehat{\boldsymbol{Q}}^{\boldsymbol{T}}(\boldsymbol{\tau^c} - \boldsymbol{\tau_p}) \tag{6.14}$$

From Eq. (6.14), the magnetic dipole moment $\boldsymbol{m_{coil}}$ can be found as:

$$\begin{bmatrix} m_{coil_x} \\ m_{coil_y} \end{bmatrix} = (1/\|\boldsymbol{b}\|)\begin{bmatrix} \dfrac{\hat{b}_1\hat{b}_2}{\hat{b}_3} & \dfrac{\hat{b}_1^2 + \hat{b}_3^2}{\hat{b}_3} \\ \dfrac{\hat{b}_1^2 + \hat{b}_3^2}{\hat{b}_3} - \hat{b}_2^2 & 0 \end{bmatrix}^{-1}\widehat{\boldsymbol{Q}}^{\boldsymbol{T}}(\boldsymbol{\tau^c} - \boldsymbol{\tau_p}) \tag{6.15}$$

Substituting back Eq. (6.15) into Eq. (6.13), the magnetic torque can be obtained as:

$$\boldsymbol{\tau_m} = \begin{bmatrix} 0 & \hat{b}_3 \\ -\hat{b}_3 & 0 \\ \hat{b}_2 & -\hat{b}_1 \end{bmatrix} \begin{bmatrix} \frac{\hat{b}_1\hat{b}_2}{\hat{b}_3} & \frac{\hat{b}_1^2+\hat{b}_3^2}{\hat{b}_3} \\ \frac{\hat{b}_1^2+\hat{b}_3^2}{\hat{b}_3} - \hat{b}_2 & 0 \end{bmatrix}^{-1} \boldsymbol{\widehat{Q}^T}(\boldsymbol{\tau^c} - \boldsymbol{\tau_p}) \tag{6.16}$$

Before proceeding to perform simulations, in order to reduce the numerical errors, Eqs. (6.1), (6.7), (6.15), and (6.16) are non-dimensionalized. To this end, the recalled non-dimensional angular velocity terms defined in Section 2.1 are:

$$\theta_i' \equiv \dot{\theta}_i/n,\ \widehat{\omega}_i \equiv \omega_i/n\ , \beta' \equiv \dot{\beta}/n \tag{6.17}$$

The non-dimensional form of the governing equations (6.1), (6.7), (6.15), and (6.16) can now be written as:

$$\boldsymbol{\hat{I}_s\widehat{\omega}'} + \boldsymbol{\widehat{\omega}} \times \boldsymbol{\hat{I}_s\widehat{\omega}} = \boldsymbol{\hat{\tau}_{gg}} + \boldsymbol{\hat{\tau}^c} + \boldsymbol{\hat{\tau}_r} \tag{6.18}$$

$$\boldsymbol{\hat{I}_f}(\boldsymbol{\widehat{\omega}'} + \boldsymbol{\beta''} + \boldsymbol{\widehat{\omega}} \times \boldsymbol{\beta'}) + \boldsymbol{\widehat{\omega}} \times \boldsymbol{\hat{I}_f}(\boldsymbol{\widehat{\omega}} + \boldsymbol{\beta'}) = \boldsymbol{\hat{\tau}_{gg_f}} - \boldsymbol{\hat{\tau}_r} - [0 \quad 0 \quad 1]^T 1/b_3(\boldsymbol{\hat{b}^T\hat{\tau}^c}) \tag{6.19}$$

$$\begin{bmatrix} \widehat{m}_{coil_x} \\ \widehat{m}_{coil_y} \end{bmatrix} = \begin{bmatrix} \frac{\hat{b}_1\hat{b}_2}{\hat{b}_3} & \frac{\hat{b}_1^2+\hat{b}_3^2}{\hat{b}_3} \\ \frac{\hat{b}_1^2+\hat{b}_3^2}{\hat{b}_3} - \hat{b}_2^2 & 0 \end{bmatrix}^{-1} \boldsymbol{\widehat{Q}^T}(\boldsymbol{\hat{\tau}^c} - \boldsymbol{\hat{\tau}_p}) \tag{6.20}$$

$$\boldsymbol{\hat{\tau}_m} = \begin{bmatrix} 0 & \hat{b}_3 \\ -\hat{b}_3 & 0 \\ \hat{b}_2 & -\hat{b}_1 \end{bmatrix} \begin{bmatrix} \frac{\hat{b}_1\hat{b}_2}{\hat{b}_3} & \frac{\hat{b}_1^2+\hat{b}_3^2}{\hat{b}_3} \\ \frac{\hat{b}_1^2+\hat{b}_3^2}{\hat{b}_3} - \hat{b}_2^2 & 0 \end{bmatrix}^{-1} \boldsymbol{\widehat{Q}^T}(\boldsymbol{\hat{\tau}^c} - \boldsymbol{\hat{\tau}_p}) \tag{6.21}$$

where $\boldsymbol{\hat{\tau}^c}$ is the non-dimensional control torque, $\boldsymbol{\hat{\tau}_{gg}}$ and $\boldsymbol{\hat{\tau}_{gg_f}}$ being the non-dimensional gravity gradient torque vectors exerted on the satellite and the fluid ring, respectively. The terms $\boldsymbol{\hat{I}_s}$ and $\boldsymbol{\hat{I}_f}$ are the non-dimensional inertia matrices defined in Eq. (2.23).

6.2. Simulation and Results

For simulations, in Eqs. (6.18)−(6.21), $\hat{\boldsymbol{\tau}}^{\boldsymbol{c}}$ is provided by a PID controller with the control law expressed below:

$$\hat{\boldsymbol{\tau}}^{\boldsymbol{c}} = K_p(\boldsymbol{\theta} - \boldsymbol{\theta_d}) + K_d(\boldsymbol{\theta}' - \boldsymbol{\theta}'_{\boldsymbol{d}}) + K_i\left(\int_0^T \boldsymbol{\theta}\, d\Gamma - \int_0^T \boldsymbol{\theta_d}\, d\Gamma\right) \tag{6.22}$$

where $\boldsymbol{\theta} = [\theta_1 \quad \theta_2 \quad \theta_3]^T$, $\boldsymbol{\theta_d}$ being the array of desired attitude angles.

The parameters of the arbitrary system assumed for the simulations reported in this section are identical to those of the system introduced in Section 2.3. For quick reference, a 100 kg satellite is considered; the inertia matrix of the whole system consisting of the satellite and the actuators with respect to the body fixed frame located at the center of mass of the satellite is assumed to be diagonal, the non-zero entries being $I_{xx} = 24.08\ \text{kgm}^2$, $I_{yy} = 27.08\ \text{kgm}^2$, and $I_{zz} = 13.67\ \text{kgm}^2$. Further, a fluid ring with the radius of 0.2 m and the cross-sectional diameter of 0.02 m is considered. The relative initial fluid angular velocity is assumed to be zero. It is also assumed that the satellite travels in a circular orbit at an altitude of 700 km. To study the effect of the fluid ring on the satellite with two magnetic torque rods, the simulation is performed initially for the system without the fluid ring. To this end, in Eqs. (6.18), (6.20), and (6.21), $\hat{\boldsymbol{\tau}}_{\boldsymbol{p}}$ and $\hat{\boldsymbol{\tau}}_{\boldsymbol{r}}$ are set to zero. The initial attitude angles and their rates are chosen as $\pi/36$ rad and 10^{-4} rad/s, respectively. The results of the simulation are shown in Figures 6.3 and 6.4.

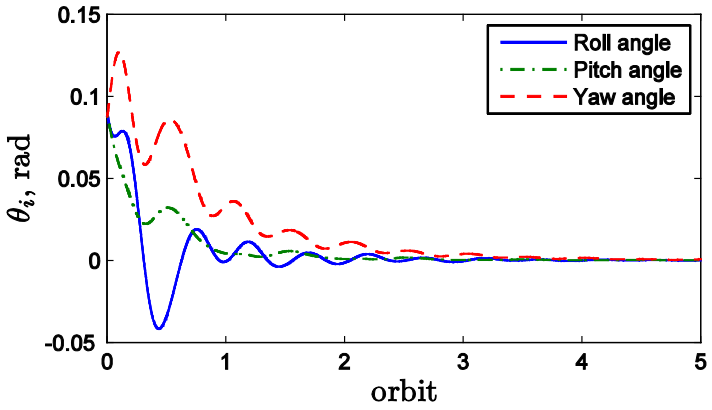

Figure 6.3: The attitude angles of a satellite using two magnetic coils with PID gains $K_p = 50$, $K_d = 60$, and $K_i = 1$

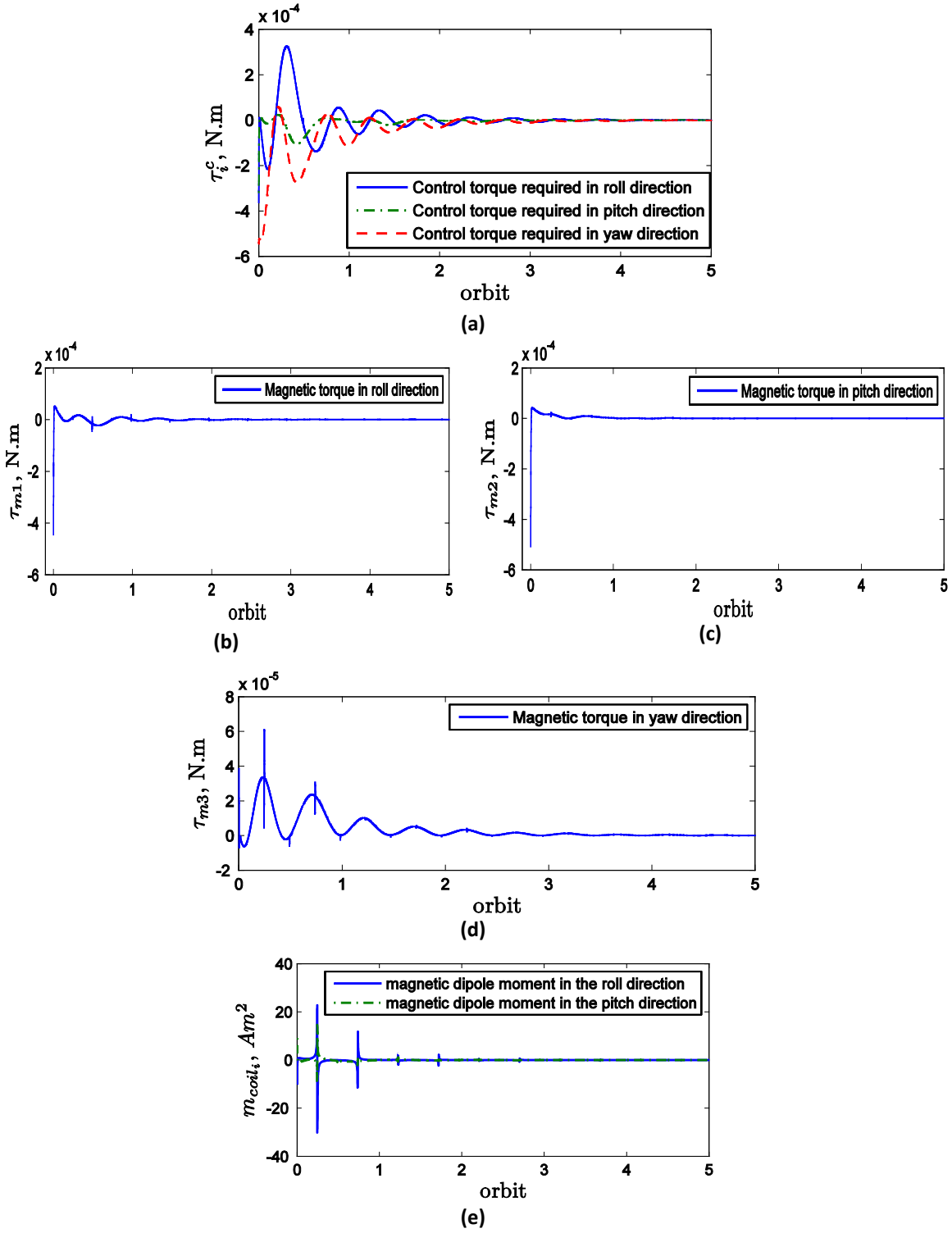

Figure 6.4: Torques produced in the satellite using only two magnetic coils with PID gains $K_p = 50$, $K_d = 60$, and $K_i = 1$: (a) Control torque; (b) Torque produced by the magnetic coils in the roll direction; (c) Torque produced by the magnetic coils in the pitch direction; (d) Torque produced by the magnetic coils in the yaw direction; (e) Magnetic dipole moments

From Figure 6.3, it can be noted that the magnetic coils can stabilize the satellite attitude angles in about four orbits. It is apparent that only $\boldsymbol{\tau}_{\perp}$ is produced by the magnetic coils, which yields a fairly slow stabilization. Considering Figure 6.4, it can be seen that the plots of the control torque components have several jumps[1]. The reason behind this is the singularities of the 2×2 matrix in Eq. (6.21). Indeed, the singular points of the dynamical model of a satellite and magnetic torquers occur where this matrix loses rank. To cope with this issue, $|\hat{b}_i| = 10^{-3}$ is used wherever the absolute amount of $\hat{b}_i$ becomes less than 10^{-3}.

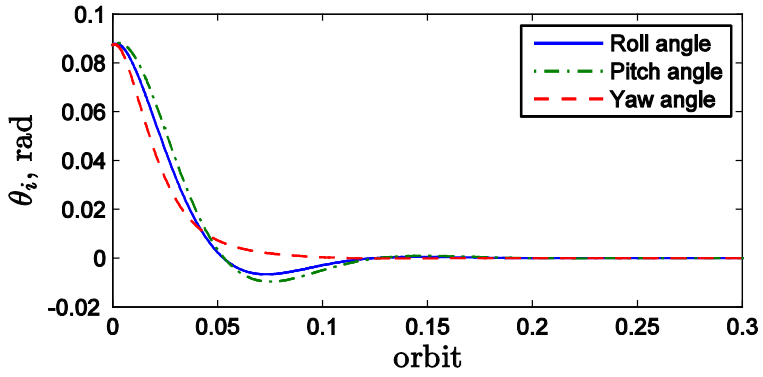

Figure 6.5: The attitude angles of a satellite using two magnetic coils and one active fluid ring with PID gains $K_p = 70$, $K_d = 100$, and $K_i = 0$

Figures 6.5 and 6.6 show the numerical solutions of the satellite with one active fluid ring and two magnetic torquers (Eqs. (6.18) – (6.21)) using the same initial conditions and system parameters as the ones introduced in the foregoing simulation.

As can be seen in Figure 6.5, the satellite stabilization occurs in about one tenth of the orbital period, while the maximum torque required is less than 2.5×10^{-4} N.m (Figure 6.6). As explained previously, the fluid ring is in charge of producing the $\boldsymbol{\tau}_{\parallel}$ component of the control torque; the maximum torque produced by the fluid ring is 3×10^{-4} N.m. According to Figure 6.6 (a), the maximum value and the trend of $\boldsymbol{\tau}^{\boldsymbol{c}}$ in the roll and pitch axes are quite similar to those of the magnetic torque plots in these two directions, which are shown in Figure 6.6 (c); it can thus be concluded that $\boldsymbol{\tau}_{\perp}$ is mainly produced by the magnetic coils. Further, the maximum τ_f is about 1.5×10^{-5} N.m; a portion of the pump energy is consumed to overcome this friction torque.

[1] The term *jump* here implies high magnitude peaks of a signal occurring in a short duration of time.

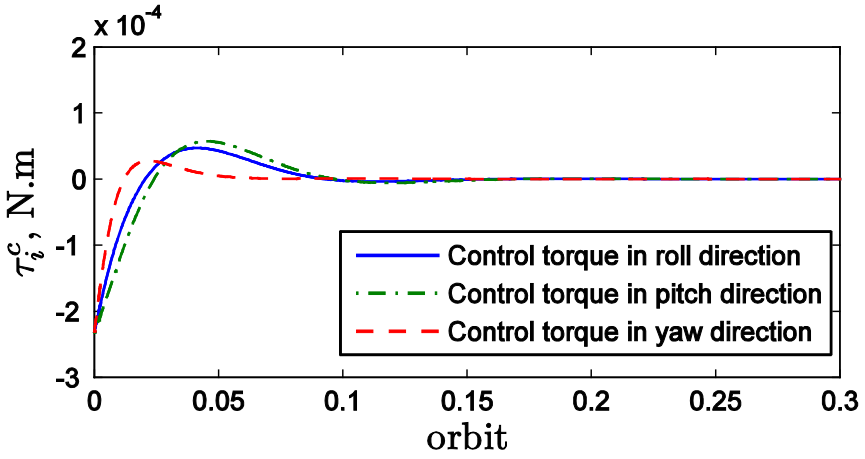
x 10^-4
2
1
0
-1
-2
-3
τ_i^c, N.m
Control torque in roll direction
Control torque in pitch direction
Control torque in yaw direction
0
0.05
0.1
0.15
0.2
0.25
0.3
orbit

(a)

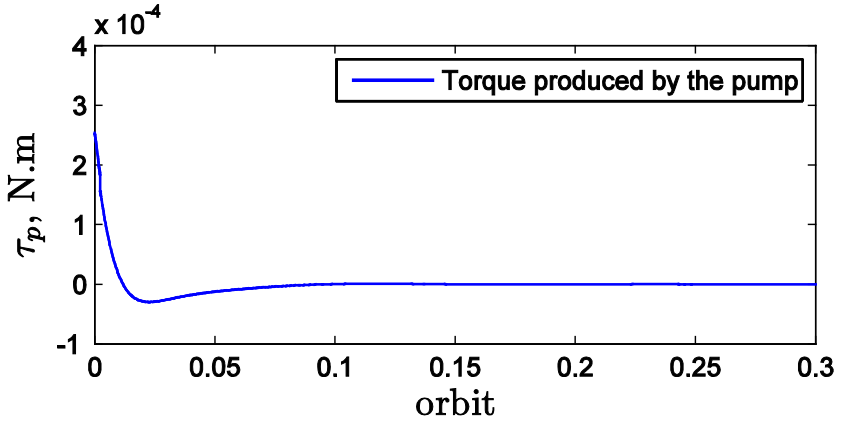
x 10^-4
4
3
2
1
0
-1
τ_p, N.m
Torque produced by the pump
0
0.05
0.1
0.15
0.2
0.25
0.3
orbit

(b)

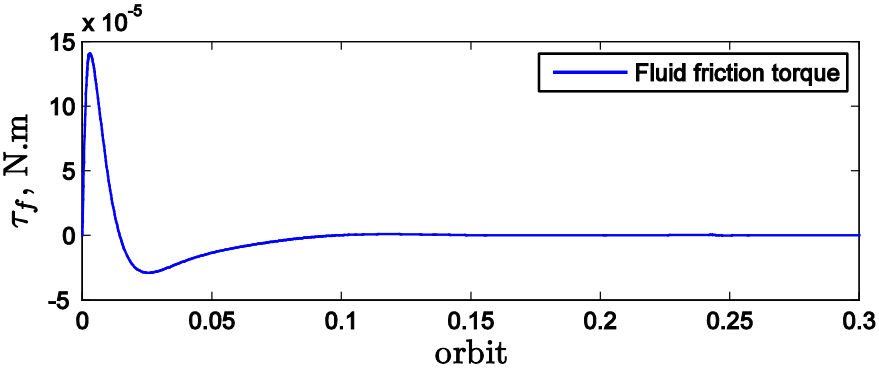
x 10^-5
15
10
5
0
-5
τ_f, N.m
Fluid friction torque
0
0.05
0.1
0.15
0.2
0.25
0.3
orbit

(c)

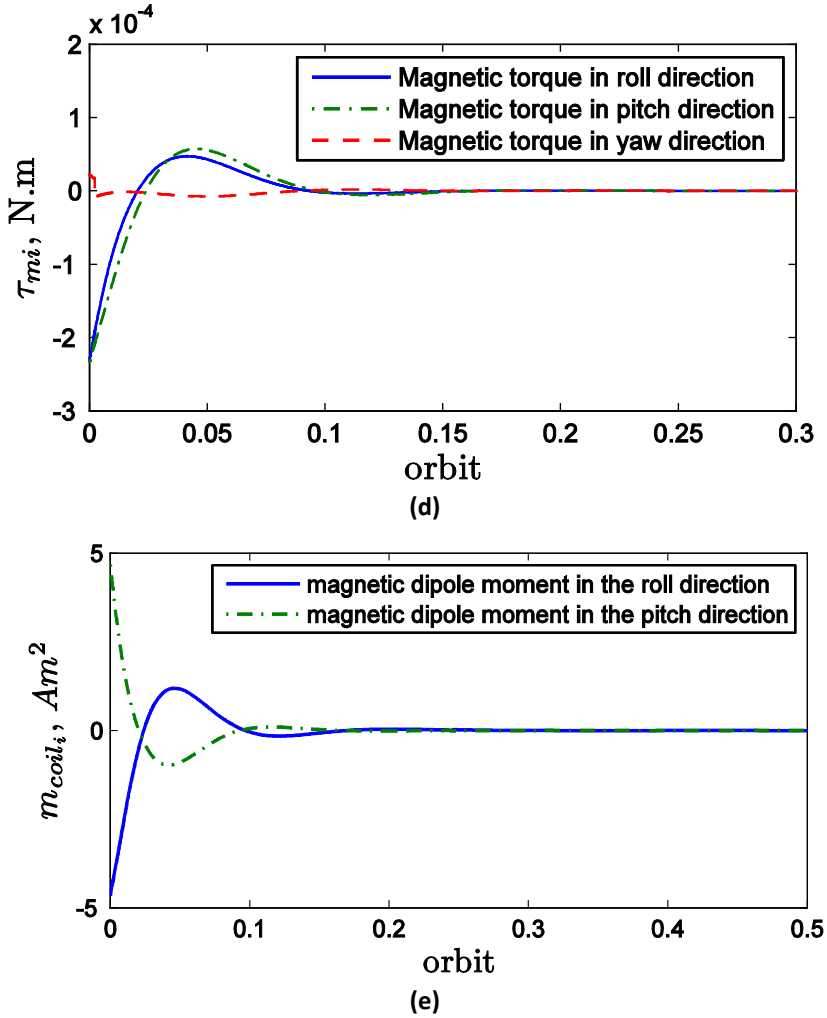

Figure 6.6: Torques produced in the satellite using two magnetic coils and one fluid ring with PID gains $K_p = 70$, $K_d = 100$, and $K_i = 0$: (a) Control torque; (b) Torque produced by the pump; (c) Fluid friction torque; (d) Torque produced by the magnetic coils; (e) Magnetic dipole moments

6.3. Failure Study

Each component used in a satellite is designed for a life span longer than that of the satellite itself. Nevertheless, to be prepared, performing the failure study of different components of a satellite is important so as to predict and control the dynamics behaviour of the system, if a failure condition occurs. In this section, the effect of failure of the fluid ring as well as that of each magnetic coil is examined.

6.3.1. Failure of the fluid ring

A fluid ring can fail due to the failure of its pump. This can lead to two different scenarios: (i) the pump is jammed and the flow is blocked inside the ring. In this case, the resulting system is similar to a satellite with two magnetic torque rods without the fluid ring, which was discussed in Section 6.2. The analysis of this condition revealed that magnetic coils can slowly stabilize the attitude angles; (ii) the pump is not functional anymore, but the flow is not blocked. This condition resembles the passive application of the fluid ring; the difference lies in that, in the case of failure of the fluid ring, the system expects to generate a component of the control torque using the pump, however in the passive case, the control torque is calculated without counting on the pump. Therefore, for the case of the failure of the fluid ring, Eqs. (6.18) and (6.19) should be modified as follows.

$$\hat{\boldsymbol{I}}_s\hat{\boldsymbol{\omega}}' + \hat{\boldsymbol{\omega}} \times \hat{\boldsymbol{I}}_s\hat{\boldsymbol{\omega}} = \hat{\boldsymbol{\tau}}_{gg} + \hat{\boldsymbol{\tau}}_m + \hat{\boldsymbol{\tau}}_r \tag{6.23}$$

$$\hat{\boldsymbol{I}}_f(\hat{\boldsymbol{\omega}}' + \boldsymbol{\beta}'' + \hat{\boldsymbol{\omega}} \times \boldsymbol{\beta}') + \hat{\boldsymbol{\omega}} \times \hat{\boldsymbol{I}}_f(\hat{\boldsymbol{\omega}} + \boldsymbol{\beta}') = \hat{\boldsymbol{\tau}}_{gg} - \hat{\boldsymbol{\tau}}_r \tag{6.24}$$

On the other hand, Eqs. (6.20) and (6.21) remain unchanged. To simulate the performance of this system, the same initial conditions as what is introduced in the foregoing section are used.

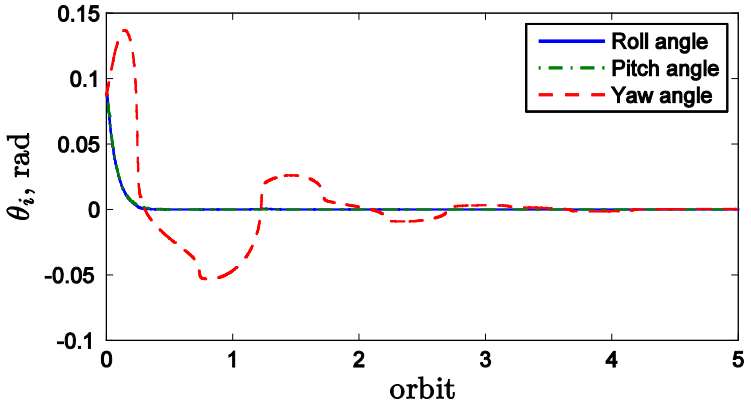

Figure 6.7: Attitude angles of the satellite in the case of failure of the fluid ring with PID gains $K_p = 60$, $K_d = 30$, **and** $K_i = 1$

Figure 6.7 shows that the attitude angles can be stabilized by the magnetic torque and the damping effect of the fluid ring. Figure 6.8 (a) shows the control torque required; the maximum control torque in the yaw direction is 1×10^{-3} N.m. Also, the fluid friction torque, that is the

only torque produced in the yaw direction, is quite small, about 5×10^{-7}N. m (Figure 6.8 (b)). Therefore, the damping effect of the fluid is negligible with minor effect on the attitude stabilization. The maximum magnetic torque in the yaw direction is about 2×10^{-4} N. m occurring after passing approximately one fourth of the orbital period, as shown in Figure 6.8 (d).

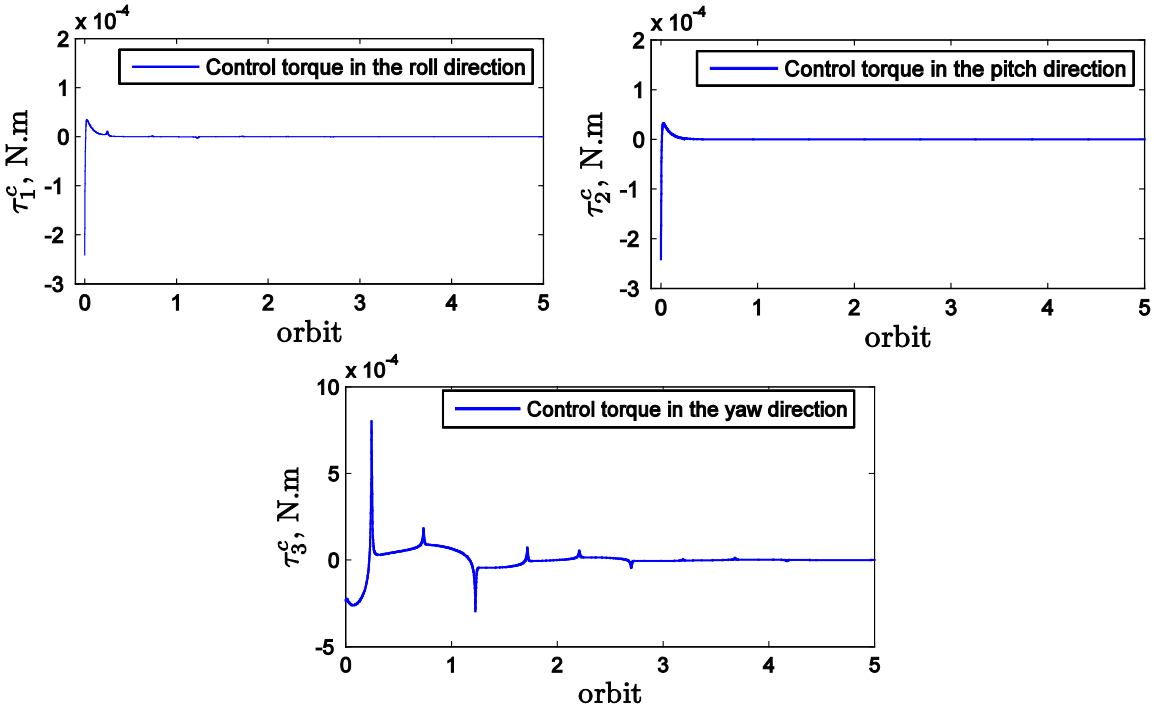

(a)

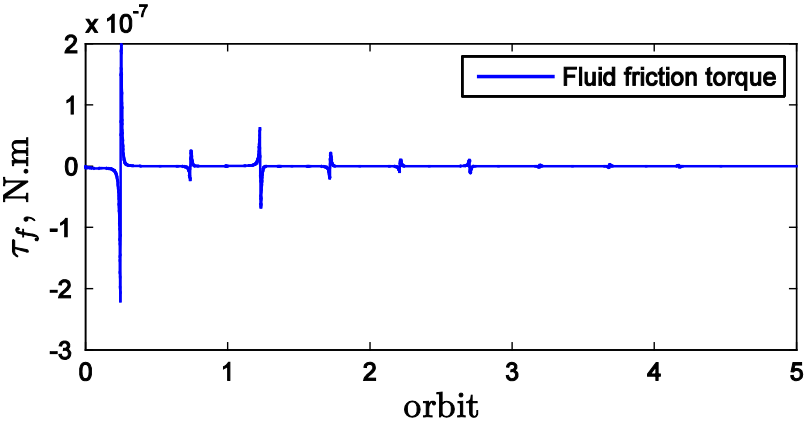

(b)

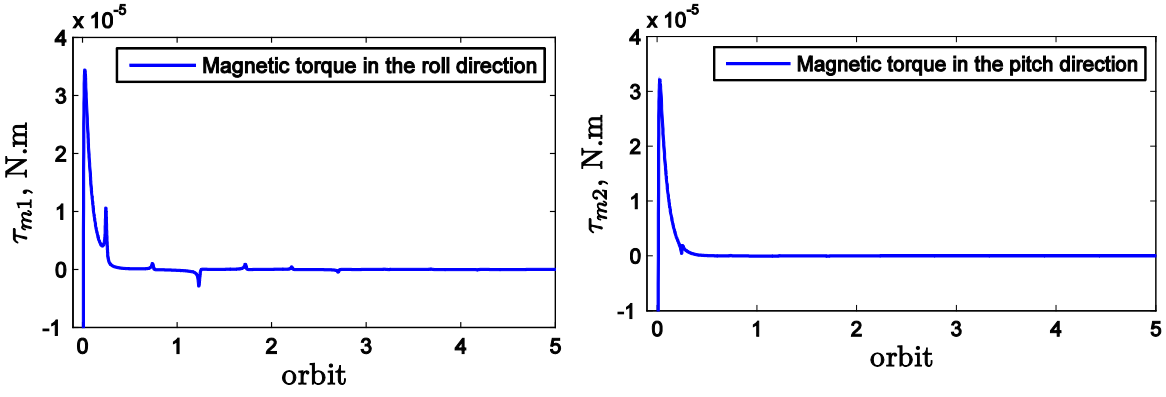

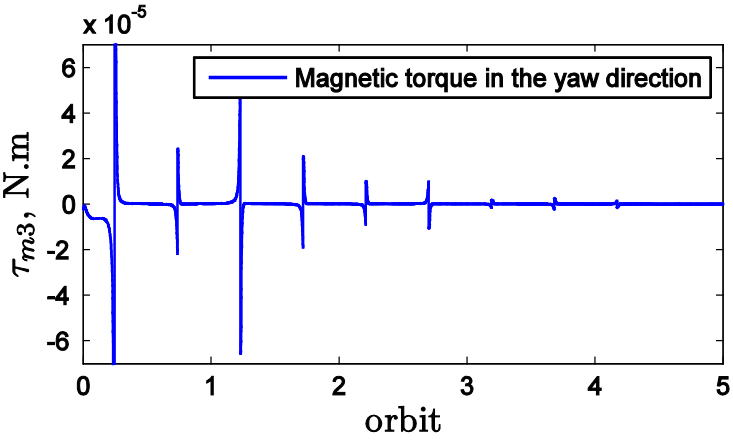

(c)

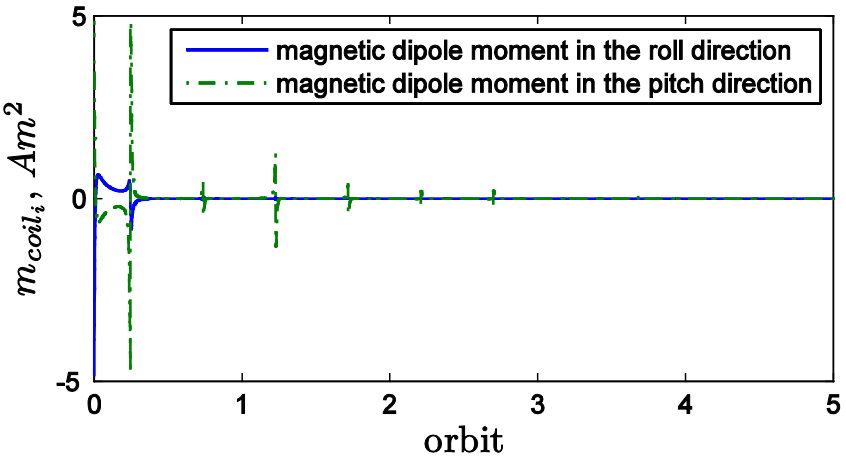

(d)

Figure 6.8: Torque produced in the satellite with the fluid ring failure with PID gains $K_p = 60$, $K_d = 30$, and $K_i = 1$: (a) Control torque; (b) Fluid friction torque; (c) Torque produced by the magnetic coils;(d) Magnetic dipole moments

6.3.2. Failure of one magnetic coil

In this section, it is assumed that one magnetic coil is broken, thus cannot comply with the control commands. The equation of motion of the satellite is accordingly modified to separate the two orthogonal components of the control torque:

$$\hat{\boldsymbol{I}}_s\hat{\boldsymbol{\omega}}' + \hat{\boldsymbol{\omega}} \times \hat{\boldsymbol{I}}_s\hat{\boldsymbol{\omega}} = \hat{\boldsymbol{\tau}}_{gg} + \hat{\boldsymbol{\tau}}_r + 1/b_3(\hat{\boldsymbol{b}}^T\hat{\boldsymbol{u}}^c)[0 \quad 0 \quad 1]^T + \boldsymbol{E}_i\hat{\boldsymbol{\tau}}_m \quad \text{for } i = 1,\ 2 \tag{6.25}$$

Further, for $i = 1$ and 2, $\boldsymbol{E}_i$ is $[\boldsymbol{e_1} \quad \boldsymbol{0} \quad \boldsymbol{0}]$ and $[\boldsymbol{0} \quad \boldsymbol{e_2} \quad \boldsymbol{0}]$, respectively, where $\boldsymbol{e_1} = [1 \quad 0 \quad 0]^T$ and $\boldsymbol{e_2} = [0 \quad 1 \quad 0]^T$. Using Eq. (6.25), the cases of failure of the coil which produces torque either along the roll or the pitch direction can be simulated. A question might arise here as why the simulation has to be performed for both cases. The answer lies in the fact that a strong dynamical coupling exists between the roll and yaw motions contrary to the weak coupling between the pitch and the roll or yaw motion. Thus, if the coil which produces torque along the roll axis fails, the torque produced by the fluid ring, whose axis of symmetry is along the yaw axis, can stabilize the attitude angle in the roll direction as well. On the other hand, the outcome of failure of the coil that produces torque along the pitch axis is not obvious. Here, the simulation is performed for both cases.

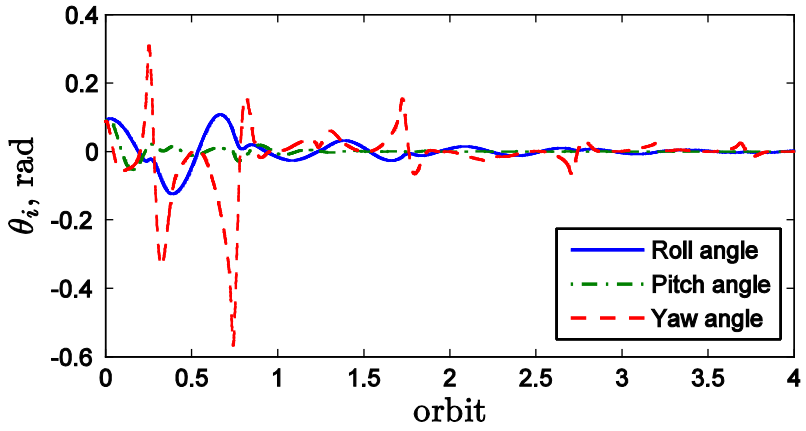

Figure 6.9: Stabilization of attitude angles in the case of failure of the roll-axis magnetic coil with PID gains $K_p = 12$, $K_d = 2$, and $K_i = 0.01$

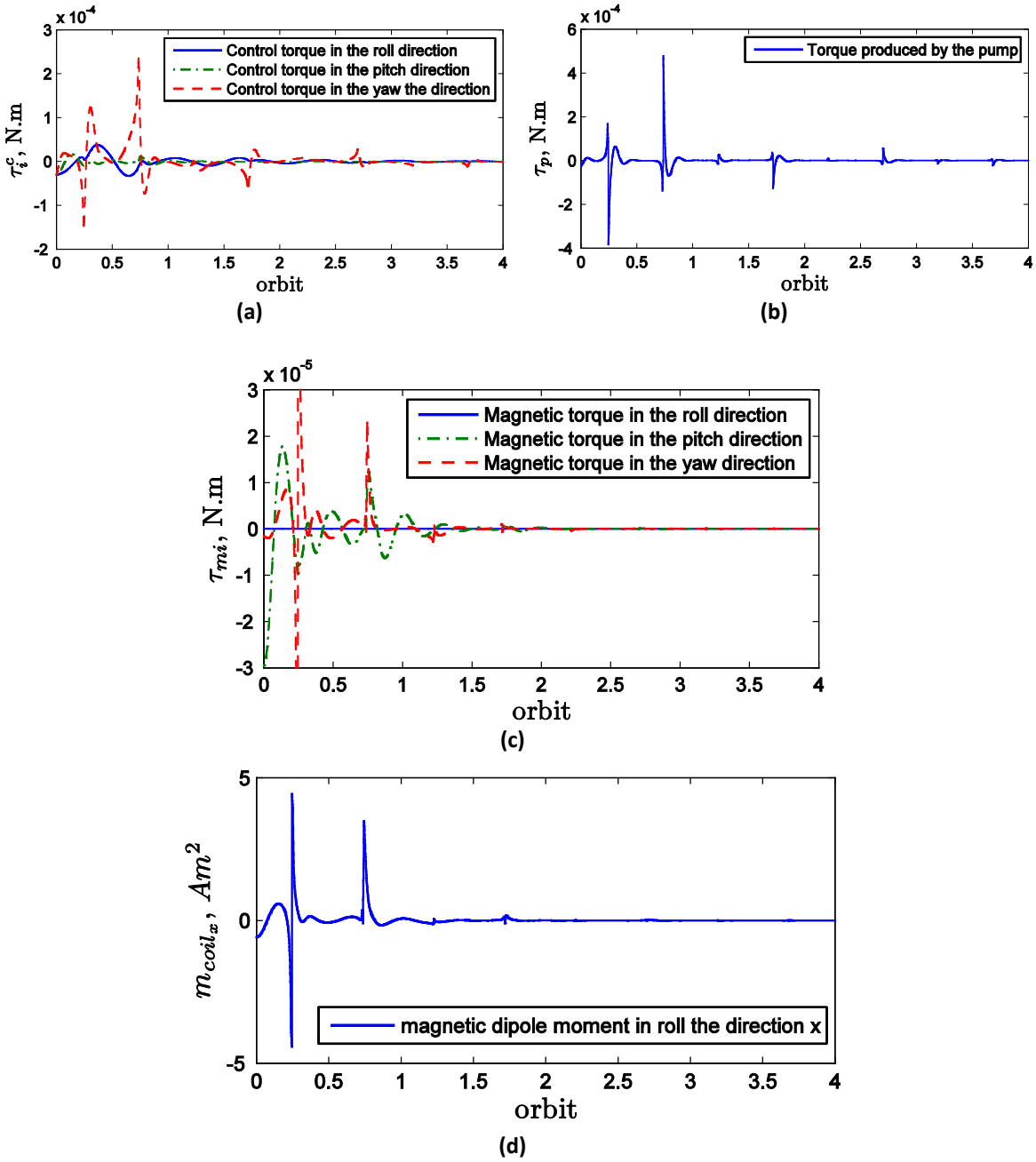

Figure 6.10: The torque produced in the case of failure of the roll-axis coil with PID gains $K_p = 12$, $K_d = 2$, and $K_i = 0.01$: (a) Control torque; (b) Torque produced by the fluid ring; (c) Torque produced by the magnetic coils; (d) Magnetic dipole moment in the pitch direction

Figures 6.9 and 6.10 illustrate the results of the failure of the roll-axis coil. Here, to stabilize the system, the PID gains have to be retuned. The stabilization time is about 4 orbital period; however, the variations in the roll and yaw angles are large. Considering Figure 6.12 (b), it can be

seen that the control torque reaches a value as high as -2×10^{-4} N. m or even 3×10^{-4} N. m at times. Also, the torque produced by the fluid ring is approximately two times larger than the control torque about the yaw axis (Figure 6.12 (b)). This shows that the yaw axis of the satellite almost lies in the plane P of Figure 6.2 to compensate the failure of the roll-axis coil.

Let us now examine the effect of failure of the pitch-axis coil. The plots illustrated in Figures 6.11 and 6.12 show that the system can be stabilized, if the PID gains are retuned. According to Figure 6.11, the yaw angle varies quite rapidly in the first half of an orbit. The reason behind this is the weak dynamical coupling between the roll or yaw and the pitch motion. As can be seen in Figure 6.12 (a), a quite large torque, of about 1.4×10^{-2} N. m, is required in the yaw direction to stabilize the attitude angles. Indeed, the fluid ring is in charge of producing this torque. It is noteworthy that, in Figure 6.12 (b), the pump pressure torque reaches the value of 1.4×10^{-2} N. m at 0.3 orbits (for the sake of illustration the vertical axis of the plot is limited to the range between -1×10^{-3} N. m and 2×10^{-3} N. m). The large torque produced by the pump also affects the pitch angle, as can be seen in Figure 6.11. Moreover, the roll-axis magnetic coil produces a torque with the maximum value of 1×10^{-3} N. m to stabilize the pitch angle. Although, in this failure case, a large amount of torque, and hence, a high pump pressure torque and a high magnetic dipole moment is required (Figure 6.12 (d)), the simulation results prove that the system still has a chance to remain stable and continue its mission objectives.

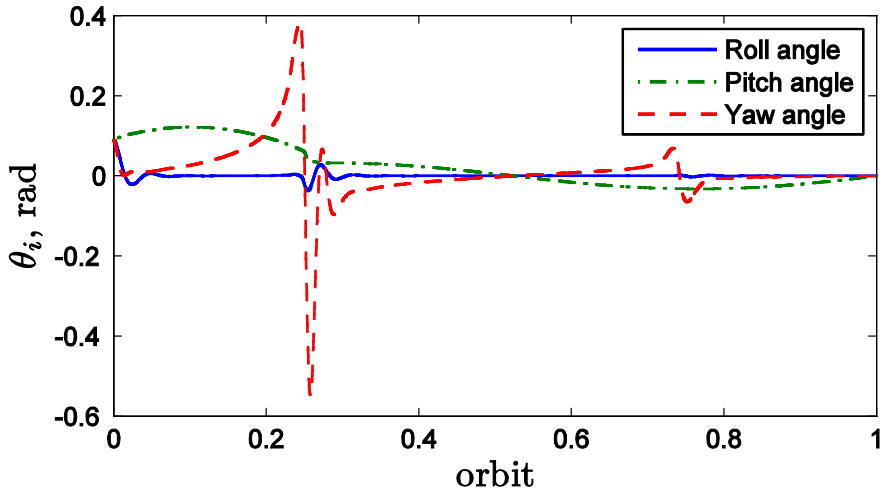

Figure 6.11: Stabilization of attitude angles in the case of failure of the pitch-axis coil with PID gains $K_p = 450$, $K_d = 15$, and $K_i = 0.01$

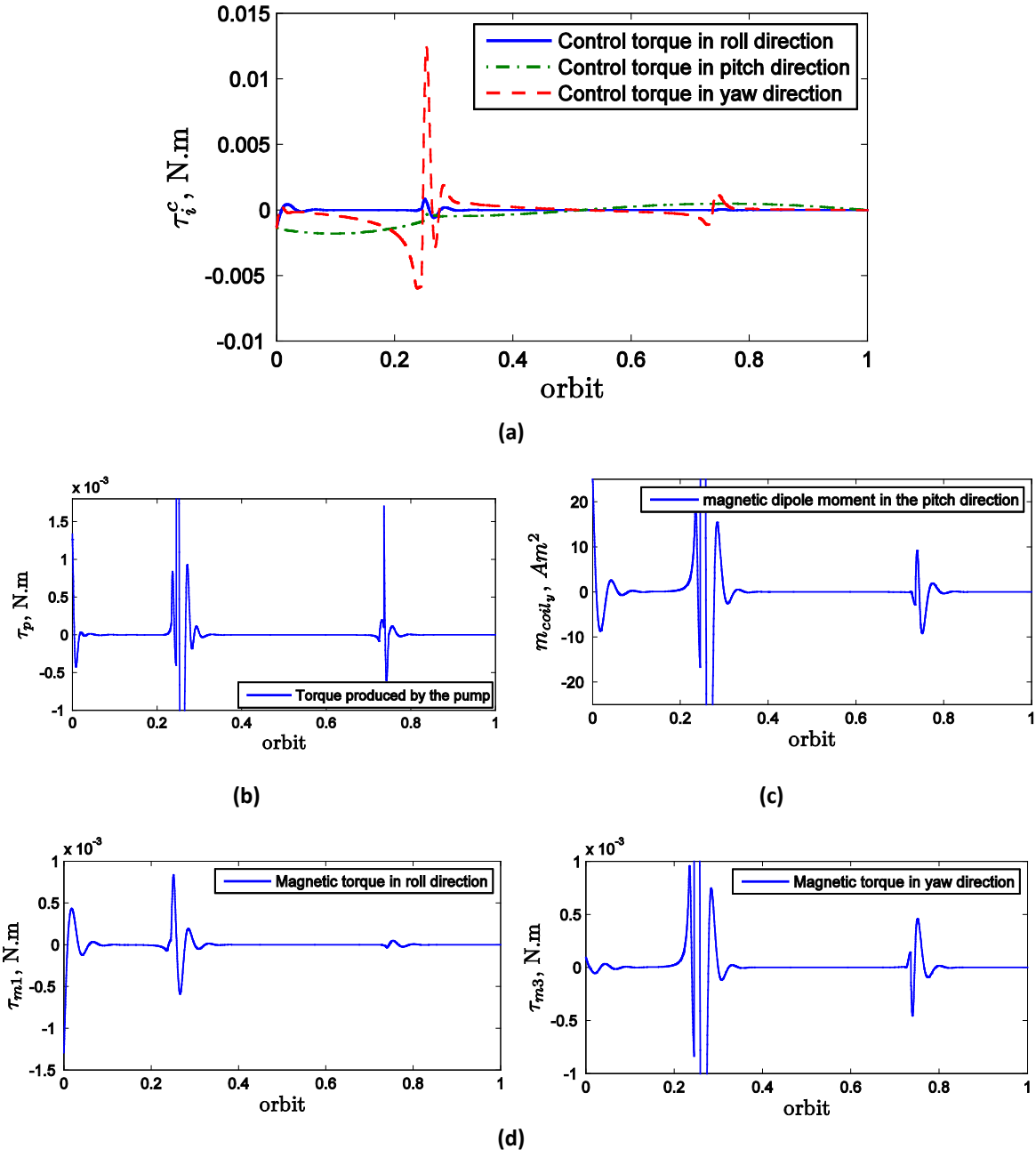

Figure 6.12: Torques produced in the case of failure of the pitch-axis coil with PID gains $K_p = 450$, $K_d = 15$, and $K_i = 0.01$: (a) Control torque; (b) Torque produced by the fluid ring; (c) Magnetic dipole moment in the roll direction; (d) Torque produced by the magnetic coils

6.4. Summary

A novel attitude control system consisting of two magnetic coils and one fluid ring was proposed in this chapter. The dynamical model of the satellite with two magnetic torque rods and a fluid ring was developed. Then, the control torque was decomposed into two orthogonal components. The part of the control torque vector that is parallel to the Earth's magnetic vector was considered to be produced by the fluid ring, the rest by the magnetic torque rods. The first simulation was performed without having the fluid ring in the system. The results showed that the satellite attitude became asymptotically stable, but slowly. It was found that the stabilization time can be reduced by a factor of 10 using an active fluid ring; a part of the actuation energy is consumed to overcome the fluid friction torque. The cases of failure of the fluid ring and one magnetic torque rod were also examined. In the case of failure of the roll-axis magnetic torque rod, the variations of the attitude angles were quite high in the first half of the orbit. However, the attitude angles were finally stabilized. In the case of failure of the pitch-axis coil, the torque required to be produced by the fluid ring was quite large due to the weak coupling of the pitch with either the roll or yaw motion. The attitude angles were finally stabilized at the cost of a high pump pressure torque and a high magnetic dipole moment.

Chapter 7

CONCLUDING REMARKS AND RECOMMENDATIONS FOR FUTURE WORK

Satellite attitude can be disturbed because of various natural perturbation sources, such as the Earth gravity gradient and solar radiation pressure. To avoid this common problem, different attitude control actuators have been designed so far. Among various control actuators, a novel type, known as fluid ring actuator, was studied in this thesis; this was motivated by the perspective of this actuator to produce a high torque to mass ratio. In fact, the goal of this thesis was the feasibility analysis of using fluid rings as attitude control actuators in satellites and also finding possible solutions to cope with their drawbacks. In this chapter, a brief summary of the previous chapters of the thesis is given, while the most significant conclusions of each chapter are highlighted. At the end, topics of future work to continue this study are proposed.

7.1. Summary and Findings

A model was developed in Chapter 2 to describe the three-dimensional attitude dynamics of a satellite with fluid ring actuators. The model in question can handle two different cases: satellites with (i) three orthogonal axes; (ii) four fluid rings in a pyramidal configuration. This mathematical model was used to evaluate the performance of the fluid rings as either a passive or active method of attitude stabilization. Although the passive application of fluid rings could stabilize the attitude angles of a satellite in a circular orbit, the simulation results showed that an asymptotic stability cannot be achieved for the pitch motion of a satellite in an elliptical orbit. Moreover, the stabilization, when achieved, was fairly slow. Therefore, a PID controller was designed to use the fluid rings actively so as to stabilize the satellite attitude angles in a reasonably short period of time. The simulation results confirmed that the satellite attitude can be effectively controlled by four fluid rings in a pyramidal configuration, if the controller gains are properly tuned. Further, according to the analysis reported in the thesis, the failure of one fluid ring in the set of actuators could be tolerated by the three remaining rings without changing the control law; however, in this condition, the steady state fluid flow rates within the rings did not vanish even when the satellite was stabilized. This is undesirable due to the unnecessary energy consumption. A remedy to this problem was found by modifying the control law to contain a feedback of the fluid angular velocity; the final conclusion was that the fluid ring actuator system is, in fact, fault-tolerant. Further, the parameter uncertainties were handled by designing a sliding mode controller, which is robust and compatible with the nonlinearities of the system. This controller stabilized the attitude angles of the satellite, while considering the parameters uncertainties in the model to be as large as 15% of their nominal values. The simulation results showed high chattering in the fluid angular velocities and control torques. To eliminate the chattering effect, a switching control law consisting of a sliding mode and a PID controller was developed; the PID is only activated when the error signal becomes smaller than a threshold value. The new controller performed satisfactorily.

The first experiment conducted was on a single loop fluid ring; this experiment mostly consists of qualitative tests to observe the system behaviour on a single-axis simulator. The PID controller of the setup was set to track the fluid angular velocity found from the theoretical analysis. Indeed, a dynamical model has been developed for a disk carrying a single fluid ring. The motivation behind developing this model was to obtain numerical results that could be

compared to those from the experiments in order to validate the modeling approach. It was noted that the setup was able to maintain attitude within an acceptable tolerance. The fluid ring setup has proved the feasibility of attitude control using fluid rings. However, it was noted that, to produce the desired control torque, the input voltage required to regulate the fluid is fairly high, more than $12\,V$.

The experimental validation of the theoretical results obtained for the three dimensional stabilization was also sought. However, due to various practical issues, such as the defects in the pumps and the manufacturing of the system, a complete test could not be conducted. Therefore, a hardware-in-the-loop experiment was performed. The results showed that the system can follow the control command to produce the fluid flow required for attitude stabilization with quite high accuracy.

According to the experimental results, producing large torques (higher than 5×10^{-3} N.m) by fluid rings requires high input voltage (more than $12\,V$), that may not be easily achievable in satellites. Hence, the feasibility of using fluid rings as auxiliary actuators combined with other types of attitude stabilization methods was investigated. In this regard, first, a spinning satellite with two fluid rings normal to the roll and yaw axes was considered. Designing a controller for this system with time-varying coefficient in the equations of motion was not straightforward. Therefore, in order to obtain a preliminary understanding of the system dynamics, simplifying assumptions regarding the magnitude of the attitude angles were made. Based on these assumptions, the linear dynamical model of the system was developed, for which a controller was designed using the pole placement method. The insight obtained from the linear model became very helpful in the design of a controller for the original nonlinear model. The attitude angles of the system were stabilized fast, while the effective control torque required was lower than 10^{-3} N.m. As a second instance of using fluid rings, a new actuation system that includes one fluid ring with two magnetic torquers was proposed. In order to determine the components of the stabilization torque to be generated from the fluid ring and the magnetic torquers, the control torque was decomposed into two components: one parallel to the Earth's magnetic field vector; the other its complement. In the case study reported, the control torque needed to be produced by the fluid ring was less than $2 \times 10^{-3}\ N.m$; the satellite attitude angles were also stabilized within a short time period. The cases of failure of the fluid ring and each magnetic torquer were also examined. It was shown that the failure of the fluid ring can be compensated by the two magnetic

torquers due to the nonlinear coupling which exists between the roll and yaw motions. However, the failure of the magnetic torquers, especially the one that produces the torque along the pitch direction, can cause instability in the satellite orientation. In this case, the attitude angles could be stabilized via modifying the control law. It is noteworthy that the torque required to be produced by the fluid ring when one magnetic torquer fails remained below 2×10^{-3} N.m. In conclusion, it seems that combining the fluid ring actuator with magnetic torquers is the most efficient application of the former. Indeed, for such system, the controller design is not complex, while the torque required to be produced by the fluid ring is quite small.

7.2. Recommendations for Future Work

The recommendations for future work are listed below:

i. **Three dimensional control validation:** The three dimensional control experiment reported in this thesis was of hardware-in-the-loop experiment type. However, testing the performance of the fluid rings with a full three dimensional setup mounted on the simulator can validate the theoretical results more accurately.

ii. **Using an observer in the experimental testing:** As mentioned in Chapter 4 the computer used in the experiments was quite limited in terms of computational speed. This fact did not allow the real time application of the Kalman filter. Therefore, the online usage of an observer, such as a Kalman filter is recommended for further experimental work.

iii. **Flexibility analysis of the satellite:** Considering the satellite as a rigid body is an acceptable assumption for the feasibility analysis reported in this thesis. However, there is still room for more accurate modeling and simulations, which can be done by modeling the satellite as a flexible body.

iv. **Considering the interaction of the fluid and the ring:** Due to the interaction between the fluid and the ring, vibrations can be induced into the system, something which adversely affects the control system. Hence, studying the fluid structure interaction in the rings is a topic which requires further attention.

REFERENCES

Ahmed, J., and Bernstein, D.S. "Adaptive Control of Double-Gimbal Control-Moment Gyro with Unbalanced Rotor." *Journal of Guidance, Control, and Dynamics*, 2002: 105-115.

Akiyama, K. "Feedback-Based Time Optimal Control System for Rapid Attitude Maneuver with Micro Control Moment Gyros." *Advances in the Astronautical Sciences*, 2010: 91-102.

Ashrafiuon, H., and Erwin, R.S. "Shape Change Maneuvers for Attitude Control of UnderActuated Satellites." *American Control Conference.* Portland, OR, USA, June 2005. 895-900.

Ayoubi, M.A., and Longuski, J.M. "Asymptotic Theory for Thrusting, Spinning-up Spacecraft Maneuvers." *Acta Astronautica*, 2009: 810-831.

Barba, P.M., and Aurbrun, J.N. "Satellite Attitude Acquisition by Momentum Transfer." *AIAA Journal*, 1976: 1382-1386.

Battagliere, M.L., Fiorillo, F., Ferrara, E., and Santoni, F. "Permeable Rods Ground Testing System for Cubesat Angular Velocity and Residual Oscillations Damping." *61st International Astronautical Congress (IAC).* Prague, Sept 2010. 2217-2225.

Bolandi, H., Bayat, F., and Nasirian, M. "Attitude Control of Spinning Satellite Subject to Actuators Restriction Using Eigenstructure Assignment." *1st International Symposium on Systems and Control in Aerospace and Astronautics.* Harbin, Jan 2006. 1413-1419.

Chen, M., Zhang, S.J., Liu, F.R., and Zhang, Y.C. "Combined Attitude Control of Small Satellite Using One Flywheel and Magnetic Torquers." *2nd International Symposium on System and Control in Aerospace and Astronautics*, *ISSCAA.* Shenzhen, China, Dec 2008. 1-6.

Das, S., Sinha, M., Kumar, K.D., and Misra, A. "Reconfigurable Magnetic Attitude Control of Earth-pointing Satellite." *Journal of Aerospace Engineering*, 2010: 1309-1326.

De Ruiter, A. "A Fault-Tolerant Magnetic Spin Stabilizing Controller for the JS2Sat-FF Missin." *Acta Astronautica*, 2011: 160-171.

Forbes, J.R., and Damaren, C.J. "Geometric Approach to Spacecraft Attitude Control Using Magnetic and Mechanical Actuation." *Journal of Guidance, Control and Dynamics*, 2010: 590-594.

Fortescue, P., and Stark, J. *Spacecraft Systems Engineering.* 2nd Edition. England: Wiely, 1995.

Godard, Abreu, N., and Kumar, K.D. "Fault-Tolerant Attitude Control of Miniature Satellite Using Reaction Wheels." *Advances in the Astronatical Sciences*, 2010: 159-178.

Hablani, H.B. "Momentum Accumulation Due to Solar Radiation Torque, and Reaction Wheel Sizing, with Configuration Optimization." *AIAA Journal of Guidance, Control, and Dynamics*, 1994: 805-814.

Haga, R.A., and Saleh, J.H. "Epidemiology of Satellite Anomalies and Failures: A Subsystem-Centric Approach." *Acta Astronautica*, 2011: 676-690.

Horri, N.M., and Palmer, P. "Practical Implemention of Attitude-Control Algorithms for Underactuated Satellite." *Journal of Guidance, Control, and Dynamics* , 2012: 40-50.

Hsu, D., Latombe, J.C., and Motwani, R. "Path Planning in Expansive Configuration Spaces." *International Journal of Computational Geometry and Applications*, 1999: 495-512.

Hughes, C.P. *Spacecraft attitude dynamics.* New York: Wiely, 1986.

Huo, X.a, Xiao, B., and Hu, Q. "Adaptive Sliding Mode Attitude Tracking Control for Spacecraft Under Actuator Misalignment." *Journal of South University*, 2011: 233-239.

Hur-Diaz, S., Wirzburger, J., and Smith, D. "Three Axis Control of the Hubble Space Telescope Using Two Reaction Wheels and Magnetic Torquer Bars for Science Observations." *Advances in the Astronautical Sciences*, 2008: 335-350.

Iskenderian, T.C. "Liquid Angular-Momentum Compensator." *NASA Tech Brifes*, 1989: 80-85.

Ismail, Z., and Varatharajoo, R. "A Study of Reaction Wheel Configurations for a 3-axis Satellite Attitude Control." *Advances in Space Research*, March 2010: 750-759.

Jiang, Y., Yao, Y., and He, F.H. "Scheme of Mass Moment Spacecraft and It's Control Problem." *Systems Engineering and Electronics*, 2008: 320-323.

Jin, J., and Hwang, L."Attitude Control of A Spacecraft With Single Variable-Speed Control Moment Gyroscope." *Journal of Guidance, Control, and Dynamics*, 2011: 1920-1924.

Kalman, R.E. "A New Approach to Linear Filtering and Prediction Problems." *Journal of Basic Engineering*, 1960: 35-45.

Kaplan, M.H. *Modern Spacecraft Dynamics & Control.* New York: Wiley, 1976.

Kataoka, J., and Kawai, N. "Design of Tokyo Tech Nano-Natellite Cute-1.7+APD II and Its Operation." *Acta Astronautica*, 2010: 1412-1424.

Kazinczy, B., and Liebing, L. "Development of a Plasma-Ablation-Accelerator for Satellite Attitude Control." *Dtsch Luft Raumfahrt Forschungsber*, 1975.

Kelly, A., McChesney C., Smith P.Z.C., and Waltena S. "A Performance Test of a Fluidic Momentum Controller in Three Axes." NASA Technical Report, May 2004.

Kennel, H.F. "A Control Law for Double-Gimballed Control Moment Gyros Used for Space Vehicle Attitude Control." NASA Report, TM-64536, 1970.

Kim, E., Bang, H., and Lee, S.H. "Attitude-Independent Magnetometer Calibration Considering Magnetic Torquer Coupling Effect." *Journal of Spacecraft and Rockets*, 2011: 691-694.

Kowalchuk, S.A., and Hall, C.D. "Spacecraft Attitude Sliding Mode Controller Using Reaction Wheels." *AIAA/AAS Astrodynamics Specialist Conference and Exhibit.* Hawaii, Aug 2008.

Krishnan, S., and Vadali, S.R. "An Inverse-Free Technique for Attitude Control of Spacecraft Using CMGS." *Acta Astronautica*, 1996: 431-438.

Kumar K.D. "Satellite Attitude Stabilization Uing Fuid Rings." *Acta Mechanica*, January 2009: 117-131.

Kurokawa, H. "Constrained Steering Law of Pyramid-Type Control Moment Gyros and Ground Tests." *Journal of Guidance, Control, and Dynamics*, 1997: 445-449.

Kusuda, Y., and Takahashi, M. "Design of Feedback Control System Using Nominal Inputs for Satellite Attitude Maneuver Using Control Moment Gyros." *AIAA Conference of Guidance, Navigation, and Control.* Chicago, Aug 2009.

Kwakernaak, H., and Sivan, R. *Linear Optimal Control Systems.* New York: Wiley, 1972.

Lappas, V., and Wie, B. "Robust Control Moment Gyroscope Steering Logic with Gimbal Angle Constraints." *Journal of Guidance, Control, and Dynamics*, 2009: 1662-1666.

Larson, W.J., and Wertz, J.R. *Space Mission Analysis and Design.* Kluwer Academic Publishers, 1992.

Laughlin, D.R., Sebesta, H.R., and Ckelkamp-Baker, D.E. "A Dual Function Magneto Hydrodynamic (mhd) Device for Angular Motion Measurement and Control." *Advances in the Astronautical Sciences*, 2002: 335-348.

Lee, H., Kim, Y., Cheon, Y.J., and Kim, H.S. "Reconfigurable Satellite Attitude Control Scheme Using Two Reaction Wheels for Limited Mission." *60th International Astronautical Congress (IAC).* Daejeon, Sept 2009. 4934-4944.

Leeghim, H., Lee, D., Bang, H., and Lee, K. "Spacecraft Attitude Control by Combination of Various Torquers." *International Journal of Systems Science*, 2009: 995-1009.

Leeghim, H., Bang, H., and Park, J.O. "Singularity Avoidance of Control Moment Gyros by One-Step Ahead Singularity Index." *Acta Astronautica*, 2009: 935-945.

Leimanis, E. *The General Problem of the Motion of Coupled Rigid Bodies About a Fixed Point.* New York: Springer-Verlag, 1965.

Li, F., and Bainum, P.M. "Numerical Approach for Solving Rigid Spacecraft Minimum Time Attitude Maneuvers." *Journal of Guidance, Control, and Dynamics*, 1990: 38-45.

Li, J., and Kumar, K.D. "Fault Tolerant Synchronization Control During Formation Flying." *Journal of Aerospace Engineering*, 2011: 251-263.

liu, H., Wanng, H., Feng, C., and Ye, W. "Attitude Control of Micro Satellite Using Thruster Plus Bias Momentum Wheel." *ICIC Express Lertters*, 2010: 1269-1274.

Lurie, B.J., and Schier, J.A. "Liquid-Ring Attitude-Control System for Spacecraft." *NASA Tech Briefs*, 1990: 82.

Lurie, B.J., Schier, J.A., and Iskenderian, T.C. Fluid-Loop Reaction System. US Patent 5026008. 1991.

Maeda, K., Hidaka, T., and Uo, M. "A Magnetic Libration Control Scheme for Gravity-Gradient Stabilized Small Satellite." *Advances in the Astronautical Sciences*, 1997: 887-8896.

Marshall, T., Gunderman, T., and Mobley, F. "Reaction Wheel Control of the MSX Satellite." *Advances in the Astronautical Sciences*, 1991: 119-138.

Martinellia, M.I. and Sanchez, P.R.S. "Passive 3 Axis Attitude Control of MSU-1 Pico-Satellite." *Acta Astronautica*, 2004: 507-518.

Maynard, R.S. Fluid Momentum Controller. US Patent 4776541. Oct. 11, 1988.

McMahon, J., and Schaub, H. "Simplified Singularity Avoidance Using Variable Speed Control Moment Gyroscope Null Motion." *Advances in the Astronautical Sciences*, 2010: 1611-1623.

Nanamori, Y., Takahashi, M., Tanikimi, S., Yoshida, K., and Ohkani, Y. "Singularity Avoidance of Control Moment Gyros Using Optimization of Initial Gimbal Angles and Application to Multi Target Pointing for Satellite Attitude Control." *Advances in the Astronautics Sciences*, 2008: 2337-2352.

Navabi, N., and Nasiri, N. "Three-axis Stabilization of a Low Earth Orbit Spacecraft Utilizing Magnetorquers and Reaction Wheels Combinations, According to Energy Consumption." *61st International Astronautical Congress*. Prague, Sept 2010. 4769-4777.

Ogata, K. *Modern Control Engineering.* 5. New York: Prentice-Hall, 2009.

Patel, S., and Kumar, K.D. *Design and Development of Fluid Based Attitude Control System.* Technical Report, Toronto, Canada: Ryerson University, 2010.

Raus, R., Gao, Y., and Watt., M. "Review and Analysis of Single-Thruster Attitude Control Techniques for Spinning Spacecraft." *61st International Astronautical Congress (IAC).* Prague, Sept 2010. 3358-3369.

Richie, D.J., and Lappas, V.J. "Saving Mass in Optimally Sizing a Small Satellite Energy Storage and Attitude Control System." *Advances in the Astronautical Sciences*, 2007: 1161-1177.

Sands, T.A., Kimz, J.J., and Agrawal, B. "Control Moment Gyroscope Singularity Reduction Via Dicoupled Control." *IEEE Southeastcon.* Atlanta, March 2009. 388-391.

Schaub, H., and Junkins, J.L. *Analytical Mechanics of Space Systems.* Reston, Virginia: AIAA Education Series, 2003.

Shames, H. I. *Mechanics of Fluids.* New York: McGraw-Hill, 1992.

Slotine, J.J., and Weiping, L. *Applied Nonlinear Control.* 1st Edition. New Jersey: Englewood Cliffs, 1991.

Sofyali, A., and Jafarov, E.M. "Three-axis Attitude Control of a Small Satellite by Magnetic Pd-like Controller Integrated with Passive Pitch Bias Momentum Method." *5th International Conference on Recent Advances in Space Technologies.* Istanbul, Turkey, June 2011. 307-331.

Srikant, S., and Akella, M.R. "Persistence Filter Based Attitude Stabilization of Micro Satellites with Variable Amplitude Thrusters." *Advanced in the Astronautical Sciences*, 2010: 649-659.

Stenmark, L., and Lang, M. "Micro Propulsion Thrusters and Technologies." *European Space Agency, (Special Publication) ESA SP*, 1997: 399-405.

Steyn, W.H. "Fuzzy Control for a Non-Linear MIMO Plant Subject to Control Constraints." *IEEE Transactions on Systems, Man and Cybernetics*, 1994: 1565-1571.

Sun, Z., Yang, X., and Yang, D. "Active Magnetic Control Methods for Small Satellite." *Journal of Aerospace Engineering*, 2003: 38-44.

Tang, H.B., Zi, Z.P., Jin, X., Jiang, J., Zau, Y., and Yan, Z.Y. "A Micro-Propulsion System with Propane Propellent for Small Satellite." *Advanced Science Letters*, 2011: 2015-2021.

Terui, F., Kimura, S., Nagai, Y., Yamamoto, H., Yoshiharo, K., Yamamoto, T., Nakasuka, S. "Moon Tracking Attitude Control Experiment of A Controlled Bias Momentum Micro Matellite." *AIAA Guidance, Navigation, and Control Conference.* San Francisco,California, Aug 2005. 1587-1601.

Topland, M.P., and Gravdahl, J.T. "Nonlinear Attitude Control of the Micro-satellite ESEO." *55th International Astronautical Federation.* Vancouver, Canada, Oct 2004. 757-767.

Tsiotras, P., Shen, H., and Hall, C. "Satellite Attitude Control and Power Tracking with Energy/Momentum Wheels." *Journal of Guidance, Control, and Dynamics*, 2001: 23-34.

Vadali, S.R., and Junkins, J. "Optimal Open-Loop and Stable Feedback Control of Rigid Spacecraft Attitude Maneuvers." *Journal of the Astronautical Sciences*, 1984: 105-122.

Wang, P., Zheng, W., Zhang, H., and Wu, Z. "Attitude Control of Low-orbit Micro-satellite with Active Magnetic Torque and Aerodynamic Torque." *International Symposium on Systems and Control in Aeronautics and Astronautics.* Harbin, China, June 2010. 1460-1464.

Wertz, J.R. *Spacecraft Attitude Determination and Control.* Netherlands: Academic Publishers, 1999.

Wie, B. *Space Vehicle Dynamics and Control.* Reston, Virginia: AIAA Education Series, 1998.

Ye, D., Zhaowei, S., and Shunan, W. "Hybrid Thrusters and Reaction Wheels Strategy for Large Angle Rapid Reorientation with High Precision." *Acta Astronautica*, 2011: 149-155.

Zhang, S.F., Qian, S., and Li, P.K. "Study on the Minimal Energy Maneuvering Control of a Rigid Spacecraft with Momentum Transfer." *Journal of Astronautics*, 2009: 1504-1515.